

**SURFACTANT ENHANCED VOLUMETRIC SWEEP EFFICIENCY**

**Final Report**

**By**

**Jeffrey H. Harwell**

**John F. Scamehorn**

**October 1989**

**Performed Under Contract No. AC19-85BC10845**

**University of Oklahoma**

**Norman, Oklahoma**

**Bartlesville Project Office  
U. S. DEPARTMENT OF ENERGY  
Bartlesville, Oklahoma**



**FOUNDAZON**

This report has been reproduced directly from the best available copy.

Available to DOE and DOE contractors from the Office Of Scientific and Technical Information, P.O. Box 62, Oak Ridge, TN 37831; prices available from (615)576-8401, FTS 626-8401.

Available to the public from the National Technical Information Service, U.S. Department of Commerce, 5285 Port Royal Rd., Springfield, VA 22161

Price: Printed   A05    
Microfiche A01

**Surfactant Enhanced Volumetric Sweep Efficiency**

**Final Report**

**By**

**Jeffrey H. Harwell**

**John F. Scamehorn**

**October 1989**

**Work Performed Under Contract No. AC19-85BC10845**

**Prepared for**

**U. S. Department of Energy**

**Assistant Secretary for Fossil Energy**

**Jerry F. Casteel, Project Manager**

**Bartlesville Project Office**

**P. O. Box 1398**

**Bartlesville, OK 74005**

**Prepared by**

**University of Oklahoma**

**School of Chemical Engineering & Materials Science**

**100 E. Boyd, Room F339**

**Norman, OK 73019**



## Table of Contents

LIST OF TABLES	iv
LIST OF FIGURES	v
EXECUTIVE SUMMARY	vii
ABSTRACT	x
CHAPTER 1 INTRODUCTION	1
CHAPTER 2 Experimental Verification of Surfactant-Assisted Waterflooding	3
INTRODUCTION	3
RESULTS AND DISCUSSIONS	3
CONCLUSIONS	9
CHAPTER 3 Simulation of Potential Increases in Oil Recovery by Surfactant Enhanced Selective Blocking	26
INTRODUCTION	26
RESULTS AND DISCUSSIONS	26
CONCLUSIONS	29
CHAPTER 4 Hardness Tolerance in Anionic Surfactant Solutions I. Anionic Surfactant with Added Monovalent Electrolyte	35
ABSTRACT	35
INTRODUCTION	35
EXPERIMENTAL MATERIALS	36
THEORY	37
RESULTS AND DISCUSSIONS	43
CONCLUSIONS	48
NOMENCLATURE	49
REFERENCES	52
CHAPTER 5 Hardness Tolerance of Anionic Surfactant Solutions II. Effect of Added Nonionic Surfactant	59
ABSTRACT	59
INTRODUCTION	59
EXPERIMENTAL MATERIALS	60
THEORY	60
RESULTS AND DISCUSSIONS	63
NOMENCLATURE	70
REFERENCES	73

## LIST OF TABLES

<u>Table</u>		<u>page</u>
2.1	Synthetic Field Brine Composition	10
2.2	Experimental Conditions in Flow Experiments	11
2.3	Experimental Conditions in Flow Experiments	12
2.4	Experimental Conditions in Flow Experiments	13
3.1	Characteristics of Simulated Reservoir	30
4.1	Comparison Between Calculated and Experimental Values of CMCds with Added NaCl and MgCl <sub>2</sub> (all CMCcds = $1.900 \times 10^{-3}$ M)	54
5.1	Summary of Parameters Used in Model	75
5.2	Comparison Between Calculated and Experimental Values of CMCds with Added NaCl and MgCl <sub>2</sub> (all CMCcds = $2.0 \times 10^{-3}$ M)	76

## LIST OF FIGURES

<u>Figure</u>		<u>page</u>
2.1	Permeability vs. Pore Volume Injected, Experiment # 1	14
2.2	Concentration History Curve, Experiment # 1	15
2.3	Permeability vs. Pore Volume Injected, Experiment # 2	16
2.4	Concentration History Curve, Experiment # 2	17
2.5	Permeability vs. Pore Volume Injected, Experiment # 3	18
2.6	Concentration History Curve, Experiment # 3	19
2.7	Permeability vs. Pore Volume Injected, Experiment # 4	20
2.8	Concentration History Curve, Experiment # 4	21
2.9	Permeability vs. Pore Volume Injected, Experiment # 5	22
2.10	Concentration History Curve, Experiment # 5	23
2.11	Permeability vs. Pore Volume Injected, Experiment # 6	24
2.12	Concentration History Curve, Experiment # 6	25
3.1	Production of Oil Versus Injected Volume of Water for Different Degrees of Heterogeneity (Short, Transversely Permeable Reservoirs)	31
3.2	Production of Oil Versus Injected Volume of Water in Short Reservoir (without or with Selective Blocking)	32
3.3	Production of Oil Versus Injected Volume of Water in Long Reservoir (without or with Selective Blocking)	33
3.4	Production of Oil Versus Injected Volume of Water in Short Reservoir (without or with Selective Blocking)	34
4.1	Schematic of Equilibrium Existing in System	55
4.2	Effect of Unbound Na <sup>+</sup> Concentration on CMC of Anionic Surfactant	56
4.3	Precipitation Phase Boundary without Added NaCl	57
4.4	Precipitation Phase Boundary with Various Concentration of Added NaCl	58

5.1	Schematic of Equilibrium Existing in System	77
5.2	CMC of Mixed Surfactant System at $[\text{Na}^+]_{\text{un}} = 0.01 \text{ M}$	78
5.3	CMC of Mixed Surfactant System at $[\text{Na}^+]_{\text{un}} = 0.02 \text{ M}$	79
5.4	CMC of Mixed Surfactant System at $[\text{Na}^+]_{\text{un}} = 0.01 \text{ M}$	80
5.5	Effect of Unbound $\text{Na}^+$ Concentration on W/RT	81
5.6	CMC of Mixed Surfactant System with Mixed Electrolytes Present	82
5.7	Precipitation Phase Boundary without Added NaCl and with and without Added Nonionic Surfactant	83
5.8	Precipitation Phase Boundary with Nonionic Surfactant and 0.02 M Added NaCl and without Added Nonionic Surfactant or Added NaCl	84
5.9	Precipitation Phase Boundary with Nonionic Surfactant and 0.10 M Added NaCl and without Added Nonionic Surfactant or Added NaCl	85
5.10	Comparison of Precipitation Phase Boundaries with Prediction Using Modified Model Parameters	86
5.11	Values of Fractional Counterion Binding of Calcium Required to Describe System with Nonionic Surfactant and No Added NaCl	87
5.12	Effect of W/RT on Predicted Precipitation Phase Boundaries	88

## EXECUTIVE SUMMARY

Fluids do not flow as a uniform plug through oil reservoirs. Reservoir heterogeneities result in most of the flow channelling through regions of high permeability, leaving significant fractions of the original oil still remaining in areas of low permeability, where flow rates are less. This is known as bypassing and results in zones in the reservoir of high residual levels of unproduced oil when a field is abandoned. It is the improved recovery of the oil trapped due to reservoir heterogeneity which this project addresses.

After development of water channels between the injection and production wells, the injected brine results primarily in brine production. The goal of surfactant-assisted waterflooding is to partially or completely block these water streaks by forming a plug of surfactant precipitate or coacervate deep in the water channels, far from the injection wells, without the occurrence of plugging in the immediate vicinity of the well bore. This plugging of the water channels forces subsequently injected brine into the portions of the reservoir with high residual oil saturations, resulting in an extension of the economic life of a secondary recovery project.

The process relies on the differences in the chromatographic velocities of oppositely charged surfactants as they are propagated through a porous medium and phase separation behavior of surfactants to seal off high permeability, low residual oil saturation regions of reservoirs. Though making use of surfactants, this new process is not to be confused with classical (low tension) surfactant flooding, which is designed to enhance oil recovery by reducing oil/water interfacial tensions. In the new process, a sequence of surfactant species is injected into the reservoir. The first surfactant injected is moved away from the injection well by subsequent injection of waterflood brine. The last surfactant injected is chosen to have higher chromatographic velocity than the first one. The species are also chosen so that when they mix in-situ, a phase separation occurs, resulting in formation of a pore-blocking precipitate surfactant phase or of a high viscosity gel-like coacervate surfactant phase. Because the oil recovery mechanism is completely different from that in low tension surfactant flooding, the new process can operate at much lower surfactant concentrations and higher injectivities, greatly reducing the upfront costs of the new process, improving its economic feasibility.

The technical feasibility of the surfactant-assisted waterflooding process in model porous media (an alumina sandpack with 0.15M NaCl and Berea sandstone cores saturated with 10% synthetic field brine) has been demonstrated both experimentally and theoretically. Static and dynamic single component surfactant adsorption isotherms, and static multicomponent adsorption isotherms have been measured for a model surfactant system (sodium dodecyl sulfate (SDS)/dodecyl pyridinium chloride (DPC)).

The adsorption of the mixture of surfactants was described by the use of ideal solution theory to model the formation of the admicelle or surfactant aggregates on the surface of the mineral. However, the phase separation model of surfactant adsorption failed to represent the monomer-micelle equilibrium at low surface coverages.

The effect of surfactant structures and concentrations, pH, temperature, and electrolyte type and concentration on precipitation phase boundaries for a model anionic/cationic surfactant mixture was investigated. A mathematical model was successfully developed to predict the precipitation phase boundaries. This model utilizes simple solubility product constants coupled with the assumption that only surfactant monomer concentration should be used in the solubility product expressions. Regular solution theory is used to describe monomer-micelle equilibrium. This model accurately predicts the precipitation phase boundaries of the anionic/cationic surfactant mixture. The hardness tolerance of anionic surfactant solutions was also found to be enhanced by the addition of monovalent electrolyte or nonionic surfactants. In general, the precipitation studies showed that the conditions of the injected surfactant slugs and surfactant structure can be adjusted to allow precipitation under a variety of reservoir conditions.

Experiments in simulated porous media had shown that in-situ mixing of surfactant slugs caused phase changes which were capable of blocking the permeable pore channels in which fluid was flowing, thereby reducing the permeability of the high permeability zones. The depth of plugging and plug sizes could also be controlled by adjusting the pore volumes of brine spacer or the concentration and pore volumes of surfactants injected. Optimum strategies were identified whereby the stability of plugs could be prolonged. It was also demonstrated that plugs could be made to form selectively (with respect to position) in high permeability zones of reservoir sandpacks and sandstones, both in the case of one directional flow through a core of low inlet and high outlet permeability (and vice versa), and in the case of two-directional flow originating in the center of a core and moving through regions of high, and low permeability, respectively. Microscopic examination of the precipitate showed that plate-like crystals were formed. It is likely that the mechanism of permeability reduction in the sandstone is closing of pore throats by stacks of oriented precipitate crystals. This mechanism is similar to that proposed for the effect of soft water on sandstone cores, only there is a different source for the particles which block the pores. This is a significant finding in that it indicates that the efficiency of the permeability reduction is not likely to be strongly dependent on the total volume of precipitate formed. This, in turn, means that lower concentrations of surfactant may be used to form channel-plugs of sufficient strength.

Mathematical simulation of a two dimensional reservoir with two phase flow (oil and water) was developed which could be used to determine the plug growth and resistance to bypassing and the potential increases in oil recovery when using the proposed

process in a variety of simulated reservoir conditions. These studies indicate that reservoirs in which the high-permeability streaks are one or two orders of magnitude greater than the lower permeability regions are strong candidate for this process.

In summary, the ability of surfactant-assisted waterflooding to modify permeability profiles in a beneficial way has been demonstrated both experimentally and theoretically. Experimental work and mathematical modeling has delineated the abilities and the limitations of the process. Starting from scratch in the investigation of a total new concept and process, results from the past three years lead to a great deal of optimism about this new technology.

## ABSTRACT

Surfactant-enhanced waterflooding is a novel EOR method aimed to improve the volumetric sweep efficiencies in reservoirs. The technique depends upon the ability to induce phase changes in surfactant solutions by mixing with surfactants of opposite charge or with salts of appropriate type. One surfactant or salt solution is injected into the reservoir. It is followed later by injection of another surfactant or salt solution. The sequence of injections is arranged so that the two solutions do not mix until they are into the permeable regions well away from the well bore. When they mix at this point, by design they form a precipitate or gel-like coacervate phase, plugging this permeable region, forcing flow through less permeable regions of the reservoir, improving sweep efficiency.

The selectivity of the plugging process is demonstrated by achieving permeability reductions in the high permeable regions of Berea sandstone cores. Strategies were set to obtain a better control over the plug placement and the stability of plugs. A numerical simulator has been developed to investigate the potential increases in oil production of model systems. Furthermore, the hardness tolerance of anionic surfactant solutions is shown to be enhanced by addition of monovalent electrolyte or nonionic surfactants.

# SURFACTANT ENHANCED VOLUMETRIC SWEEP EFFICIENCY

## CHAPTER 1

### INTRODUCTION

The purpose of this project is to increase the ultimate oil recovery through waterflooding in heterogeneous reservoirs by selectively blocking off high permeability zones which exist at waterflood residual oil saturation. Subsequently injected displacement fluids will be diverted into the low permeability zones of high oil content.

This process consists of three parts; first a dilute surfactant solution is injected into the reservoir which has a high adsorption loss onto the reservoir minerals. This leads to a tail region in the advancing slug with a low chromatographic velocity. Second, a brine spacer is injected. Thirdly, a second unlike surfactant solution is injected which has a lower adsorption than the first injected surfactant. The concentration of the surfactant solutions are several times the Critical Micelle Concentration (CMC); therefore surfactants are in the form of micelles which advance with a large chromatographic velocity.

Interaction of the two unlike surfactants will occur deep within the reservoir in the high permeability zones. This interaction results in the formation of a precipitate or a gel-like coacervate either of which can greatly reduce the permeability of the high permeability zones. The distance from the injection well at which permeability reduction occurs can be controlled, by altering the size of the brine spacer and the concentration of the two surfactants.

Experiments have been performed in sandstone cores which have shown that in-situ mixing of surfactant slugs causes a phase change which is capable of significantly reducing the permeability. Strategies have been identified whereby the stability of low-permeability plugs can be prolonged.

The research project has shown that selective plugging can be made to occur. For example, permeability reductions were achieved in high-permeability zones, both in the case of one directional flow through a core of low-inlet and high-outlet permeability (and vice versa), and in the case of two-directional flow originating in the center of a core and moving

through regions of high, and low permeability, respectively.

A numerical simulator has been developed which can be used to determine the potential increases in oil recovery when using the proposed process in model reservoirs. The studies indicate that reservoirs in which the high-permeability streaks are one or two orders of magnitude greater than the lower permeability regions are strong candidates for this process. It has also been shown that dramatic improvements in oil recovery are possible with the process, because the precipitate or coacervate form rapidly and selectively in the high permeability zones.

Two possible candidates for the injected slugs in this process are; a slug of anionic surfactant followed by a slug of multivalent cations, and a slug of anionic surfactant followed by a slug of nonionic surfactant. Detailed work has been done on the phase boundary behavior of such systems, without and with the addition of monovalent electrolyte.

Such studies should make it possible to predict how to formulate surfactant slugs, such that strong precipitation will take place on in-situ mixing, and such that the individual slugs themselves can be given an increased hardness tolerance to multivalent cations present in the reservoir itself.

## CHAPTER 2

### Experimental Verification of Surfactant-Assisted Waterflooding

#### INTRODUCTION

The objective of the experiments described in this report is to investigate permeability reduction in consolidated Berea sandstone cores produced by a selective plugging process. The process uses phase changes in surfactant solutions and the chromatographic movement of surfactants to improve the volumetric sweep efficiency. High permeability regions are the desired locations for surfactant precipitate formation to occur. The ultimate goal is to partially plug these regions and force the fluid flow into the low permeability zones, which have higher oil saturations after normal waterflooding.

To validate and to show the technical feasibility of the proposed process in a well-defined experimental system, experiments were designed and performed to: (1) verify that phase separation would occur in a simulated porous media composed of Berea sandstone with an anionic/cationic surfactant system, resulting in formation of either a solid precipitate or a viscous gel-like coacervate phase, which is capable of blocking the high-permeable pore channels in which fluid is flowing, thereby reducing the permeability of the high permeability zones, (2) show that the subsequently injected fluid would be selectively diverted to the low permeability and unswept regions, (3) investigate the depth of plugging and test the injection strategies so that plug placement could be controlled, (4) examine the long term stability of plugs.

#### RESULTS AND DISCUSSIONS

Berea sandstone cores were stabilized prior to each run. This was required by the presence of considerable amounts of clay minerals, which could migrate or swell to cause plugging. In order to minimize these effects, 100 pore volumes of a 10% synthetic field brine (SFB) solution was injected through one end of the core and then through the other end. The 10% SFB is a dilution of a full strength SFB whose composition is shown on Table 2.1. Several factors, such as injectivity rate, salinity, and pH were also monitored and kept constant. Brine solutions were vacuum filtered to prevent fine particles and degassed to prevent air bubbles from getting into the system and effecting the apparent permeability. A pressure tap was placed about half way from the inlet end and 1/2 inch into the surface of the core. By monitoring the pressure drop between the inlet and the outlet the approximate distance from the injection point at which plugging occurs could be determined. The pressure and flow rate were continuously monitored during the experiments. Table 2.2

through Table 2.4 list the test conditions, pore volumes of injected surfactant and brine solutions.

The effect of coacervate formation on the permeability of the core was determined by experiment 1. Figure 2.1 is a plot of permeability versus pore volumes injected and figure 2.2 is a concentration history curve for this run. During injection of Dodecyl Pyridinium Chloride (DPC), the pressure drop for the outlet section of the core decreased. This might be due to a drag reduction phenomena known to be produced by adsorbing surfactants; it may also be due to some unknown mechanism by which the surfactant interacts with the Berea surface or with clays in the column. With injection of Sodium Dodecyl Sulfate (SDS), the permeability through the outlet section first increased, but then sharply decreased within 3.14 pore volume (pv) of injection (from 143.3 md to 23.1 md - 84% reduction). However, permeability through the inlet section decreased immediately and reached almost a constant value of 23 md (40% reduction). Coacervate was observed in the effluent samples shortly after the DPC concentration reached its minimum, indicating that formation of this viscous surfactant phase was occurring in-situ. Continued flushing with brine resulted in a subsequent increase in permeability of the outlet section to 53 md (still 33% reduction overall). This was probably due to partial elution of the coacervate, or a dissolution of part of the coacervate phase. However, as is evident from figure 2.1, the permeability through both sections reached a stable condition after 70 pv had been injected. It can also be observed from figure 2.2 that continued injection of SDS would cause a partial recovery of the permeability and elution of DPC from the porous medium. After injection of 16 pv, the permeability in the outlet section increased. This coincides with an increase in effluent DPC concentration. Continued injection of 10% SFB caused both the effluent DPC concentration and the permeability in the outlet section to decrease. The effluent DPC concentration reached zero after 3.4 pv of 10% SFB was injected. Thus, it is apparent that only an optimum SDS slug size is needed to reduce the permeability to its minimum. This optimum is reached when the effluent DPC concentration reaches its minimum following SDS introduction into the system.

Experiment 2 was designed to show the effect of brine spacer on selective permeability reduction. Permeability reduction can be obtained in the outlet half of the core by monitoring the size of the brine spacer. Moreover, it was desired to demonstrate that the extent to which DPC was removed from the core after injection of SDS could be controlled by the size of the SDS slug. After injecting 10.03 pv of DPC, 0.64 pv of 10% SFB (more than 150% increase in the size of the brine spacer over the previous run), was followed by 3.5 pv of SDS. Figure 2.3 is a plot of permeability versus pore volumes injected for this run, and Figure 2.4 is the concentration history curve. As shown in Figure 2.3, after injection of SDS, a quicker response in permeability reduction can be observed for the inlet section (20%

reduction) than for the outlet section (28% reduction). When 10% SFB was injected, there was first an immediate increase in permeability through the inlet section, which subsequently remained constant at 121.6 md (11% reduction overall). However, the increase in permeability through the outlet section did not occur until 10 pv of brine had been injected into the core. This recovery could again be due to partial dissolution of the plugs. It stabilized at 83.7 md (23% reduction overall) and remained constant throughout the rest of the run. Injection of SDS was stopped when the effluent DPC concentration reached its minimum. This limited the elution of DPC from the core and resulted in a lower recovery in permeability in the outlet section. As in the first run, the presence of coacervate in the effluent solution was observed when the effluent DPC concentration was at its minimum.

In the next two experiments, cores were placed in such a way that higher permeability sections were at the outlet end and lower permeability regions were at the inlet end of the core. This allowed us to investigate the ability of formation of precipitate at the downstream side away from the inlet end and in the high permeability regions.

Experiment 3 was designed to show the effect of formation of precipitate on the permeability of the core. Figure 2.5 is a plot of permeability versus pore volumes injected and Figure 2.6 is a concentration history curve for this run. After injection of 9.96 pv of DPC, 0.68 pv of 10% SFB was followed by 3.54 pv of SDS. The optimum SDS slug size needed to control the elution of DPC from the core, occurred after 0.22 pv of SDS was injected and when the effluent DPC concentration reached its minimum following SDS introduction into the system. At this point, the permeability through the outlet section started to decrease and reached its minimum within 3.84 pv of SDS injection (from 116 md to 22.5 md - 81% reduction). However, permeability in the inlet section decreased immediately and reached almost a constant value of 15.4 md (67% reduction). Precipitate was observed in the effluent samples after the DPC concentration reached its minimum, indicating that formation of precipitate was occurring in-situ. It was also desired to achieve more permeability reduction through the outlet section by injecting 0.68 pv of brine spacer. This task was momentarily achieved after 16 pv had been injected (81% reduction in the outlet section as opposed to 67% reduction in the inlet section). Continued flushing with brine resulted in a subsequent increase in permeability which ultimately reached a stable condition after 90 pv had been injected (still 45% reduction in the outlet section as opposed to 70% reduction in the inlet section). One reason for this behavior could be that precipitate was not fully formed in the outlet section at time at which injection of brine solution was resumed. Precipitate particles are assumed to be produced as nuclei and grow in size gradually. When the size of these particles is smaller than the size of the pore throat of the porous media, they can easily pass through the pores and leave more flow paths available for fluid

to go through.

In Experiment 4, the concentration of SDS was increased from 6000  $\mu\text{M}$  to 7000  $\mu\text{M}$ . This was to produce more stable plugs and to prevent a larger recovery in permeability. A smaller slug size for the brine spacer was also used to concentrate the extent of formation of precipitate in the inlet end of the core. Figure 2.7 is a plot of permeability versus pore volumes injected for this run, and Figure 2.8 is the concentration history curve. As shown in Figure 2.7, after injection of SDS, a quicker response in permeability reduction can be observed for the inlet section (88% reduction) than for the outlet section (84% reduction). After injection of 10% SFB, permeability through both sections gradually increased. However, the permeability through the inlet section remained constant after 20 pv of injection (still 79% reduction overall), and the permeability through the outlet section never reached a constant value (46% reduction after 163 pv of injection). This recovery was probably again due to elution of precipitate, or a dissolution of part of the precipitate phase. Injection of SDS was stopped when effluent DPC concentration reached its minimum. This limited the elution of DPC from the core and resulted in a lower recovery in permeability in the outlet section. As in the last run, the presence of precipitate in the effluent solution was observed when the effluent DPC concentration was at its minimum.

To obtain a more stable plug and to prevent the elution or dissolution of part of the coacervate phase, fluid flow was stopped in Experiment 5. This resulted in a greater permeability reduction and formation of more stable plugs, which prevented a large recovery in permeability. Figure 2.9 is a plot of permeability versus pore volumes injected, and Figure 2.10 is the concentration history curve for the same experiment. After injecting 8.21 pv of DPC at 15000  $\mu\text{M}$ , 0.43 pv of 10% SFB, and 1.51 pv of SDS at 10000  $\mu\text{M}$ , the permeability in the inlet section dropped from 164 md to 50.5 md. Flow was then stopped and the core was placed in a horizontal position with a pressure tap on the top. The horizontal position was chosen in order to eliminate the gravity effect on the coacervate phase. At the injected surfactant concentrations, based on the phase diagram for the SDS-DPC system, formation of coacervate was expected. As shown in the diagram, during this time, the permeability for the inlet section changed from 57.1 md to 50.5 md; the outlet section permeability changed from 26 md to 26.5 md. These are not significant changes in permeability. With additional injection of brine the permeability through the inlet section increased to an average value of about 64 md (an overall reduction of 61% from the original permeabilities). The permeability of the outlet section averaged about 16 md (a 27% overall reduction). Since only 0.43 pv of brine spacer was used, it was expected that the permeability reduction for the inlet section would be greater than for the outlet section. Thus, by stopping the flow for the purpose of giving enough time for the completion of any interaction to occur between the SDS and the DPC, an increase in

permeability with continued injection of brine was prevented. This also suggests that large amounts of coacervate did not dissolve into the bulk solution after the phase separation. Moreover, as can be observed from Figure 2.10, there was no increase in effluent DPC concentration once 10% SFB was again injected. This implies that there was no elution of a significant part of the coacervate phase from the porous medium and that a stable plug was formed.

The objective in Experiment 6 of this report was to show the selective plug placement of the process. To achieve this goal, a core from a previous run was used. Surfactant solutions were injected into a core from the inlet end and the permeability of the inlet section was selectively reduced. The core was now a heterogeneous medium with one half having a much higher permeability than the other half. After injecting more than 50 pv of 10% SFB and reaching a stable condition, the core was flooded from a tap which had been placed in the middle of the core; i.e., injection of fluid flow was carried out through a hole 7.2 cm from one end and 6.9 cm from the other end. The initial permeability of the high permeable section (section 1) was 15.4 md; that of the low permeable section (section 2) was 3.0 md. Approximately 83% of flow was initially through section 1. After stabilization with 10% SFB, injection of 5.97 pv of DPC at 15000  $\mu\text{M}$  was followed by 0.29 pv of 10% SFB, and 2.55 pv of SDS at 10000  $\mu\text{M}$ . Figure 2.11 is a plot of permeability of both the high and low permeability sections and percent flow through the high-permeable section, versus cumulative pore volumes injected; Figure 2.12 is a concentration history curve for the two sections. Since more flow was passing through section 1, much of the DPC and brine spacer ended up in this section. This is evident from Figure 2.12, where an earlier DPC breakthrough occurs from section 1 than from section 2: DPC was first detected from section 1 at 1.97 pv, and from section 2 at 4.9 pv. The maximum effluent DPC concentration from section 2 was 7941  $\mu\text{M}$ , while from section 1 the injected concentration, 15000  $\mu\text{M}$ , was reached. A slow decrease of percent flow and permeability through both sections during injection of DPC and 10% SFB was mainly because the core was not completely devoid of any surfactant. Even with injection of more than 50 pv of 10% SFB during the first part of the process, some surfactant was still left in the core in form of coacervate or adsorbed molecules. However, they interacted slightly with the incoming DPC slug and caused minimal changes. During injection of SDS, the interaction of the two surfactants resulted in a phase separation. This diverted the fluid and forced extra SDS to pass through the low permeability section (section 2), where SDS then adsorbed on the mineral surface and interacted with the DPC which was left in this section during DPC injection. The plugging occurred rapidly as the SDS invaded section 1 at a faster rate than section 2. This is evident from the experimental results shown in Figure 2.11. At the end of SDS injection, both permeability and percent flow through section 1 dropped sharply to 1.7 md and 54% (89% and 35% reductions) respectively. At the same time the permeability

through section 2 was 1.3 md (57% reduction). After injecting 0.56 pv of 10%SFB, coacervate was observed at the effluent solution from section 1. This again indicates that coacervate had been formed in-situ and caused the permeability reduction of the higher permeability section, forcing the subsequent fluid flow to bypass this blocked, high permeability region and to divert the fluid into the other region (section 2). This is also evident from a decrease in percent flow through section 1. After 15.5 pv, permeability through section 2 (K2) started to decrease and finally reached to 0.7 md (77% reduction) at 21.51 pv. Since a smaller fraction of surfactants invaded this section, they were diluted to a lower concentration with the incoming brine. This placed the mixture nearer the solubility curve, and, as a result, decreased the relative supersaturation; thus, the rate of formation of the new phase was also decreased in this section. Continual flushing with brine resulted in a partial recovery of permeability through section 2. As described above, coacervate was not fully formed in this section because of the slow rate of formation. Also, from the ratio of relative permeabilities, which was 5.13 before plugging and 1.3 after plugging, it can be concluded that a more uniform and homogeneous medium can be prepared by using this selective plugging process.

## CONCLUSIONS

The following conclusions had been derived by the experiments:

1. permeability reduction can be achieved by forming both coacervate and precipitate in any desired region of a core.
2. The depth of plugging can be extended throughout the length of the core by increasing the size of the surfactant slug and the size of the brine spacer. The size of the brine spacer was increased from 0.25 pv in the first experiment to 0.64 pv in the second experiment. This resulted in greater permeability reduction nearer the end of the core.
3. The loss of the first surfactant from the core can be reduced by controlling the size of the second surfactant slug.
4. Plug formation is reversible; that is, injection of a large excess of the anionic surfactant may be used to remove the plug if necessary for further treatments.
5. More stable coacervate phases can be formed by stopping the flow after injection of the second surfactant. This reduces permeability recovery during subsequent injection of brine.
6. The diversion of fluid flow from the high permeable section to the low permeability section of the core suggests that plugging took place in the flooding zones and forced the flow into the unswept regions. Thus, the high permeability regions can be plugged selectively by in-situ formation of coacervate; and this results into a much more uniform and homogeneous medium.

TABLE 2.1

## SYNTHETIC FIELD BRINE COMPOSITION

COMPONENT	Kg/m <sup>3</sup>
NaCl	12.31
CaCl <sub>2</sub>	0.32
MgCl <sub>2</sub> . 6H <sub>2</sub> O	0.44
NH <sub>4</sub> Cl	0.07
Na <sub>2</sub> B <sub>4</sub> O <sub>7</sub> . 10H <sub>2</sub> O	0.34

TABLE 2.2  
EXPERIMENTAL CONDITIONS IN FLOW EXPERIMENTS

CORE DATA :

	EXPERIMENT # 1	EXPERIMENT # 2
LENGTH (cm)	16.7	14.2
CROSS SECTIONAL AREA (cm <sup>2</sup> )	9.62	10.18
DENSITY (g/cm <sup>3</sup> )	2.87	2.87
PORE VOLYUME (pv)	35.8 ml	33.4 ml
POROSITY (%)	22.3	23.1
PRESSURE TAP LOCATION DISTANCE FROM INLET (cm)	8.6	7.4
INITIAL PERMEABILITY (md)		
INLET SECTION	38.5	148.0
OUTLET SECTION	79.6	108.8
FINAL PERMEABILITY (md)		
INLET SECTION	23.1	121.6
OUTLET SECTION	53.1	83.7
% PERMEABILITY REDUCTION		
INLET SECTION	40.0	11.0
OUTLET SECTION	33.0	23.0

FLUID FLOW DATA:

pv INJECTED

1- DPC	10.96	10.03
2- BRINE SAPACER	0.25	0.64
3- SDS	12.57	3.50

EXPERIMENTAL SYSTEM : DODECYL PYRIDINIUM CHLORIDE (DPC) /  
SODIUM DODECYL SULFATE (SDS)

INJECTED SURFACTANT  
CONCENTRATION : 15000 µM DPC / 10000 µM SDS

SURFACTANT SOLUTION  
VISCOSITY : 1.11 cp (for both SDS and DPC)

INJECTED BRINE  
SOLUTION : 10% SYNTHETIC FIELD BRINE (SFB)

BRINE SOLUTION  
VISCOSITY : 0.96 cp

TABLE 2.3  
EXPERIMENTAL CONDITIONS IN FLOW EXPERIMENTS

CORE DATA :

	EXPERIMENT # 3	EXPERIMENT # 4
LENGTH (cm)	16.55	16.55
CROSS SECTIONAL AREA (cm <sup>2</sup> )	9.62	10.46
DENSITY (g/cm <sup>3</sup> )	2.97	2.64
PORE VOLUME (pv)	38.0 ml	36.8 ml
POROSITY (%)	23.9	21.3
PRESSURE TAP LOCATION DISTANCE FROM INLET (cm)	8.3	7.95
INITIAL PERMEABILITY (md)		
INLET SECTION	46.1	159.4
OUTLET SECTION	116.0	230.0
FINAL PERMEABILITY (md)		
INLET SECTION	13.8	34.0
OUTLET SECTION	63.3	123.6
% PERMEABILITY REDUCTION		
INLET SECTION	70.0	79.0
OUTLET SECTION	45.0	46.0

FLUID FLOW DATA:

pv INJECTED		
1- DPC	9.96	9.50
2- BRINE SAPACER	0.68	0.58
3- SDS	3.54	4.46
INJECTED SURFACTANT CONCENTRATION (μM)		
DPC	15000	15000
SDS	6000	7000
EXPERIMENTAL SYSTEM	DODECYL PYRIDINIUM CHLORIDE (DPC)/ SODIUM DODECYL SULFATE (SDS)	
SURFACTANT SOLUTION VISCOSITY	: 1.11 cp (for both SDS and DPC)	
INJECTED BRINE SOLUTION	: 10% SYNTHETIC FIELD BRINE (SFB)	
BRINE SOLUTION VISCOSITY	: 0.96 cp	

TABLE 2.4  
EXPERIMENTAL CONDITIONS IN FLOW EXPERIMENTS

CORE DATA :

	EXPERIMENT # 5	EXPERIMENT # 6
LENGTH (cm)	14.8	14.1
CROSS SECTIONAL AREA (cm <sup>2</sup> )	10.18	10.75
DENSITY (g/cm <sup>3</sup> )	2.74	2.72
PORE VOLUME (pv)	33.94 ml	32.01 ml
POROSITY (%)	22.5	21.1
PRESSURE TAP LOCATION DISTANCE FROM INLET (cm)	7.75	7.2
INITIAL PERMEABILITY (md)		
INLET SECTION	164.1	15.4
OUTLET SECTION	22.1	3.0
FINAL PERMEABILITY (md)		
INLET SECTION	54.7	1.8
OUTLET SECTION	16.1	1.4
% PERMEABILITY REDUCTION		
INLET SECTION	67.0	88.0
OUTLET SECTION	27.0	53.0

FLUID FLOW DATA:

pv INJECTED		
1- DPC	8.21	5.97
2- BRINE SAPACER	0.43	0.29
3- SDS	1.51	2.55
INJECTED SURFACTANT CONCENTRATION (μM) :		
DPC	15000	15000
SDS	10000	10000
EXPERIMENTAL SYSTEM :	DODECYL PYRIDINIUM CHLORIDE (DPC)/ SODIUM DODECYL SULFATE (SDS)	
SURFACTANT SOLUTION VISCOSITY :	1.11 cp (for both SDS and DPC)	
INJECTED BRINE SOLUTION :	10% SYNTHETIC FIELD BRINE (SFB)	
BRINE SOLUTION VISCOSITY :	0.96 cp	

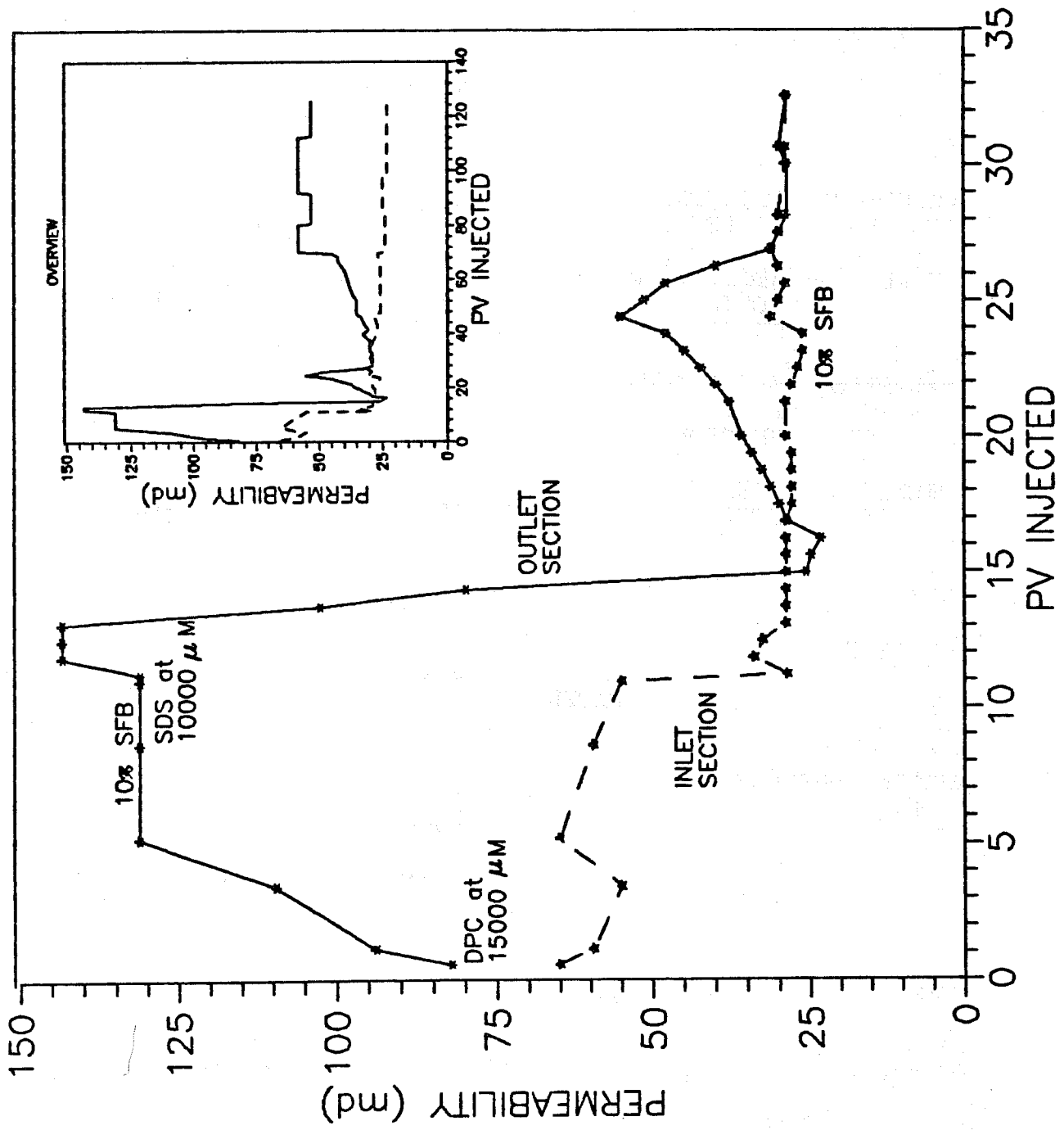


FIGURE 2.1- PERMEABILITY vs. PORE VOLUME INJECTED, EXPERIMENT # 1

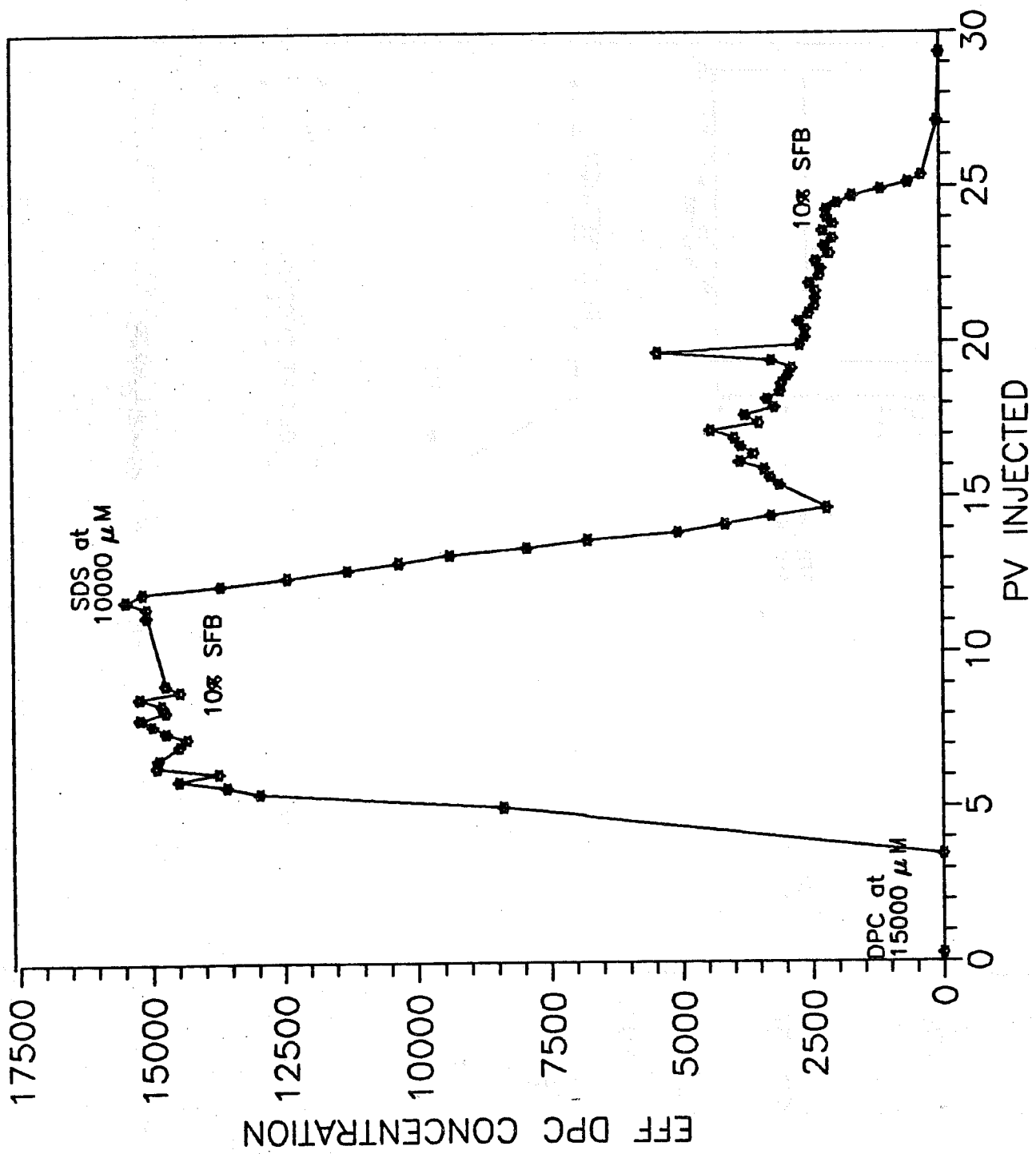


FIGURE 2.2- CONCENTRATION HISTORY CURVE, EXPERIMENT # 1

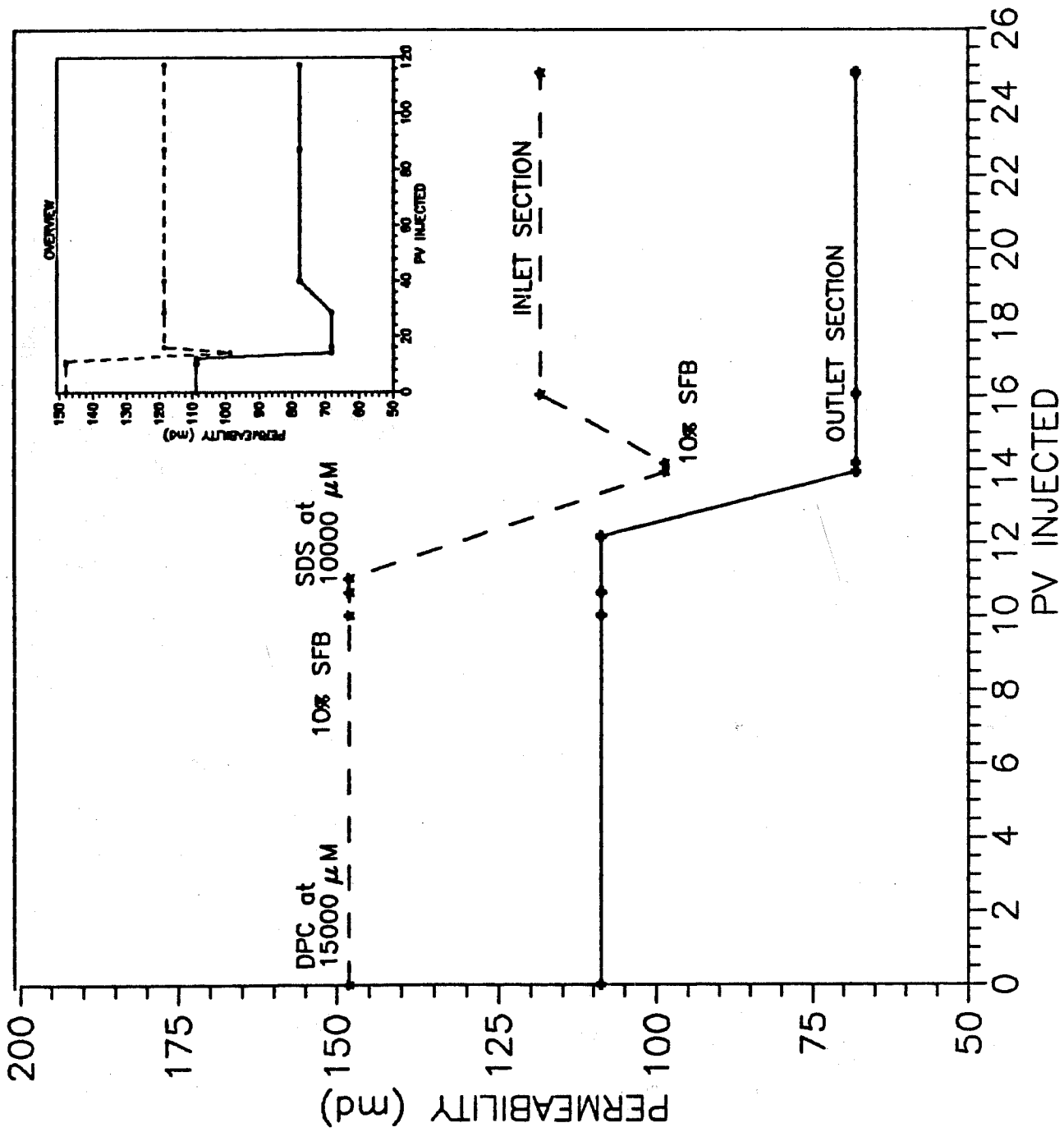


FIGURE 2.3-- PERMEABILITY vs. PORE VOLUME INJECTED, EXPERIMENT # 2

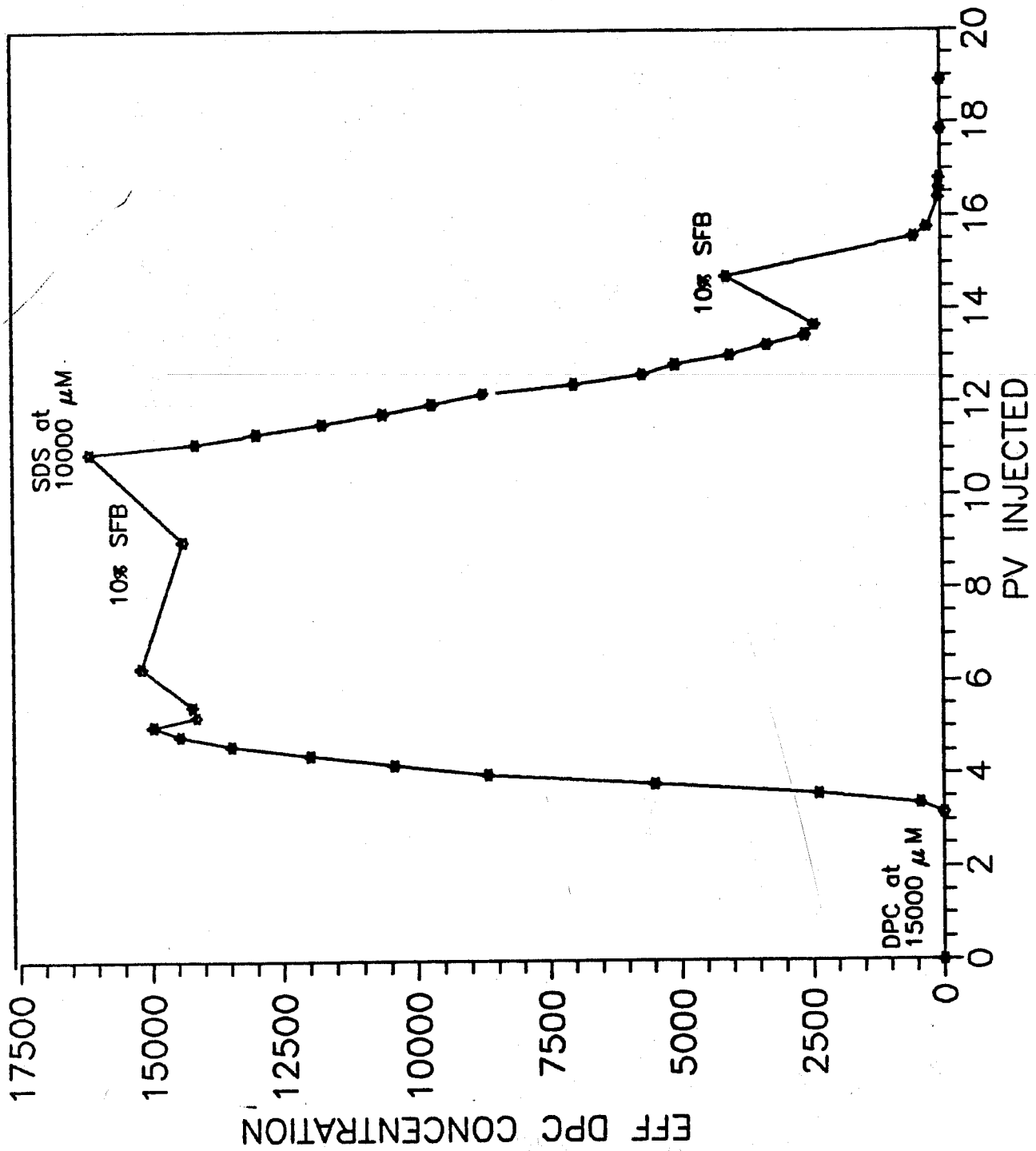


FIGURE 2.4- CONCENTRATION HISTORY CURVE, EXPERIMENT # 2

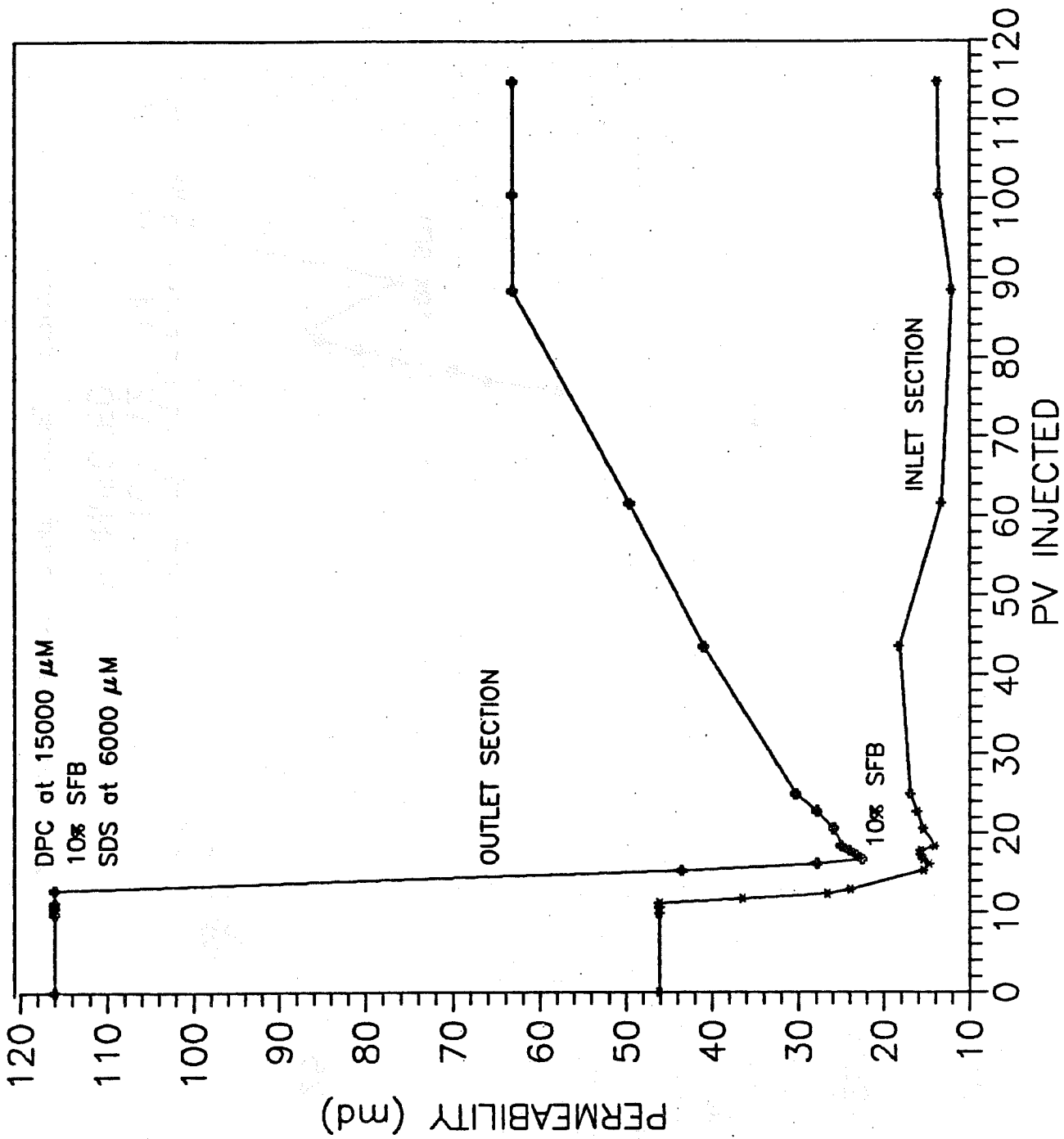


FIGURE 2.5- PERMEABILITY vs. PORE VOLUME INJECTED, EXPERIMENT # 3

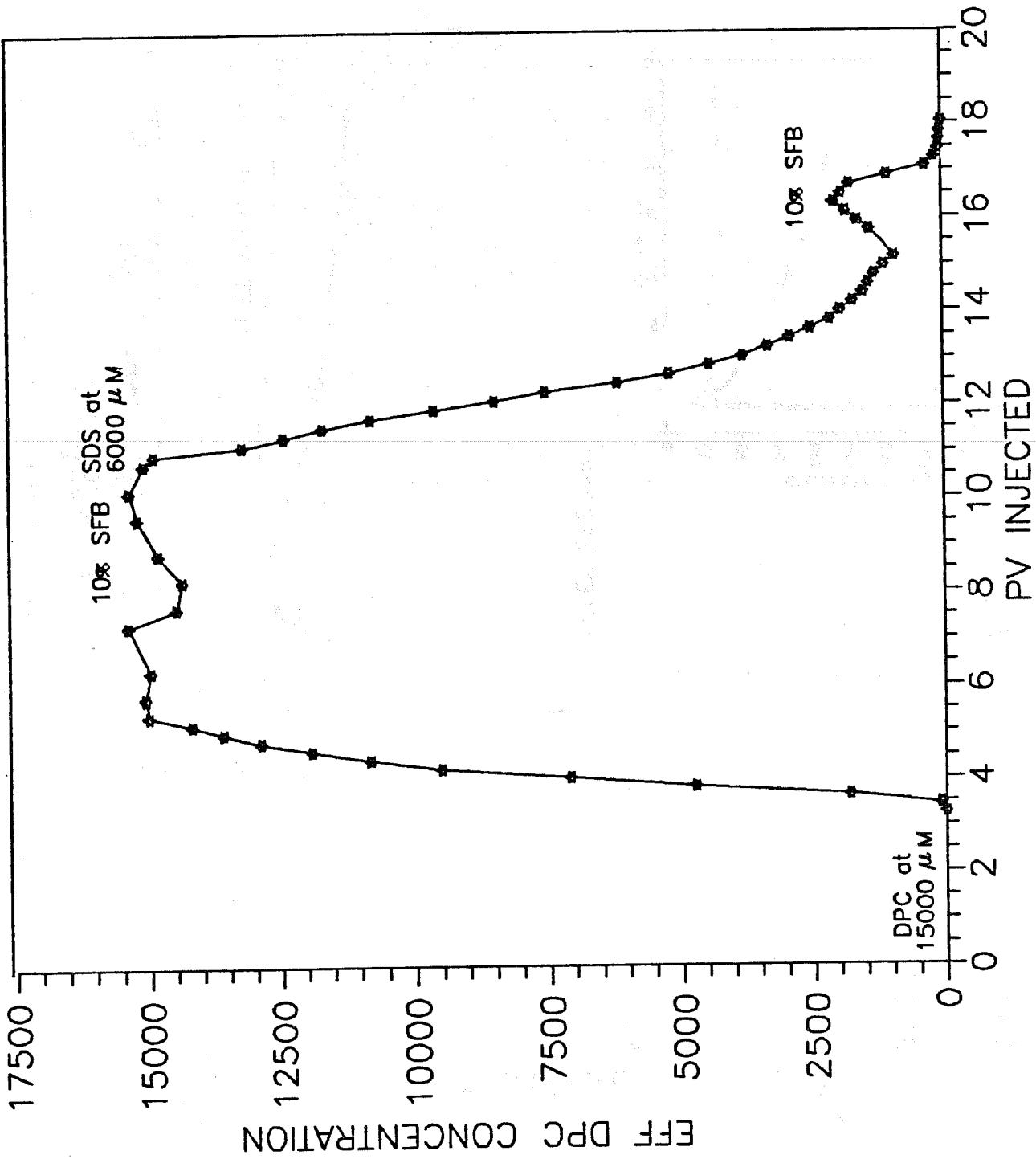


FIGURE 2.6— CONCENTRATION HISTORY CURVE, EXPERIMENT # 3

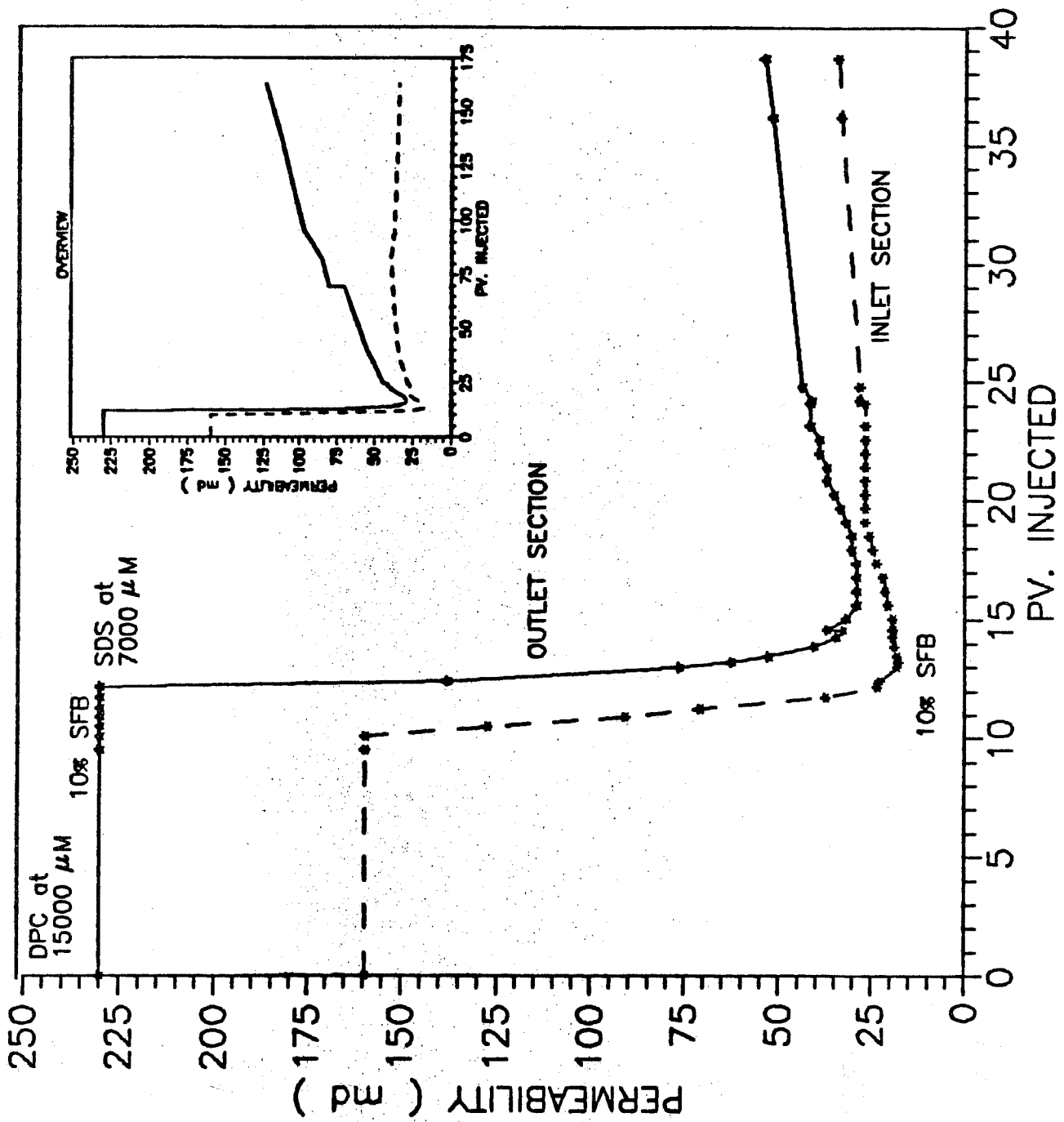


FIGURE 2.7- PERMEABILITY vs. PORE VOLUME INJECTED, EXPERIMENT # 4

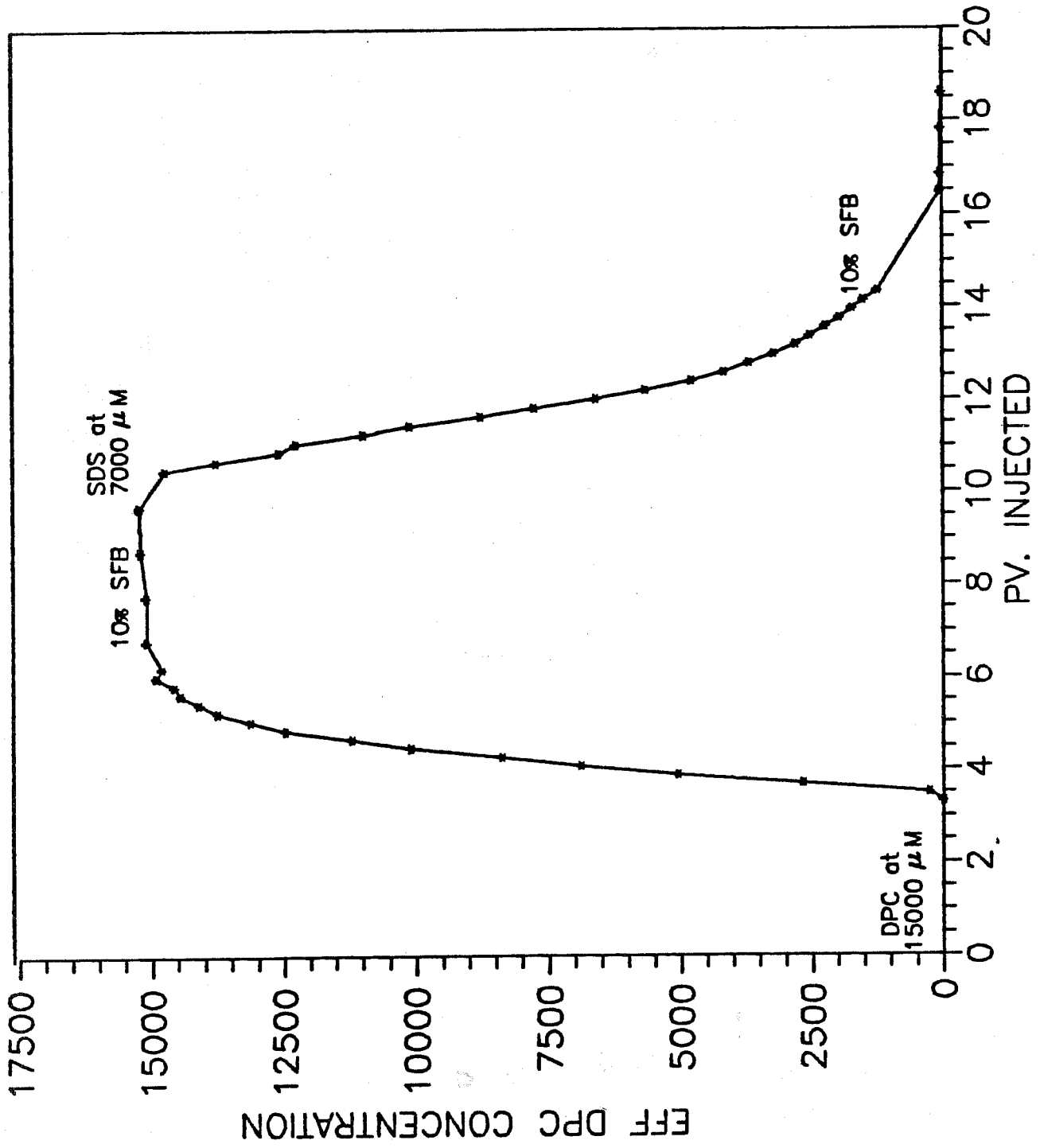


FIGURE 2.8-- CONCENTRATION HISTORY CURVE, EXPERIMENT # 4

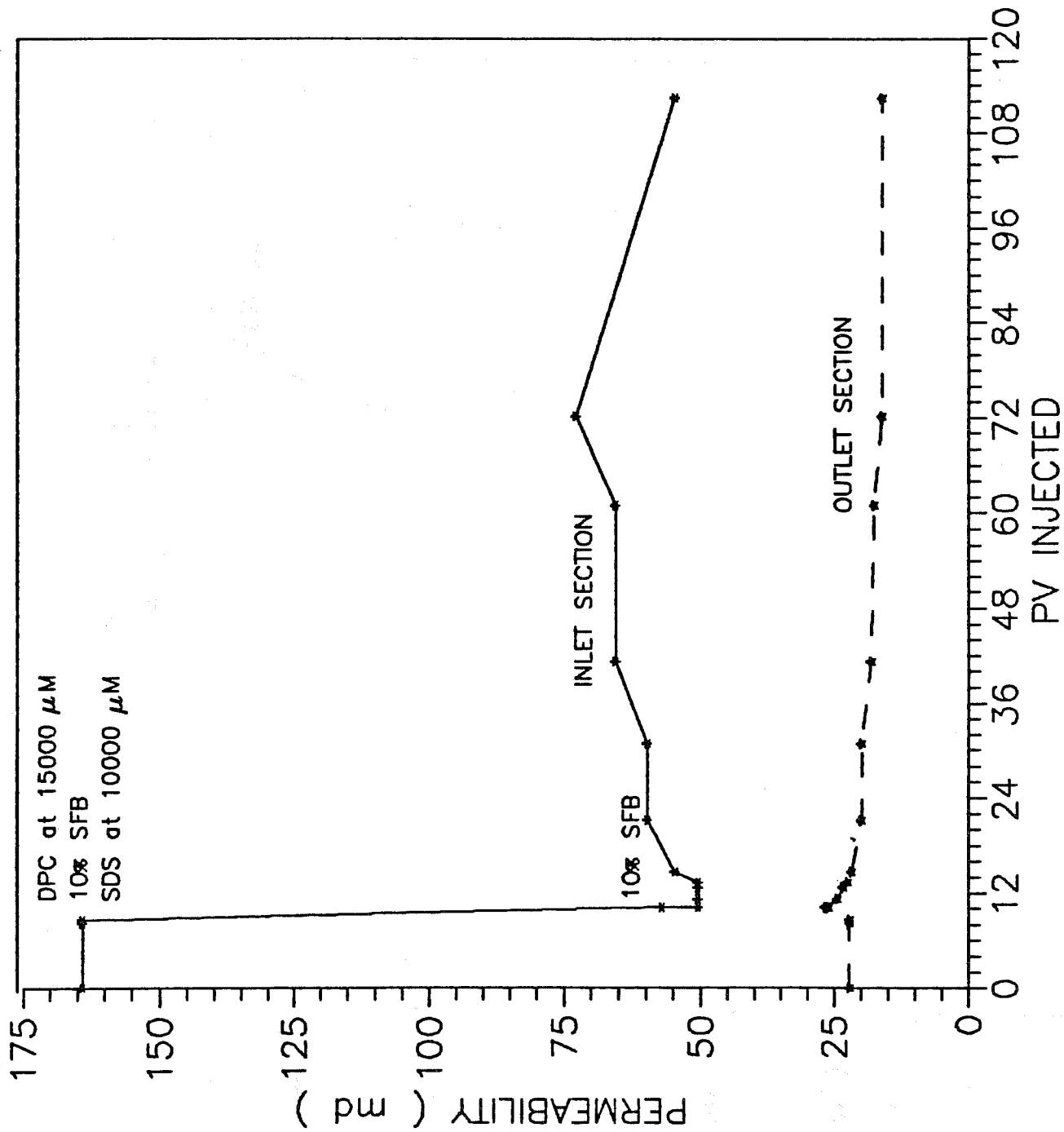


FIGURE 2.9- PERMEABILITY vs. PV INJECTED, EXPERIMENT # 5

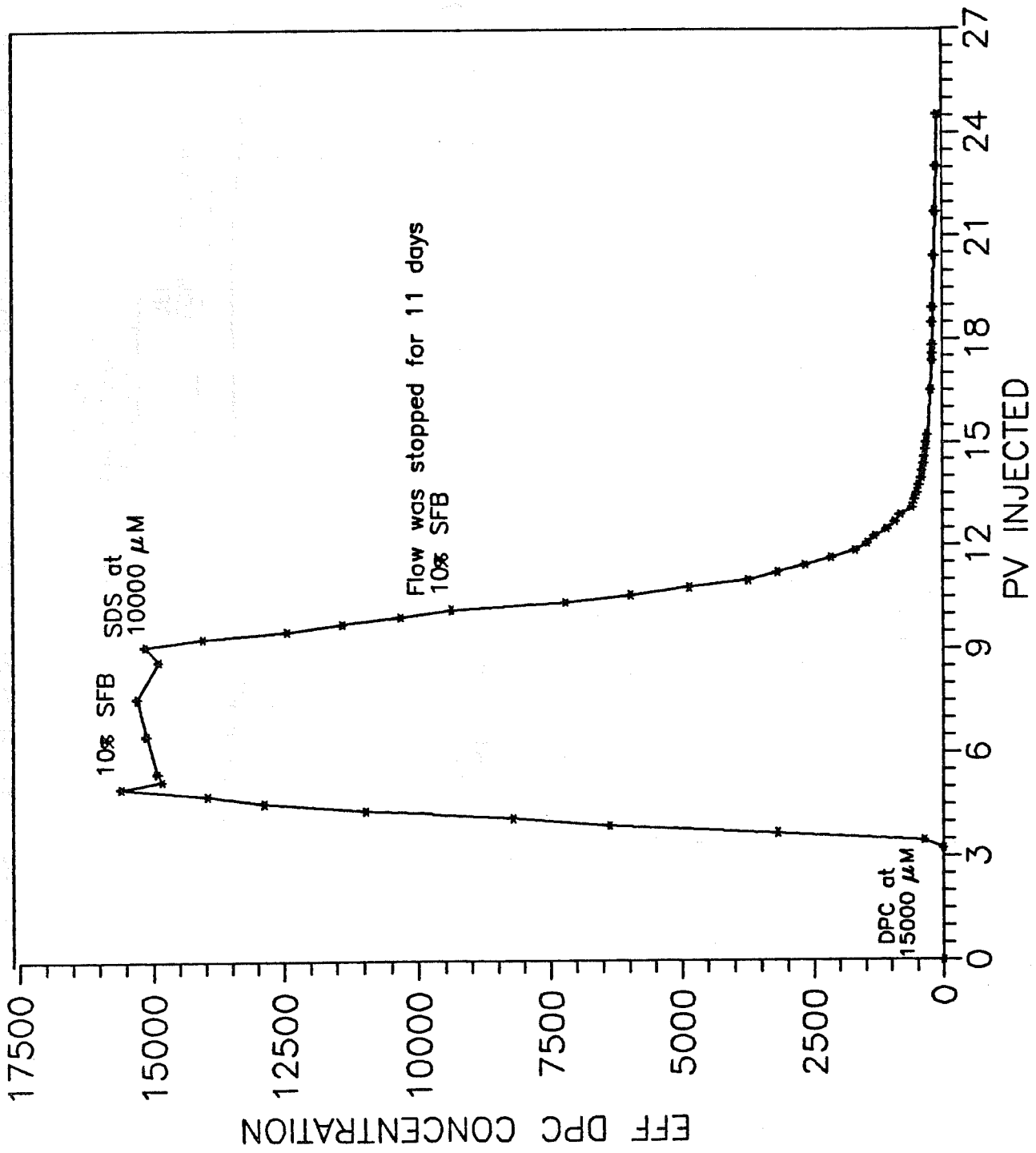


FIGURE 2.10— CONCENTRATION HISTORY CURVE, EXPERIMENT # 5

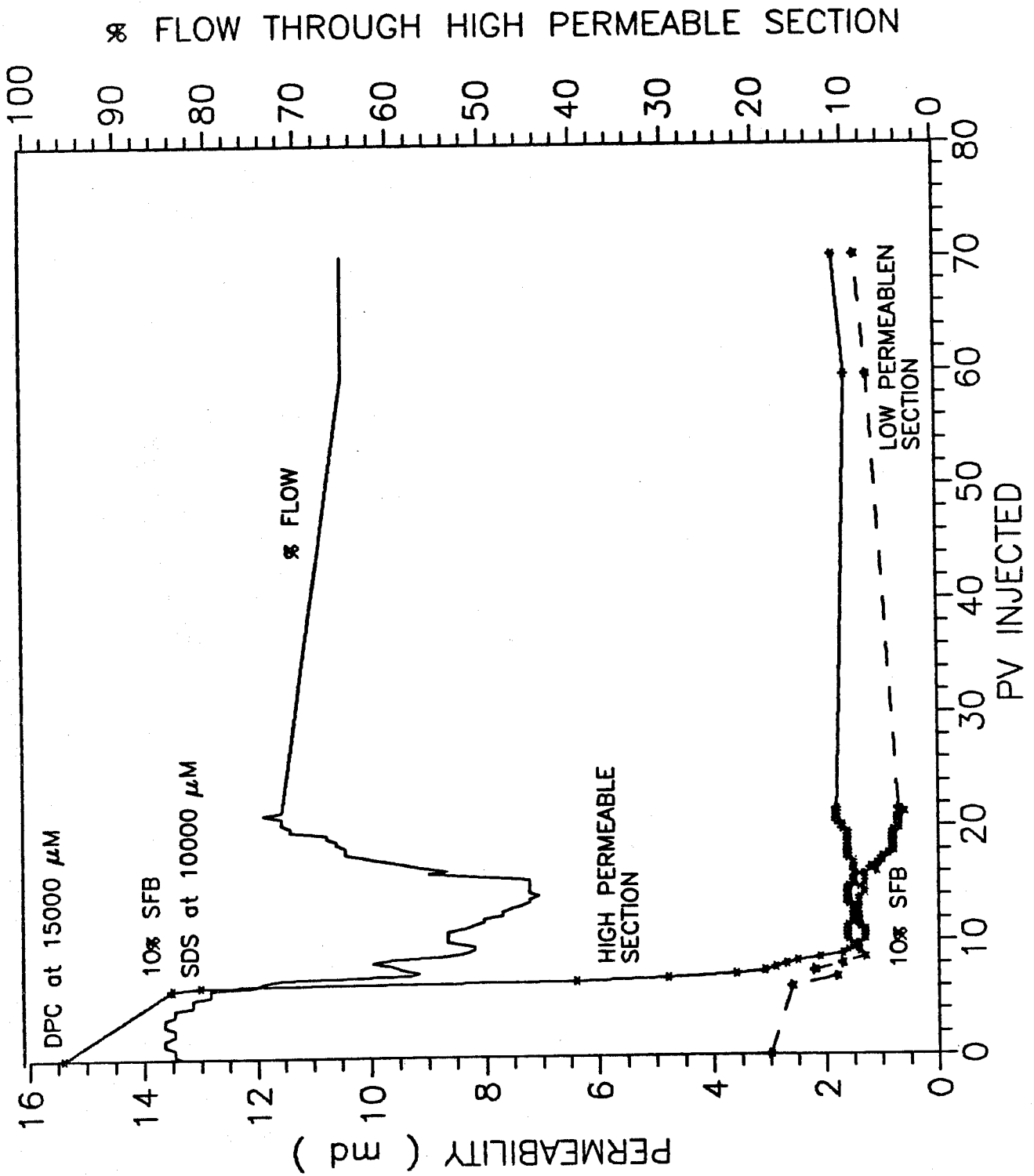


FIGURE 2.11 - PERMEABILITY & %FLOW vs. PV INJECTED, EXPERIMENT # 6

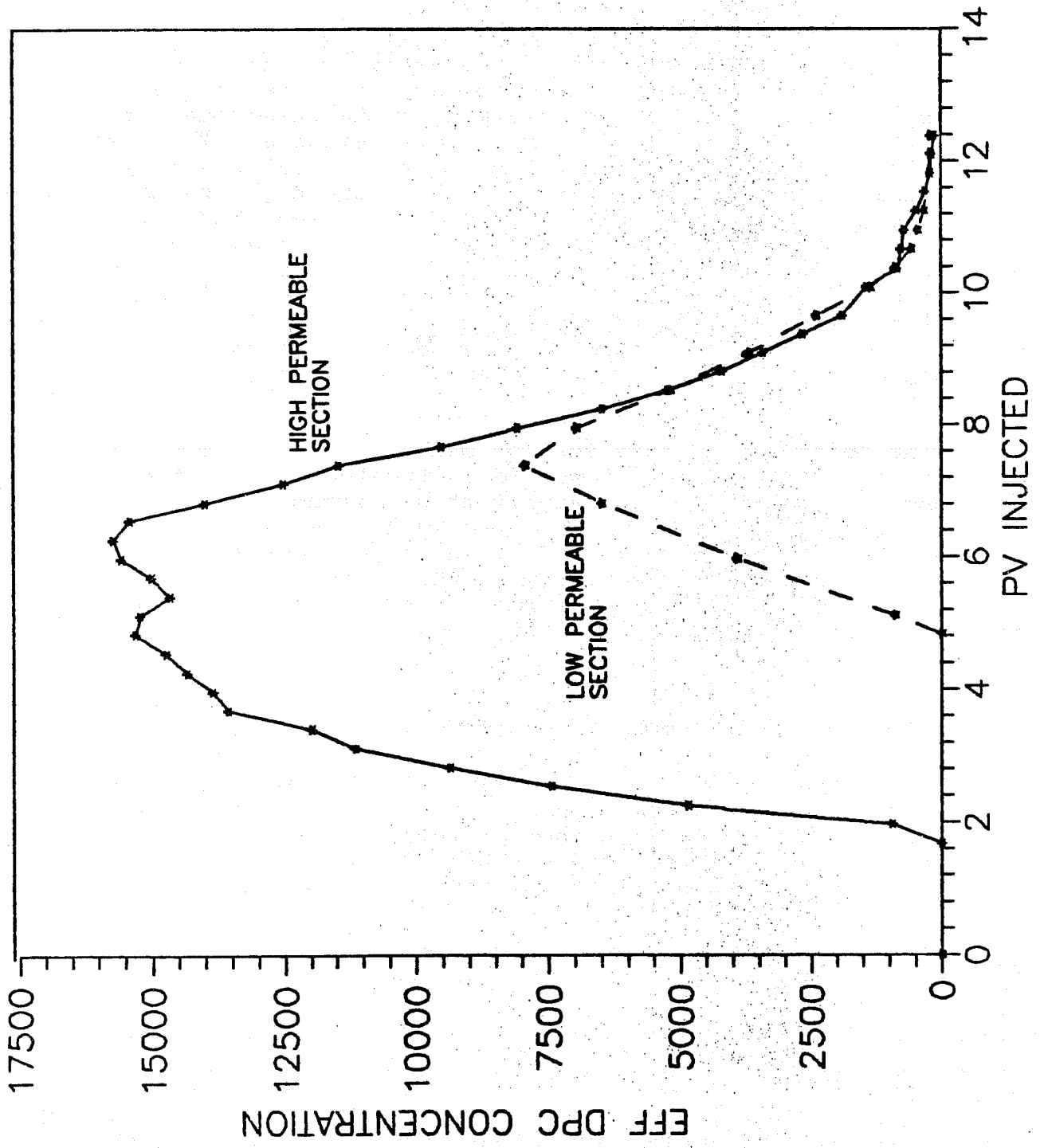


FIGURE 2.12- CONCENTRATION HISTORY CURVE, EXPERIMENT # 6

## CHAPTER 3

### SIMULATION OF POTENTIAL INCREASES IN OIL RECOVERY BY SURFACTANT ENHANCED SELECTIVE BLOCKING

#### INTRODUCTION

In earlier reports (third quarterly report, 1987), the development of a mathematical model for the process was described. The model was used to simulate the development of low permeability plugs, in model reservoir systems. The results showed that, under most circumstances, it was possible to grow a low permeability plug selectively within the high permeability zone. Some important modifications have been made to the simulation, making it possible to monitor more accurately the distribution of oil saturation "characteristics" within the reservoir, and interpolate the values of grid block oil saturation. This modification is particularly important when strong reductions of reservoir permeability lead to drastic rearrangements in the reservoir flow patterns and induce strong crossflows.

The objective of this section has thus been to monitor the oil production in model systems, for untreated and treated cases. This makes it possible to identify those circumstances in which the net oil production without treatment is very poor, the potential increases in oil production if treatment can be made selectively, and the optimum way in which this treatment should be administered. Finally, these guidelines are used as a means of optimising a full process simulation in which the net potential increase in oil production can be assessed.

#### RESULTS AND DISCUSSIONS

Model systems were chosen with the parameters given in table 3.1. Figure 3.1 presents results for the total produced volume of oil from different short heterogeneous reservoirs as a function of the injected volume of water. The arrows on the figure represent the points at which the water to oil ratio (WOR) in the production wells exceeds 50; this is chosen arbitrarily as the point at which it is no longer economically feasible to continue waterflooding the reservoir. For the homogeneous reservoir, oil recovery is pistonlike up to 64 % recovery of oil in place (O.I.P.) after which breakthrough occurs and the sweep efficiency rapidly declines, oil recovery reaching an ultimate value of 72%. A reservoir with a 10 fold difference in permeability between the middle streak and outside layers shows almost the same performance. However, when the difference is 100 fold, sweep efficiency is much poorer, with an early breakthrough and a final recovery of only 45%. For a 1000 fold difference in permeability, this has dropped to 23%.

Figure 3.2 presents the effect of ideal selective blocking on the sweep efficiency in a short (100 feet) reservoir in which the low-permeability zone is 10 md and the high permeability zone is 1000 md. Low-permeability plugs are introduced artificially inside the high permeability zone when the WOR exceeds 50. The various curves then represent the effect of a 100 fold reduction in permeability ("plugging") at various locations within the high permeability zone at water out. Relatively short plugs were chosen to minimize the reduction in fluid injectivity. A plug close to the injection well hardly improves the sweep efficiency at all, while reducing the injectivity of displacement fluid, and is thus detrimental to the oil recovery process. However, a plug placed between one half and three quarters of the length along the high permeability zone causes an immediate and dramatic improvement in sweep efficiency, yielding a final oil recovery of 74% (24% increase) by injecting an extra one pore volume of fluid only. Other cases yield oil recoveries intermediate between these two extremes.

Figure 3.3 presents exactly the same results for a long, 5000 foot reservoir; a plug near the injection well produces no observable improvement in sweep efficiency, while one between one half and three-quarters along the high permeability zone produces a significant improvement in sweep efficiency. The final recovery is 74% (20 % increase) but this requires an additional 5 pore volumes of injected water. In general, the improvement in sweep efficiency for the same fractional length and position of plug is rather lower in the long reservoir than in the short reservoir. Clearly, a solution is to use longer plugs but this must be assessed against the further reduction in overall injectivity. Furthermore, previous results indicated that the selectivity of plug formation for high permeability zones was worse in long reservoirs.

Finally, a full process simulation was performed based on the previous findings (Figure 3.4). First, the process was applied to a 10 and 1000 md reservoir in which plug formation was controlled to start in the middle of the reservoir and the size of the slugs chosen so that plug formation ceased three quarters of the way along the reservoir. Plug formation began when the WOR exceeded 50. The local permeability reduction was chosen as 100. In this case, the improvement in sweep efficiency is almost as good as in the ideal case resulting in a 24% increase in oil recovery for one pore volume of subsequent injection. Reduction in injectivity is also similar to the ideal case. Thus, the plug formation proceeds rapidly enough to give an almost instantaneous and dramatic diversion of injected fluid into the regions of low permeability and high residual oil content. Secondly, the process was applied to the same reservoir in which the plug was allowed to grow along the entire second half of the reservoir with a permeability reduction of only 10. Again, an improvement in sweep efficiency (though less dramatic) leads to a 20% increase in oil recovery. The advantage of using a longer and weaker plug is that

it causes a smaller reduction in overall injectivity.

## CONCLUSIONS

1. Short reservoirs in which the high permeability streaks have a permeability at least one or two orders of magnitude higher than the low permeability regions are strong candidates for this process.
2. From all stand points, short reservoirs are expected to perform better than long reservoirs.
3. The optimum position of plug formation would appear to be between one half and three quarters of the distance along the high permeability streak; longer plugs of lower permeability reduction may yield the same results. The use of longer plugs of high permeability reduction should be avoided since it will not lead to any great increase in sweep efficiency, while leading to further unnecessary decreases in injectivity.
4. The process method of plug formation is able to emulate the ideal improvement in sweep efficiency quite closely; the final injectivities are also close to those in the ideal cases. The occurrence of auxiliary plugging near the injection well has no serious detrimental effect.

Finally, the economic effect of an overall reduction in injectivity (i.e. increased pumping costs or lower injection rates), which is inevitable since the average permeability of the reservoir is lowered considerably, has not been considered here but is a factor to be considered in addition to the economic improvement in oil recovery as a result of a greatly improved displacement efficiency.

TABLE 3.1  
 Characteristics of simulated reservoir

Rock density	=	2.65 g/cm <sup>3</sup>
Porosity	=	0.2
Oil viscosity	=	5.0 cp
Water viscosity	=	1.0 cp
Injection pressure gradient (maintained constant)	=	1.5 psi/ft
Fluid densities	=	1.0 g/cm <sup>3</sup>
Depth of injection face	=	50 ft
Width of central high permeability streak	=	10 ft
Length of reservoir	=	100 ft or 5000 ft
Trapped oil saturation	=	0.2
Initial water saturation	=	0.1
Henry's law constant: DPC (liter/gm)	=	8.3*10 <sup>-5</sup>
or : SDS	=	2.71*10 <sup>-4</sup>
CMC values : DPC	=	800
(micromoles/liter) : SDS	=	4000

Both surfactants injected at 10 CMC.

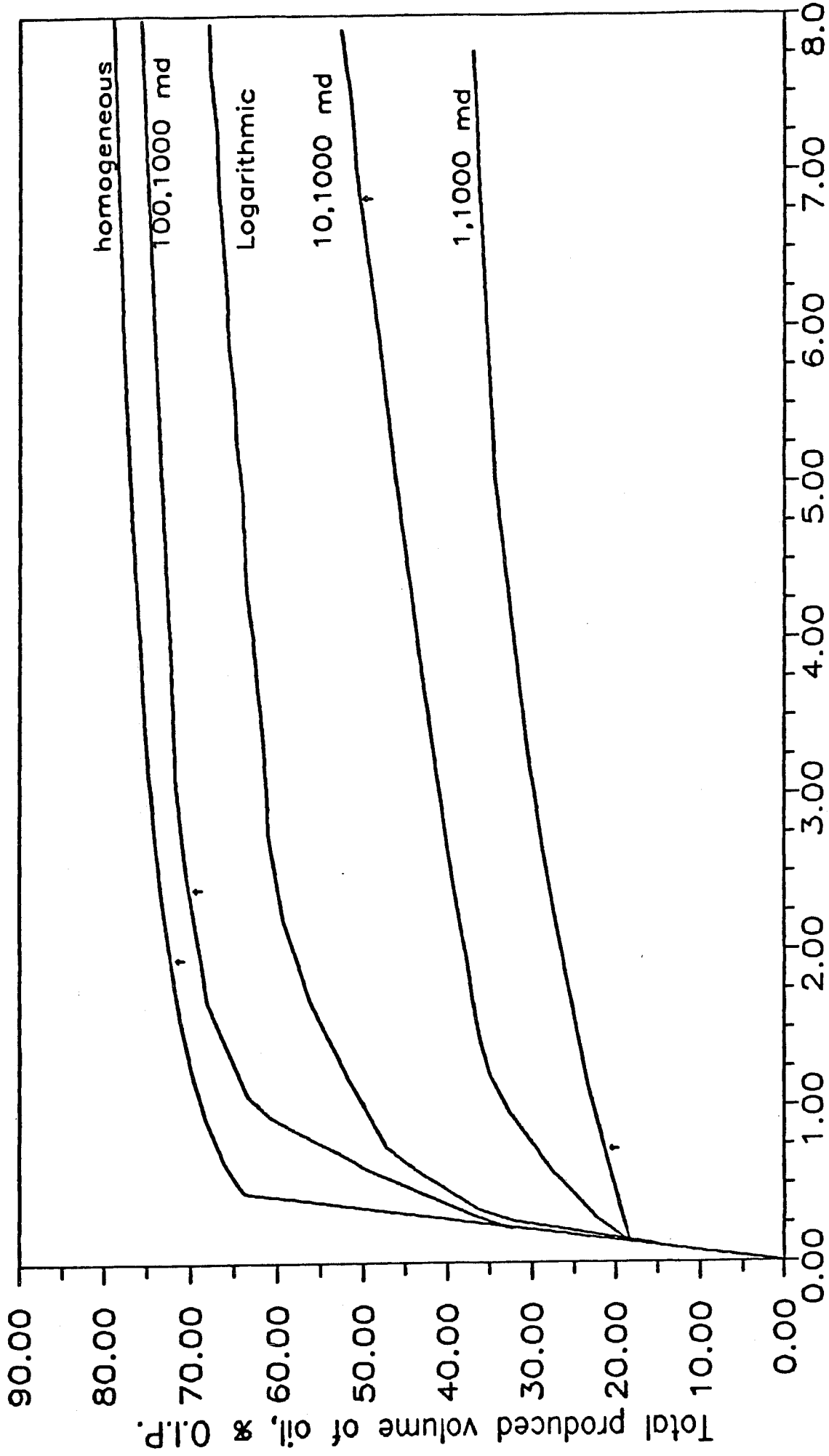


Figure 3.11 Production of Oil Versus Injected Volume of Water for Different Degrees of Heterogeneity (Short, Transversely Permeable reservoirs.)

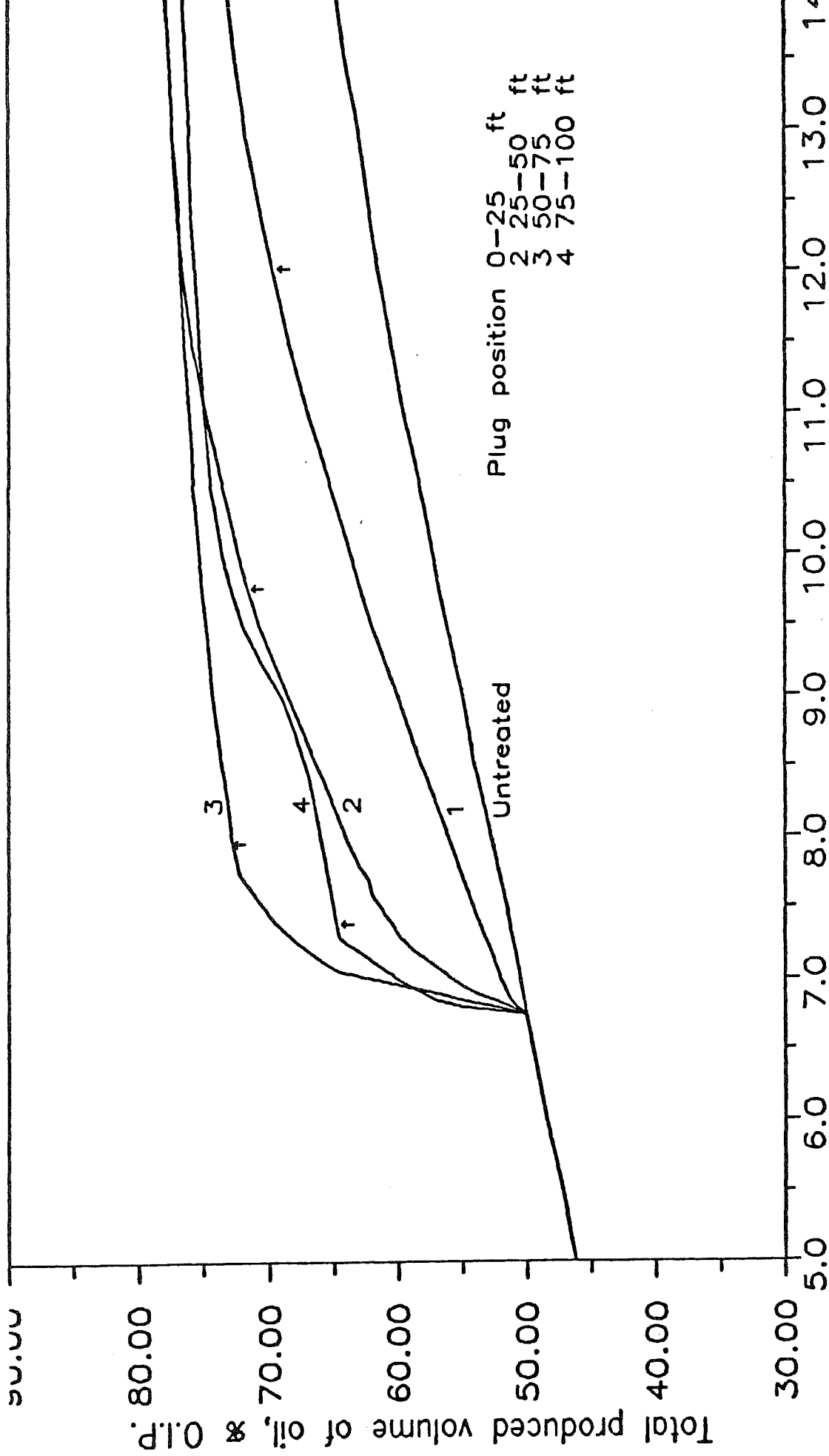


Figure 3.2: Production of Oil Versus Injected Volume of Water in Short Reservoir (Without or With Selective Blocking.)

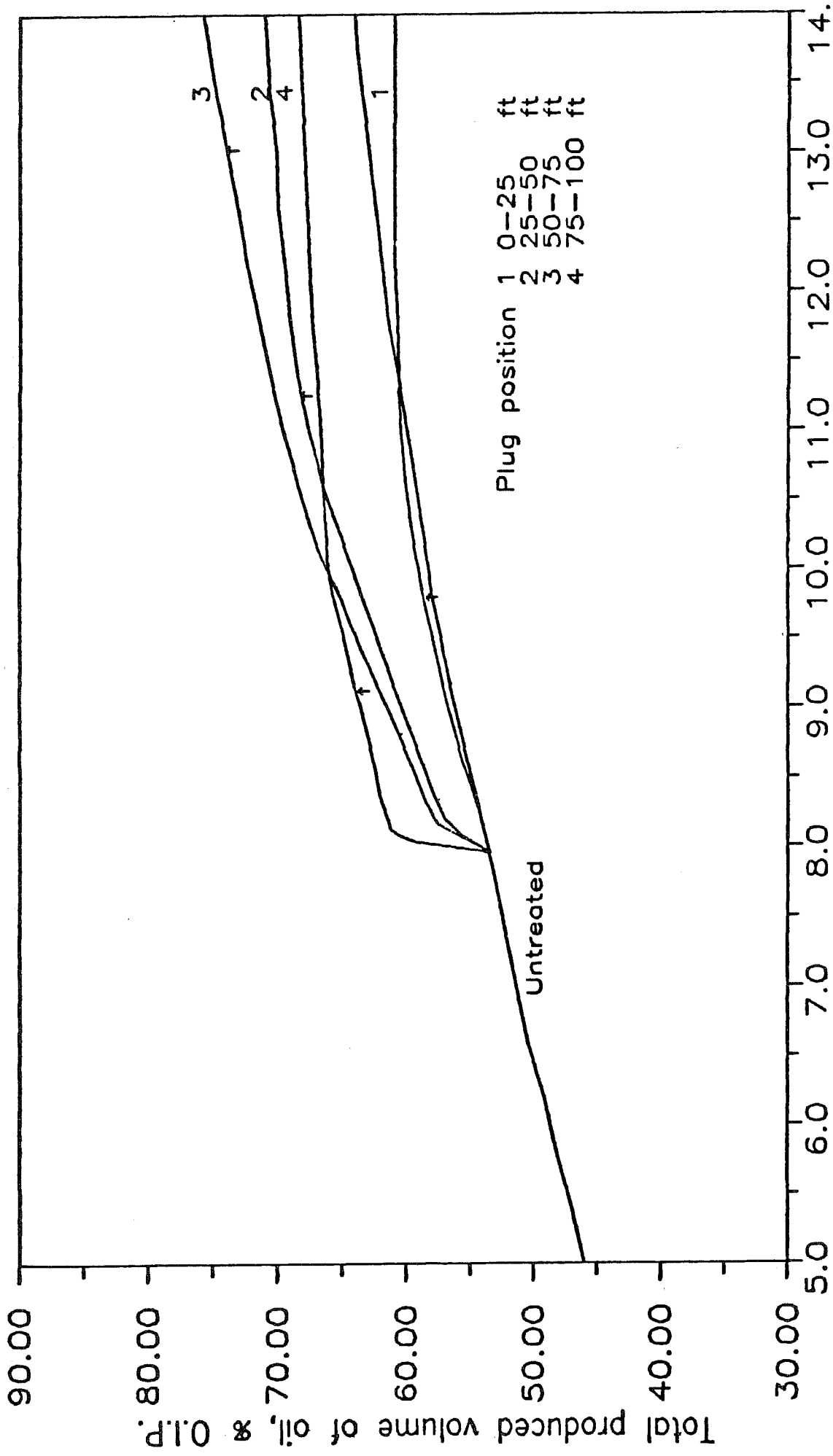


Figure 3.3: Production of Oil Versus Injected Volume of Water in Long Reservoir (Without or With Selective Blocking.)

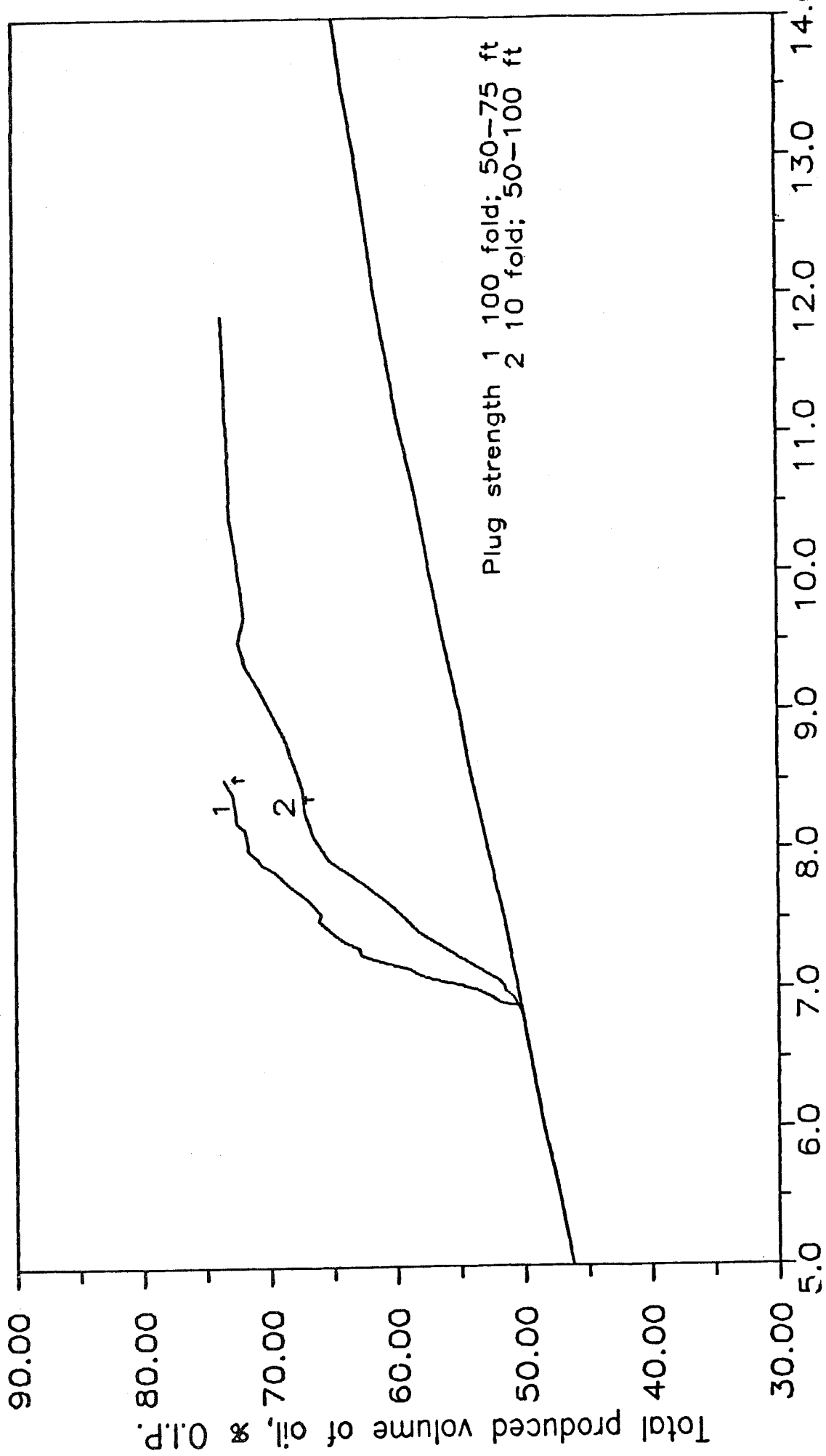


Figure 3.4: Production of Oil Versus Injected Volume of Water in Short Reservoir (Without or With Selective Blocking.)

## CHAPTER 4

### HARDNESS TOLERANCE IN ANIONIC SURFACTANT SOLUTIONS: I. ANIONIC SURFACTANT WITH ADDED MONOVALENT ELECTROLYTE

#### ABSTRACT

Precipitation of sodium dodecylsulfate by calcium has been reported over a wide range of concentrations with and without added sodium chloride. Below the CMC, when no micelles are present, surfactant precipitation can be described by an activity-based solubility product written between the surfactant and the calcium. Above the CMC, where micelles exist, the solubility product must be written between the unbound (unassociated) divalent counterion and the monomeric (unassociated) anionic surfactant activities. A model has been developed that can predict the precipitation boundary using the solubility product combined with material balances for each species and information about binding of counterions on the charged micelles. Hardness tolerance (minimum calcium concentration required to cause precipitation) of this system has been shown to increase by as much as a factor of 25 by addition of 0.1 M NaCl, indicating the value of monovalent electrolyte in enhancing hardness tolerance of anionic surfactant solutions.

#### INTRODUCTION

Hardness tolerance of an anionic surfactant is defined as the minimum concentration of multivalent cation necessary to cause precipitation of the surfactant. Precipitation is an important phenomenon because it is well known to potentially limit the usefulness of anionic surfactants in detergency applications in hard water (water containing a high concentration of calcium and/or magnesium). It can also restrict the ability to apply surfactants in surfactant enhanced waterflooding, or in micellar enhanced oil recovery, in reservoirs with high hardness levels. However, the hardness tolerance of the anionic slug to reservoir-borne multivalent cations can be increased by the correct use of monovalent electrolyte to formulate the surfactant solution.

Conversely, the use of multivalent cations to precipitate anionic surfactant can be useful in surfactant enhanced waterflooding, where the multivalent cations are injected as a slug behind a leading anionic surfactant slug. The trailing edge of the surfactant slug is overtaken by the slug of cations deep inside the high permeability zone. Another use of multivalent cations to precipitate anionic surfactant as illustrated by a proposed process for the recovery of surfactant from surfactant-based separation processes<sup>1</sup>.

In this study, the precipitation phase boundary (boundary between the region where precipitate forms and where solutions remain isotropic) is reported for mixtures of sodium dodecylsulfate (SDS) and calcium chloride ( $\text{CaCl}_2$ ) over a wide range of concentrations. A model is developed which can be used to predict the precipitation phase boundary for this system when  $\text{NaCl}$  is also added. In the next chapter, the model is expanded to include the addition of nonionic surfactant to the system to enhance hardness tolerance and tested against experimental precipitation phase boundaries for that system. In previous related work, we have studied salinity tolerance of anionic surfactant solutions in the presence of nonionic surfactant<sup>2</sup> and precipitation of anionic/cationic surfactant mixtures<sup>3</sup>.

### EXPERIMENTAL MATERIALS

Sodium dodecylsulfate (NaDS) obtained from Fisher Scientific had a purity greater than 95%. This was recrystallized twice from a 50/50 mixture of water and ethanol, then dried under vacuum with low heat.

The  $\text{NaCl}$ ,  $\text{CaCl}_2$ , and  $\text{MgCl}_2$  were Fisher reagent grade and were used as received. The water was distilled and deionized.

### METHODS

Precipitation Boundaries. A series of solutions, each with the same concentration of NaDS and  $\text{NaCl}$  (when present), but with varying  $\text{CaCl}_2$  concentrations, were prepared in 100 ml volumetric flasks. All experiments in this study were performed at  $30^\circ \pm 0.05^\circ\text{C}$ , since precise temperature control is essential to obtain accurate precipitation phase boundaries. Surfactant solutions can remain supersaturated for long periods of time before precipitation is complete<sup>4,5</sup>; therefore, all solutions were cooled to near freezing temperatures to force precipitation to occur. The solutions were then placed in the  $30^\circ\text{C}$  water bath, shaken periodically, and allowed to equilibrate for at least 4 days.

Whether or not crystals were present after equilibration determined if the initial solution composition was inside the precipitation phase boundary. Using simple visual detection, the concentration of  $\text{CaCl}_2$  that determined a point on the precipitation boundary was accurate to within  $\pm 10\%$  at all NaDS concentrations. Other workers<sup>6,7</sup> have used laser scattering to obtain more accurate phase boundaries in similar systems. However, the observed precipitation phase boundaries were not significantly different when laser techniques were used for detection in this work. We have found that the laser technique can give improved detection results in precipitating anionic/cationic surfactant systems<sup>3</sup>.

CMC Determination. Surface tension measurements were used to determine the critical micelle concentration (CMC) for each system of interest by a break in the surface tension versus logarithm of surfactant concentration curve. A DuNuoy ring tensiometer (Central Scientific) with a platinum-iridium ring was used and all the necessary precautions were taken to maximize accuracy<sup>8</sup>. Solution temperatures were held constant at 30° C and measurements were taken every 15 minutes until 3 successive readings were the same. If readings did not stabilize in 3.5 hours, the final surface tension measurement was arbitrarily used.

## THEORY

Figure 4.1 is a schematic diagram which represents precipitation in these mixtures when micelles are present. The anionic surfactant is present in 3 environments: 1) as monomer (unassociated molecules), 2) incorporated in mixed micelles, and 3) as precipitate. Monovalent counterions (not shown in Figure 4.1 for clarity) and divalent counterions, both exist 1) as unbound (unassociated) species and 2) bound onto the micelle surface. In addition, the divalent counterion is present in any precipitate that forms.

To develop a model for surfactant precipitation in mixed electrolyte systems, it is necessary to determine how the surfactant monomer concentration varies as a function of the concentration of all unbound counterions (those not bound to micelles) at total surfactant concentrations above the CMC. This is a difficult problem and very little work in the literature addresses it. Fortunately, in hardness tolerance studies where only anionic surfactant is present, the concentration of unbound  $\text{Ca}^{+2}$  is usually negligible compared to the unbound  $\text{Na}^{+}$  concentration, so that a simple relationship can be used to relate the surfactant monomer concentration to the unbound  $\text{Na}^{+}$  concentration.

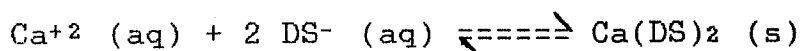
In this paper, two different approaches will be discussed to model precipitation phase boundaries. A simplified model is developed that ignores the effect of  $\text{Ca}^{+2}$  on the surfactant monomer concentration. This model is then extended to a generalized model where the effect of unbound  $\text{Ca}^{+2}$  is included. Although the simplified approach is adequate for the anionic surfactant-only data presented in this paper, the generalized model must be used in the anionic-nonionic surfactant mixtures presented in Part II of this series.

## SIMPLIFIED MODEL

In hardness tolerance studies, there are two different counterions which must be included in the model. In this case, sodium ions originate from the NaDS and added NaCl,

while calcium ions originate from added  $\text{CaCl}_2$ . Theoretically, either  $\text{Ca}^{+2}$  or  $\text{Na}^+$  could cause anionic surfactant to precipitate in these solutions. Practically, however, very high  $\text{NaCl}$  concentrations<sup>2</sup> (ca. 0.9 M) are required to precipitate surfactant as  $\text{NaDS}$  (compared to a maximum  $\text{Na}^+$  concentration of 0.2 M in this work), so it can be assumed that  $\text{Ca}^{+2}$  is the only counterion involved in the precipitation reaction.

The precipitation reaction can be represented by:



which can be described by a simple solubility product relationship between the free or unassociated species involved. Therefore:

$$K_{sp} = [\text{Ca}^{+2}]_{un} ([\text{DS}^-]_{mon})^2 f_{ca} (f_{ds})^2 \quad (4.1)$$

where  $K_{sp}$  is the activity-based solubility product,  $[\text{Ca}^{+2}]_{un}$  is the concentration of unbound calcium,  $[\text{DS}^-]_{mon}$  is the monomer concentration of anionic surfactant, and  $f_{ca}$  and  $f_{ds}$  represent the activity coefficients of unbound  $\text{Ca}^{+2}$  and monomeric  $\text{DS}^-$  in solution, respectively.

Activity coefficients for each species are given by an extended Debye-Huckel expression<sup>9</sup>:

$$\log(f_{ca}) = -0.5139(2)^2(I)^{0.5}/(1 + 1.9782(I)^{0.5}) \quad (4.2)$$

$$\log(f_{ds}) = -0.5139(-1)^2(I)^{0.5}/(1 + 2.3079(I)^{0.5}) \quad (4.3)$$

where  $I$  is the ionic strength. The ion size parameter in the denominator of equations 2 and 3 is reported or estimated using data or techniques from reference 9. The ionic strength is calculated from:

$$I = \sum 0.5 c_i (z_i)^2 = [\text{NaCl}] + [\text{SDS}] + 3[\text{CaCl}_2] \quad (4.4)$$

where  $c_i$  is the total concentration of ion  $i$  in solution,  $z_i$  is the charge of species  $i$ , and  $[\text{NaCl}]$ ,  $[\text{SDS}]$ , and  $[\text{CaCl}_2]$  are the total concentrations of each species represented. Calculating activity coefficients in micellar solutions can be a difficult problem. Burchfield and Woolley<sup>10</sup> have calculated mean stoichiometric activity coefficients by treating the micelles as a separate species contributing only a fraction of their total charge to ionic strength. The work of other researchers has suggested that activity coefficients of ions in solutions can be calculated by assuming the surfactant is a simple strong electrolyte in solution (discussed in Reference 10). In this study, the contribution of surfactant to ionic strength will be considered to be the same as a simple electrolyte, as shown in eq 4. The model is not very sensitive to the value of the resulting activity coefficients, so inaccuracies introduced by these assumptions

do not have a significant effect on the final model predictions.

The purpose of the theory is to predict the precipitation phase boundary; i.e., the minimum  $\text{CaCl}_2$  concentration required to cause precipitation at any given surfactant concentration. Along the precipitation phase boundary, therefore, only an infinitesimal amount of precipitate is present and it can be neglected in material balance equations, even though eq 1 is still satisfied. A material balance on the anionic surfactant yields:

$$[\text{SDS}] = [\text{DS}^-]_{\text{mon}} + [\text{DS}^-]_{\text{mic}} \quad (4.5)$$

where  $[\text{DS}^-]_{\text{mic}}$  represents the concentration of  $\text{DS}^-$  present in micelles. Similarly, the total concentration of sodium ions in solution,  $[\text{Na}^+]_{\text{tot}}$  is given by:

$$[\text{Na}^+]_{\text{tot}} = [\text{NaCl}] + [\text{SDS}] = [\text{Na}^+]_{\text{un}} + [\text{Na}^+]_{\text{b}} \quad (4.6)$$

where  $[\text{Na}^+]_{\text{un}}$  is the concentration of unbound  $\text{Na}^+$ , and  $[\text{Na}^+]_{\text{b}}$  is the concentration of  $\text{Na}^+$  bound on the charged micelles. Eq 6 shows that sodium is contributed by both added  $\text{NaCl}$  (when present) and surfactant, and that all  $\text{Na}^+$  in solution must either be unassociated or bound onto the micelles. The amount of sodium bound is related to the fractional counterion binding on a pure anionic micelle,  $\beta_{\text{Na}^0}$ , by:

$$\beta_{\text{Na}^0} = [\text{Na}^+]_{\text{b}} / [\text{DS}^-]_{\text{mic}} \quad (4.7)$$

The material balance for  $\text{Ca}^{+2}$  on the precipitation phase boundary yields:

$$[\text{CaCl}_2] = [\text{Ca}^{+2}]_{\text{un}} + [\text{Ca}^{+2}]_{\text{b}} \quad (4.8)$$

where  $[\text{Ca}^{+2}]_{\text{b}}$  represents the concentration of calcium ions that are bound onto the micelles. Here however, the counterion binding of calcium,  $\beta_{\text{Ca}^0}$ , is defined by:

$$\beta_{\text{Ca}^0} = 2[\text{Ca}^{+2}]_{\text{b}} / [\text{DS}^-]_{\text{mic}} \quad (4.9)$$

because the total number of charges of the micelle that are neutralized by calcium is twice the concentration of  $\text{Ca}^{+2}$  bound on the micelle. Therefore, in this study, fractional counterion binding is defined as the ratio of neutralized charges in a micelle (from bound  $\text{Na}^+$  or  $\text{Ca}^{+2}$ ) to the total number of anionic surfactant molecules in the micelle.

In this work, the monomer concentration, when micelles are present, will be assumed to be equal to the CMC of the surfactant. This CMC used is that measured when the total concentration of counterions is equal to the corresponding concentration of unbound counterions in the solution of interest above the CMC. These unbound counterion

concentrations are the same as the total counterion concentrations in CMC measurements because a negligible amount of surfactant is in micellar form at the CMC (hence, negligible micellar binding of counterion). Therefore, we can discuss the monomer concentration of surfactant ( $[DS^-]_{mon}$ ) in terms of the CMC of the surfactant under appropriate conditions.

If the concentration of unbound  $Ca^{+2}$  is small enough so as not to affect CMC, the surfactant monomer concentration can be described by the following equation<sup>11</sup>:

$$\ln([DS^-]_{mon}) = K_1 - K_g \ln([Na^+]_{un}) \quad (4.10)$$

where  $K_1$  and  $K_g$  are constants.

When a precipitation phase boundary is determined experimentally, total surfactant concentration and salt concentration are independent variables. When  $[SDS]$  and  $[NaCl]$  are set, the dependent variable of interest is the minimum concentration of calcium required to cause surfactant precipitation,  $[CaCl_2]$ . If  $K_{sp}$ ,  $\beta_{Na^0}$ ,  $\beta_{Ca^0}$ ,  $K_1$ , and  $K_g$  are known, eqs 1 - 10 can be solved simultaneously to obtain  $[CaCl_2]$ ,  $[Ca^{+2}]_{un}$ ,  $[Ca^{+2}]_b$ ,  $[Na^+]_{un}$ ,  $[Na^+]_b$ ,  $[DS^-]_{mon}$ ,  $[DS^-]_{mic}$ ,  $I$ ,  $f_{ca}$ , and  $f_{ds}$ . Therefore, it should be possible to predict hardness tolerance for any anionic surfactant concentration at any salinity.

### GENERALIZED MODEL

In general it is not always possible to neglect the effect of  $Ca^{+2}$  on  $[DS^-]_{mon}$  (which is the case for anionic-nonionic mixtures presented in Part II of this series). In this case, equations 1-9 remain the same; however a new relationship must now replace equation 10. Although a considerable amount of data has been published concerning the effect of a single counterion species on the CMC of ionic surfactants, far less has been published on mixtures of monovalent and divalent counterions. Shinoda<sup>12,13</sup> derived theoretical equations that can be used to describe mixed electrolyte systems and applied these to data presented by Lange<sup>14</sup>. Moroi et. al.<sup>15,16</sup> have modified the Shinoda equations to produce a successful model for mixtures of NaDS and divalent metal dodecyl sulfates without other added electrolyte. The derivation presented here is a generalization of the approach taken by Moroi et. al. and it allows calculation of the CMC for any concentration of added  $Na^+$  and  $Ca^{+2}$ . The equations that follow are written specifically for  $Na^+$  and  $Ca^{+2}$  but they apply for any mixture of monovalent and divalent counterions.

By making the proper assumptions<sup>13</sup>, the Poisson-Boltzmann equation can be applied to micelles to give:

$$2000 \pi E_c S^2 / (DNkT) = \sum c_i \{ \exp(-z_i e \Phi_0 / kT) - 1 \} \quad (4.11)$$

where  $S$  is the surface charge density of the micelle,  $D$  is the dielectric constant of the solution,  $N$  is Avogadro's number,  $k$  is the Boltzmann constant,  $T$  is absolute temperature,  $E_c$  is a conversion constant to give proper units,  $c_i$  and  $z_i$  represent the concentration and charge of each counterion in solution, respectively,  $e$  is the charge of an electron, and  $\Phi_0$  is the electrical potential at the surface of the charged micelle. Since the micelle is composed of negatively charged molecules,  $\Phi_0$  is negative and the exponential term in eq 11 is generally considered much larger than 1 so equation 11 can be written as:

$$K_2 S^2 = \sum c_i \exp(-z_i e \Phi_0 / kT) \quad (4.12)$$

where  $K_2$  is a constant that can be calculated from the parameters in eq 11.

For a system of NaDS with added NaCl, equation 12 can be written as:

$$K_2 (S_{Na})^2 = [Na^+]_{un} P \quad (4.13)$$

where  $S_{Na}$  is the surface charge density when only sodium ions are present, and  $P$  is given by:

$$P = \exp(-e \Phi_0 / kT) \quad (4.14)$$

Similarly, for  $Ca(DS)_2$  with added  $CaCl_2$ , one obtains:

$$K_2 (S_{Ca})^2 = [Ca^{+2}]_{un} P^2 \quad (4.15)$$

where  $S_{Ca}$  is the surface charge density of the micelle when  $Ca^{+2}$  is the only counterion present in solution. For solutions that contain both  $Na^+$  and  $Ca^{+2}$ , equation 12 is written as:

$$K_2 S^2 = [Na^+]_{un} P + [Ca^{+2}]_{un} P^2 \quad (4.16)$$

$S$  is assumed to be a linear combination of  $S_i$  multiplied by the ratio of ion concentrations at the micelle surface in the mixed electrolyte system to the concentrations at the micelle surface with only one type of counterion present:

$$S = [Na^+]_s S_{Na} / [Na^+]_{s^0} + [Ca^{+2}]_s S_{Ca} / [Ca^{+2}]_{s^0} \quad (4.17)$$

where  $[Na^+]_s$  and  $[Ca^{+2}]_s$  represent the concentrations of each species at the micelle surface in the mixed counterion system, and  $[Na^+]_{s^0}$  and  $[Ca^{+2}]_{s^0}$  are the surface concentrations at the CMC for each pure surfactant. The Boltzmann equation<sup>17</sup> can be used to relate surface concentrations to bulk concentrations so that:

$$[Na^+]_s = [Na^+]_{un} P \quad (4.18)$$

$$[Na^+]_s^0 = CMC_{SDS} P_{SDS} \quad (4.19)$$

$$[Ca^{+2}]_s = [Ca^{+2}]_{un} P^2 \quad (4.20)$$

$$[Ca^{+2}]_s^0 = 0.5 CMC_{CDs} (P_{CDs})^2 \quad (4.21)$$

where  $CMC_{SDS}$  and  $CMC_{CDs}$  are the CMCs of pure sodium dodecylsulfate and pure calcium dodecylsulfate, without added electrolyte, and  $P_{SDS}$  and  $P_{CDs}$  are the values of  $P$  at  $CMC_{SDS}$  and  $CMC_{CDs}$ , respectively.

In this work, CMC is defined as the concentration of dodecylsulfate anion where micelles begin to form. Therefore,  $CMC_{CDs}$  is twice the concentration of pure calcium dodecylsulfate ( $[Ca^{+2}]_{un} = 0.5 CMC_{CDs}$ ), whereas at the CMC of pure sodium dodecylsulfate without added electrolyte,  $CMC_{SDS}$  is equal to the sodium concentration ( $[Na^+]_{un} = CMC_{SDS}$ ). Substituting equations 18 -21 into equation 17 gives:

$$S = [Na^+]_{un} P(S_{Na}) / \{ CMC_{SDS} P_{SDS} \} + [Ca^{+2}]_{un} P^2 (S_{Ca}) / \{ 0.5 CMC_{CDs} (P_{CDs})^2 \} \quad (4.22)$$

which allows calculation of  $S$  at any unbound  $Na^+$  and  $Ca^{+2}$  concentration.

Shinoda<sup>13</sup> has developed equations which relate the CMC to electrical potential:

$$\ln(CMC) = \ln(1000/Nv) - mw/kT - 1 - K_g e \Phi_0 / kT \quad (4.23)$$

where  $v$  is the free volume per surfactant molecule in the micelle,  $m$  is the carbon number in the surfactant molecule, and  $w$  is cohesive energy difference per molecule between micellar and singly dispersed state. Using our nomenclature, equation 23 is written:

$$\ln[DS^-]_{mon} = K_3 + K_g \ln(P) \quad (4.24)$$

where  $K_3$  can be calculated from parameters in equation 23 and is constant for a given surfactant.

For a system of  $NaDS + NaCl$ , equation 24 is combined with equation 13 to give:

$$\ln([DS^-]_{mon}) = K_3 + (K_g, Na) \ln\{K_2 (S_{Na})^2\} - (K_g, Na) \ln[Na^+]_{un} = K_1 - (K_g, Na) \ln[Na^+]_{un} \quad (4.25)$$

where  $K_g, Na$  is the value of  $K_g$  when only  $Na^+$  is present. equation 25 is actually eq 10 written in more specific detail. Similarly, for  $Ca(DS)_2 + CaCl_2$ , combining eqs 24 and 15 yields:

$$\ln([DS^-]_{mon}) = K_3 + 0.5(K_g, Ca) \ln\{K_2 (S_{Ca})^2\} - 0.5(K_g, Ca) \ln[Ca^{+2}]_{un} \quad (4.26)$$

where  $K_g, Ca$  is the value of  $K_g$  when only  $Ca^{+2}$  is present. Finally, for  $SDS + NaCl + CaCl_2$ , eq 24 is written as:

$$\ln([DS^-]_{\text{mon}}) = K_3 + K_g \ln(P) \quad (4.27)$$

where  $K_g$  is a linear combination of  $K_{g,i}$  analogous to equation 17. By combining equations 18 - 21,  $K_g$  is given by:

$$K_g = [Na^+]_{\text{un}} P (K_{g,Na}) / \{CMC_{SDS} P_{SDS}\} + [Ca^{+2}]_{\text{un}} P^2 (K_{g,Ca}) / \{0.5 CMC_{CaDS} (P_{CaDS})^2\} \quad (4.28)$$

When eq 24 is written for pure sodium dodecylsulfate and pure calcium dodecylsulfate, respectively:

$$\ln(CMC_{SDS}) = K_3 + (K_{g,Na}) \ln(P_{SDS}) \quad (4.29)$$

$$\ln(CMC_{CaDS}) = K_3 + (K_{g,Ca}) \ln(P_{CaDS}) \quad (4.30)$$

If the constants  $K_2$ ,  $K_3$ ,  $K_{g,Na}$ ,  $K_{g,Ca}$ ,  $S_{Na}$ ,  $S_{Ca}$ ,  $CMC_{SDS}$ ,  $CMC_{CaDS}$ ,  $P_{SDS}$ , and  $P_{CaDS}$  are known, equations 16, 22, 27, and 28 can be solved simultaneously for  $[DS^-]_{\text{mon}}$ ,  $P$ ,  $S$ , and  $K_g$  at any given concentrations of  $[Na^+]_{\text{un}}$  and  $[Ca^{+2}]_{\text{un}}$ . These four equations can be used in the place of eq 10 to predict hardness tolerance as in the simplified model, except that there are now a total of 13 equations, instead of 10 equations, which must be solved simultaneously.

## RESULTS AND DISCUSSION

### DETERMINATION OF PARAMETERS IN SIMPLIFIED MODEL

Before equations 1 - 10 can be solved to predict hardness tolerance, it is necessary to determine  $K_1$ ,  $K_g$ ,  $K_{sp}$ ,  $\beta_{Na^0}$ , and  $\beta_{Ca^0}$ .

From eq 10 it can be seen that  $K_1$  and  $K_g$  can be obtained from CMC data over a range of salinities. The CMC of the sodium dodecylsulfate under variable conditions will be referred to as  $CMC_{DS}$ , which is equal to  $[DS^-]_{\text{mon}}$ , but will be referred to separately when it is a measured CMC value. Figure 4.2 shows  $CMC_{DS}$  as a function of unbound  $Na^+$  concentration from which  $K_1 = -8.5134$  and  $K_g = 0.698$  were obtained. At the CMC,  $[Na^+]_{\text{un}}$  is equal to the total sodium ion concentration.

Figure 4.3 shows the entire precipitation boundary for the SDS +  $CaCl_2$  system, from which these parameters can be obtained. Below the CMC, where no micelles are present, precipitation data are described by eqs 1 - 4 where  $[Ca^{+2}]_{\text{un}}$  and  $[DS^-]_{\text{mon}}$  are equal to the total calcium concentration ( $[CaCl_2]$ ) and total surfactant concentration ( $[NaDS]$ ), respectively. Therefore, it is possible to calculate  $K_{sp}$  from any precipitation point below the CMC. In this case, all precipitation data below the CMC was fit simultaneously to obtain the best value of  $K_{sp} = 5.02 \times 10^{-10} M^3$  as shown in Figure 4.3.

Well above the CMC, virtually all of the surfactant is

present as micelles so that  $[DS^-]_{mic}$  can be considered equal to  $[SDS]$ . Similarly, the concentration of unbound calcium in solution is insignificant compared to the total amount present so it is assumed  $[Ca^{+2}]_b = [CaCl_2]$ . Therefore, from equation 9,  $\beta_{Ca^0}$  can be determined from precipitation data far above the CMC where  $[CaCl_2]$  versus  $[SDS]$  is constant. From the data in Figure 4.3, a value of  $\beta_{Ca^0} = 0.20$  is obtained. Although it would be useful to confirm this value with independent experiments using a calcium specific electrode, it was not possible in this system because the concentration of unbound  $Ca^{+2}$  was so low that interference from  $Na^+$  ions prevented accurate measurements. Other workers<sup>4, 18, 19</sup> have used precipitation boundary to infer values for counterion binding. Kallay et. al.<sup>18</sup> report  $\beta_{Ca^0} = 0.16$  for the SDS +  $CaCl_2$  system at 25°C.

To calculate a value for  $\beta_{Na^0}$ , it is assumed that the total fraction of negative charges (from  $DS^-$ ) that are neutralized in the micelles is constant. The counterion binding of  $Na^+$  (without  $Ca^{+2}$  present) was found to be 0.65 on a pure dodecylsulfate micelle<sup>20</sup>. If it is assumed that 65% of all charges are still neutralized in the  $Na^+/Ca^{+2}$  mixture; then,  $\beta_{Na^0} = 0.45$ .

## RESULTS USING SIMPLIFIED MODEL

The precipitation phase boundary shown in Figure 4.3 is the result of simultaneous solution of equations 1-10 and it is seen to represent the data very well. Actually, the curve in Figure 4.3 is a composite of the curve below the CMC, using equations 1-4, and the curve above the CMC, using all 10 equations.

Below the CMC, surfactant precipitation as  $Ca(DS)_2$  behaves the same as any simple electrolyte; i.e., as the concentration of one ion is increased, the concentration of the other ion required to cause precipitation decreases as dictated by equation 1. At the CMC, however, micelles begin to form and the precipitation boundary drastically changes slope. This is primarily due to counterion binding of  $Ca^{+2}$  onto any micelles that form. The steepness of the curve at surfactant concentrations just above the CMC can be explained by considering the concentration of unbound (total)  $Ca^{+2}$  relative to the concentration of SDS at the CMC. Any surfactant added beyond the CMC can be considered to form micelles. So then, if  $1.0 \times 10^{-3}$  M of NaDS is added above the CMC, approximately  $1.0 \times 10^{-4}$  M of additional  $CaCl_2$  can be added (dictated by binding). In Figure 4.3 therefore, a small change in  $[NaDS]$  beyond the CMC results in a relatively large change in  $[CaCl_2]$ .

It has been demonstrated that the model is able to describe the data in Figure 4.3 quite well. This is to be expected however, because this data has been fit to determine

the best value for  $K_{sp}$  and  $\beta_{Ca^0}$ . Using these same parameters, the model is able to predict what the precipitation boundary for NaDS + CaCl<sub>2</sub> should be for any concentration of added NaCl as shown in Figure 4.4 for [NaCl] = 0.02 M and 0.1 M. The results for [NaCl] = 0.02 M, are excellent. However for [NaCl] = 0.1 M, agreement between experimental values and calculations from the model are less impressive. The error at the higher salinity in Figure 4.4 could be caused by several factors. For instance, equations 2 and 3 are only valid for ionic strengths up to about 0.1 M which is exceeded in each solution with [NaCl] = 0.1 M. Error in activity coefficient calculations would affect the calculated value of  $[Ca^{+2}]_{un}$  in equation 1 and thereby affect predicted hardness tolerance in these mixtures since unbound Ca<sup>2+</sup> accounts for most of the Ca<sup>2+</sup> in solution under these conditions.

Assumptions that were made about counterion binding may also account for some of the discrepancy between predicted and experimental values at 0.1 M NaCl. It seems reasonable to believe that there must be competition between both Na<sup>+</sup> and Ca<sup>2+</sup> to bind on the charged micelle. Although divalent calcium ions bind preferentially,  $\beta_{Ca^0}$  may decrease as the ratio of  $[Na^+]_{un}/[Ca^{+2}]_{un}$  increases. Therefore, the binding of Ca<sup>2+</sup> may be less than 0.2 when the concentration of NaCl is raised to 0.1 M. Although a lower value for  $\beta_{Ca^0}$  at this salinity would give a better fit to the data at 0.02 M added NaCl, it still would not account for the minimum that is observed in the precipitation boundary above the CMC. Baviere and co-workers<sup>21,22</sup> have also observed minima in precipitation boundaries when NaCl is added and attributed this to competitive binding of Na<sup>+</sup> and Ca<sup>2+</sup>. It is interesting to note that, at high NaDS concentrations, precipitation data converge along the same line, implying a constant value of  $\beta_{Ca^0}$ .

Competitive binding between Na<sup>+</sup> and Ca<sup>2+</sup> could also explain why the value of  $\beta_{Ca^0}$  presented here is lower than one would expect from binding without Na<sup>+</sup> present. Koshinuma<sup>23</sup> has shown that  $\beta_{Ca^0} = 0.88$  for micelles composed of decylsulfate anions when sodium ions are not present in solution. Binding of Ca<sup>2+</sup> on dodecylsulfate micelles is expected to give a similar value, but in these systems it is much lower, indicating the competition with Na<sup>+</sup>. That paper also shows (Figure 8 of Reference 23) that the total fraction of charges neutralized ( $\beta_{Ca^0} + \beta_{Na^0}$ ) is approximately constant at higher Na<sup>+</sup>/Ca<sup>2+</sup> ratios. This seems to verify the assumption made in this work that the total binding ( $\beta_{Na^0} + \beta_{Ca^0}$ ) is constant.

The most striking general observation from Figure 4.4 is that as the concentration of added NaCl increases, the minimum hardness tolerance for each system increases. For instance, when 0.02 M NaCl is added, the minimum point in the

precipitation boundary is shifted up by 400% (experimental values) to a higher  $[CaCl_2]$ . When 0.1 M NaCl is added, a 2500% increase is realized in the minimum hardness tolerance compared to the precipitation boundary without added NaCl. This can be explained by Figure 4.2 which shows that  $[DS^-]_{mon}$  or CMC<sub>ds</sub> decreases as  $Na^+$  is increased. When the monomer concentration of anionic surfactant decreases, a higher  $Ca^{+2}$  is required to cause precipitation as dictated by equation 1.

#### CALCULATION OF PARAMETERS IN GENERALIZED MODEL

To calculate  $[DS^-]_{mon}$  at any  $Na^+$  and  $Ca^{+2}$  concentration, it is necessary to obtain the appropriate constants. For NaDS, Moroi et. al.<sup>15</sup> reports  $Nv = 32.7 \text{ cm}^3$  and  $w = 1.08kT$  so that with  $m = 12$ , parameters in equation 23 can be used to calculate  $K_3 = -10.5396$ . Similarly, with a value<sup>24</sup> of  $E_c = 8.9876 \times 10^9 \text{ Nm}^2 \text{ C}^{-2}$ ,  $D = 78$ , and  $T = 303.15 \text{ K}$ ,  $K_2$  is found from equation 11 so that  $K_2 = 2.8724 \times 10^5 \text{ (mol)m}^4/\text{C}^2\text{L}$ .

When equation 25 is combined with data presented in Figure 4.2, one obtains  $K_{g,Na} = 0.69832$  and, from the intercept,  $S_{Na} = 7.960 \times 10^{-3} \text{ (C/m}^2\text{)}$ . When this value is converted to  $esu/\text{cm}^2$ , it is much lower than the value which Moroi et. al.<sup>15</sup> reports due to using a different  $K_{g,Na}$  value and an error they made in units associated with  $K_2$  (which does not affect their ultimate results since it was made throughout). When the data in Figure 4.2 are extrapolated back to the CMC of pure NaDS (or equation 25 is solved for  $[DS^-]_{mon} = [Na^+]_{un} = \text{CMC}_{ds}$ ), it gives a value of  $\text{CMC}_{ds} = 6.652 \times 10^{-3} \text{ M}$ . This is used in equation 29 to obtain  $P_{ds} = 2736.32$ . The value of  $\text{CMC}_{ds}$  reported here is slightly lower than the accepted literature value<sup>15,25</sup> of about  $8.25 \times 10^{-3} \text{ M}$  (although wide variations are reported). For example, Fan et. al.<sup>5</sup> recently reported a  $\text{CMC}_{ds}$  of  $5.3 \times 10^{-3} \text{ M}$  in another study of the precipitation of this surfactant.

In an analogous way, the constants  $K_{g,ca}$ ,  $S_{ca}$ ,  $\text{CMC}_{cds}$ , and  $P_{cds}$  could be obtained from  $\ln(\text{CMC}_{cds})$  versus  $\ln([Ca^{+2}]_{un})$  data for  $Ca(DS)_2 + CaCl_2$ . This would give all the required constants so that equations 16, 22, 27, and 28 could be used to calculate  $[DS^-]_{mon}$  for any concentrations of unbound  $Na^+$  and  $Ca^{+2}$ . Using a different method, Moroi et. al. measured the CMC of pure divalent metal dodecylsulfates,  $\text{CMC}_{cds}$ , and used  $K_{g,ca}$  as an adjustable parameter to give the best fit for CMC data in SDS +  $Ca(DS)_2$  mixtures.

In this work,  $K_{g,ca}$  is used as an adjustable parameter to give the best fit for CMC data in electrolyte mixtures. At 30° C it is not possible to measure  $\text{CMC}_{cds}$  in electrolyte mixtures containing  $Ca^{+2}$  because precipitation occurs at even low concentrations. Therefore, it is very difficult to measure the effect of  $Ca^{+2}$  on  $\text{CMC}_{cds}$  in SDS +  $CaCl_2$  + NaCl

systems. This obstacle can be bypassed by studying the effects of other divalent metals on CMC<sub>ds</sub>. Generally, ions with the same charge have the same effect on the CMC<sup>15, 25-27</sup> because it is an electrostatic phenomenon; i.e., there is little specificity between ions of similar charge. The Krafft temperature of magnesium dodecylsulfate, Mg(DS)<sub>2</sub>, is much lower<sup>28</sup> than that of calcium dodecylsulfate (or the solubility product of the Mg(DS)<sub>2</sub> is higher<sup>5</sup>), so the system NaDS + Mg(DS)<sub>2</sub> + NaCl can be used to study the effect of divalent metal concentrations on CMC<sub>ds</sub>. Table 1 summarizes the results of some CMC measurements for this system.

Table 4.1 shows there is good agreement between experimental values of CMC<sub>ds</sub> and calculations from eqs 16, 22, 27, and 28 with  $K_{g,ca} = 0.895$  and  $CMC_{c,ds} = 1.900 \times 10^{-3}$  M. For a given CMC<sub>ds</sub>, the corresponding value of PC<sub>ds</sub> is obtained from equation 30 and when an arbitrary  $K_{g,ca}$  is chosen,  $S_{ca}$  can be calculated from equation 26 using the point  $[DS^-]_{mon} = CMC_{c,ds} = 2[Ca^{+2}]_{un}$ . In essence then, two parameters have been manipulated in this case (CMC<sub>ds</sub> and  $K_{g,ca}$ ) to give the best fit to the CMC<sub>ds</sub> data. Using these values for CMC<sub>ds</sub>, PC<sub>ds</sub>,  $K_{g,ca}$ , and  $S_{ca}$ , it is possible to accurately calculate  $[DS^-]_{mon}$  (or CMC<sub>ds</sub>) at any Na<sup>+</sup> and Ca<sup>+2</sup> concentration.

## RESULTS USING GENERALIZED MODEL

Results for the generalized model will not be shown here because they are essentially the same as those of the simplified model at  $[NaCl] = 0.0$  and  $0.02$  M. Simply stated, this means that the effect of  $[Ca^{+2}]_{un}$  on  $[DS^-]_{mon}$  is negligible compared to the effect of  $[Na^+]_{un}$  because at each point,  $[Na^+]_{un} \gg [Ca^{+2}]_{un}$ . At  $[NaCl] = 0.1$  M, the predicted precipitation boundary here gives a slightly worse fit (a maximum of 10 % difference in the hardness tolerance) than the simplified model. When  $[Ca^{+2}]_{un}$  is accounted for, it causes  $[DS^-]_{mon}$  to be decreased even more than in the simplified model so that hardness tolerance predictions are higher and therefore more in error.

In this work, and the work of others for these types of systems, using the simplified model gives an accurate fit to precipitation data since the effect of Ca<sup>+2</sup> on the CMC is negligible. However, this will not always be the case in anionic-only surfactant systems. For instance, if  $K_{sp}$  were greater, a higher concentration of unbound divalent metal ( $[Ca^{+2}]_{un}$ ) would be required to cause precipitation for the same  $[SDS]$  and  $[NaCl]$ . In this case,  $[Ca^{+2}]_{un}$  would no longer have a negligible affect on  $[DS^-]_{mon}$  and it would be necessary to use the generalized model. Similarly, in anionic-nonionic surfactant mixtures (presented in Part II of this series),  $[Ca^{+2}]_{un}$  is not negligible and this generalized approach must be used to determine anionic surfactant monomer concentration.

## RELATIONSHIP TO PREVIOUS WORK

Much work has been done on precipitation of anionic surfactants by calcium<sup>4-6,18,21-23,29-33</sup>. Because of this, a basic understanding has developed concerning phenomena that are important in these systems. For instance, most workers agree that: precipitation is governed by a solubility product; hardness tolerance increases when micelles form due to binding; and increasing NaCl concentration increases hardness tolerance due to lowering of CMC. In addition, several approaches have been used to model these systems<sup>4,5,18,22,29,30</sup> and generally with good qualitative results. Interestingly, Chou et. al.<sup>30</sup> shows the same result at high salinities (0.1 M) as are presented here (i.e., predictions that are higher than actual data) but likewise has good success at moderate salinities.

Several authors have reported coprecipitation of surfactant by both Na<sup>+</sup> and Ca<sup>2+</sup> in these types of systems although in the work presented in this chapter, only Ca(DS)<sub>2</sub> was assumed to precipitate. There are no conditions studied here where the K<sub>sp</sub> of NaDS is exceeded. Researchers<sup>22,34</sup> that have reported coprecipitation have used longer chain surfactant molecules with lower K<sub>sp</sub> values for Na<sup>+</sup>. Therefore at high enough total Na<sup>+</sup> concentrations, the K<sub>sp</sub> of the sodium surfactant salt has been exceeded and coprecipitation occurs.

## CONCLUSIONS

In general, there are two mechanisms by which hardness tolerance can be increased in an anionic-only surfactant system. First, hardness tolerance increases as surfactant concentration is increased above the CMC. This is due to binding of divalent counterions onto any micelles that form above the CMC. Secondly, the minimum hardness tolerance for a precipitation boundary increases as the added monovalent electrolyte concentration is increased. The reason for this is a reduction in the monomer concentration of anionic surfactant when NaCl is added. As anionic surfactant monomer concentration decreases, a higher concentration of divalent counterion is required in solution to cause precipitation (as dictated by the solubility product).

## NOMENCLATURE

$c_i$	concentration of ion $i$ in solution, $\text{kmol/m}^3$
$[\text{CaCl}_2]$	total concentration of $\text{CaCl}_2$ in solution, $\text{kmol/m}^3$
$[\text{Ca}^{+2}]_b$	concentration of $\text{Ca}^{+2}$ bound on micelles, $\text{kmol/m}^3$
$[\text{Ca}^{+2}]_s$	concentration of $\text{Ca}^{+2}$ at the micelle surface when both $\text{Ca}^{+2}$ and $\text{Na}^+$ are present in solution, $\text{kmol/m}^3$
$[\text{Ca}^{+2}]_s^0$	concentration of $\text{Ca}^{+2}$ at the micelle surface at the CMC of pure $\text{Ca}(\text{DS})_2$ , $\text{kmol/m}^3$
$[\text{Ca}^{+2}]_{un}$	concentration of unbound $\text{Ca}^{+2}$ in solution, $\text{kmol/m}^3$
$[\text{Ca}^{+2}]_{un}^0$	concentration of unbound $\text{Ca}^{+2}$ at the CMC of pure $\text{Ca}(\text{DS})_2$ , $\text{kmol/m}^3$
CMC	critical micelle concentration, $\text{kmol/m}^3$
CMC <sub>CaDS</sub>	CMC of pure $\text{Ca}(\text{DS})_2$ , $\text{kmol/m}^3$
CMC <sub>SDS</sub>	CMC of SDS under various conditions, $\text{kmol/m}^3$
CMC <sub>NaDS</sub>	CMC of pure $\text{NaDS}$ , $\text{kmol/m}^3$
$D$	dielectric constant of water
$[\text{DS}^-]_{mic}$	concentration of $\text{DS}^-$ present in micelles, $\text{kmol/m}^3$
$[\text{DS}^-]_{mon}$	concentration of $\text{DS}^-$ present as monomer, $\text{kmol/m}^3$
$e$	charge of an electron, $1.6 \times 10^{-19} \text{ C}$
$E_c$	conversion constant ( $8.9876 \times 10^9 \text{ N m}^2/\text{C}^2$ )
$f_{Ca}$	activity coefficient of unbound $\text{Ca}^{+2}$ in solution
$f_{DS}$	activity coefficient of monomeric $\text{DS}^-$ in solution
$I$	ionic strength, $\text{kmol/m}^3$
$k$	Boltzmann constant, $1.38 \times 10^{-23} \text{ J}/(\text{molecule K})$
$K_1, K_3, K_g$	constants
$K_2$	constant, $\text{Mm}^4/\text{C}^2$
$K_{g, Ca}$	value of $K_g$ when $\text{Ca}^{+2}$ is the only counterion

	present in solution
$K_{g, Na}$	value of $K_g$ when $Na^+$ is the only counterion present in solution
$K_{sp}$	solubility product, $M^3$
$m$	carbon number of surfactant molecule
$N$	Avogadro's number, $6.023 \times 10^{26}$ molecules/kmol
$[Na^+]_b$	concentration of $Na^+$ bound on micelles, $kmol/m^3$
$[Na^+]_s$	concentration of $Na^+$ at the micelle surface when both $Na^+$ and $Ca^{+2}$ are present in solution, $kmol/m^3$
$[Na^+]_{s^0}$	concentration of $Na^+$ at the micelle surface at the CMC of pure NaDS, $kmol/m^3$
$[Na^+]_{tot}$	total concentration of $Na^+$ ions in solution, $kmol/m^3$
$[Na^+]_{un}$	concentration of unbound $Na^+$ in solution, $kmol/m^3$
$[Na^+]_{un^0}$	concentration of unbound $Na^+$ at the CMC of pure NaDS, $kmol/m^3$
$[NaCl]$	total concentration of NaCl in solution, $kmol/m^3$
$P$	term related to $\Phi_0$
$P_{cDs}$	the value of $P$ at the CMC of pure $Ca(DS)_2$
$P_{sDs}$	the value of $P$ at the CMC of pure NaDS
$R$	gas constant, $1.987 \text{ kcal}/(\text{kmol K})$
$S$	surface charge density of micelle, $C/m^2$
$S_{ca}$	surface charge density of micelle when $Ca^{+2}$ is the only counterion present in solution, $C/m^2$
$[SDS]$	total concentration of NaDS in solution, $kmol/m^3$
$S_{Na}$	surface charge density of micelle when $Na^+$ is the only counterion present in solution, $C/m^2$
$T$	absolute temperature, $K$
$v$	free volume per surfactant molecule in micelle, $m^3/\text{molecule}$
$w$	cohesive energy difference per molecule between micellar and singly dispersed state, $J/\text{molecule}$

$z_i$  valence of species  $i$   
 $\beta_{Ca^0}$  fractional counterion binding of  $Ca^{+2}$  on micelle  
 $\beta_{Na^0}$  fractional counterion binding of  $Na^+$  on micelle  
 $\Phi_0$  electrical potential at the micelle surface, V

## REFERENCES

1. Brant, L.W.; Stellner, K.L.; Scamehorn, J.F. in Surfactant-Based Separation Processes; Scamehorn, J.F.; Harwell, J.H., Eds.; Marcel Dekker: New York, Chapter 12, In Press.
2. Stellner, K.L.; Scamehorn, J.F. J. Am. Oil Chem. Soc., 1986, 63, 566.
3. Stellner, K.L.; Amante, J.C.; Scamehorn, J.F.; Harwell, J.H. J. Colloid Interface Sci., 1988, 123, 186.
4. Peacock, J.M.; Matijevic, E. J. Colloid Interface Sci. 1980, 77, 548.
5. Fan, X.-J., Stenius, P., Kallay, N., and Matijevic, E., J. Colloid Interface Sci. 1988, 121, 571.
6. Matheson, K.L.; Cox, M.F.; Smith, D.L. J. Am. Oil Chem. Soc. 1985, 62, 1391.
7. Smith, D.L.; Matheson, K.L.; Cox, M.F. J. Am. Oil Chem. Soc. 1985, 62, 1399.
8. Lunkenheimer, K.; Wantke, K.D. Colloid Polym. Sci. 1981, 259, 354.
9. Klotz, I.M.; Rosenberg, R.M., Chemical Thermodynamics, 3rd ed.; Benjamin Cummings: Menlo Park, California, 1972; p 384.
10. Burchfield, T.E.; Woolley, E.M. J. Phys. Chem. 1984, 88, 2149.
11. Shinoda, K. In Colloidal Surfactants (Shinoda, K.; Tamamushi, B.; Nakagawa, T.; Isemura, T., Eds.; Academic Press: New York, 1963; p 58.
12. Shinoda, K. Bull. Chem. Soc. Jpn. 1955, 28, 340.
13. Shinoda, K. In Colloidal Surfactants (Shinoda, K.; Tamamushi, B.; Nakagawa, T.; Isemura, T., Eds.; Academic Press: New York, 1963; p 39-42.
14. Lange, H. Kolloid-Z 1951, 121, 66.
15. Moroi, Y.; Motomura, K.; Matuura, R. J. Colloid Interface Sci. 1974, 46, 111.
16. Moroi, Y.; Nishikido, N.; Matuura, R. J. Colloid Interface Sci. 1975, 50, 344.

17. Hiemenz, P.C. Principles of Colloid and Surface Chemistry; Marcel Dekker: New York, 1977; p 366.
18. Kallay, N.; Pastuovic, M.; Matijevec, E. J. Colloid Interface Sci. 1985, 106, 452.
19. Gerbacia, W.E.F. J. Colloid Interface Sci. 1983 93, 556.
20. Rathman, J.F.; Scamehorn, J.F. Langmuir 1987 3, 372.
21. Baviere, M.; Bazin, B.; Aude, R. J. Colloid Interface Sci. 1983, 92, 580.
22. Noik, C.; Baviere, M.; Defives, D. J. Colloid Interface Sci. 1987, 115, 36.
23. Koshinuma, M. Bull. Chem. Soc. Jpn. 1983, 56, 2341.
24. Hiemenz, P.C. Principles of Colloid and Surface Chemistry; Marcel Dekker: New York, 1977; p 360.
25. Mukerjee, P.; Mysels, K.J. Critical Micelle Concentrations of Aqueous Surfactant Systems" (NSRDS-NBS 36); U.S. Government Printing Office: Washington, 1971.
26. Oko, M.U.; Venable, R.L. J. Colloid Interface Sci. 1971, 35, 53.
27. Satake, I.; Iwamatsu, I.; Hosokawa, S.; and Matuura, R. Bull. Chem. Soc. Jpn. 1963, 36, 204.
28. Miyamoto, S., Bull. Chem. Soc. Jpn. 1960, 33, 371.
29. Bozic, J.; Krznaric, I.; Kallay, N. Colloid Polym. Sci. 1979, 257, 201.
30. Chou, S.I.; Bae, J.H. J. Colloid Interface Sci. 1983, 96, 192.
31. Matheson, K.L. J Am. Oil Chem. Soc. 1985, 62, 1269.
32. Somasundaran, P.; Ananthapadmanabhan, K.P.; Celik, M.S.; Manev, E.D. Soc. Pet. Eng. J. 1984, 24, 667.
33. Tartar, H.V.; Cadle, R.D. J. Phys. Chem. 1939, 43, 1173.
34. Celik, M.S.; Manev, E.D.; Somasundaran, P. AIChE Symp. Ser. 1982, 78, 86.

Table 4.1: Comparison Between Calculated and Experimental Values of CMC<sub>ds</sub> with Added NaCl and MgCl<sub>2</sub> (all Concentrations in mM).  $K_{g,ca} = 0.895$ ,  $CMC_{cds} = 1.900 \times 10^{-3}$  M.

[NaCl]	[Mg <sup>+2</sup> ] <sub>un</sub> <sup>a</sup>	[Na <sup>+</sup> ] <sub>un</sub> <sup>b</sup>	Calc. <sup>c</sup> CMC <sub>ds</sub>	Exper. CMC <sub>ds</sub>	error
0.0	0.100	4.5711	4.5711	4.450	+2.7%
0.0	0.300	3.0360	3.0360	2.800	+8.4%
0.0	1.000	1.8303	1.8303	1.930	-5.2%
10.0	1.000	11.695	1.6954	1.750	-3.1%
20.0	0.500	21.982	1.9820	1.900	+4.3%
20.0	3.000	21.041	1.0408	1.150	-9.5%
100.0	0.600 <sup>d</sup>	101.01	1.0116	0.965	+4.8%

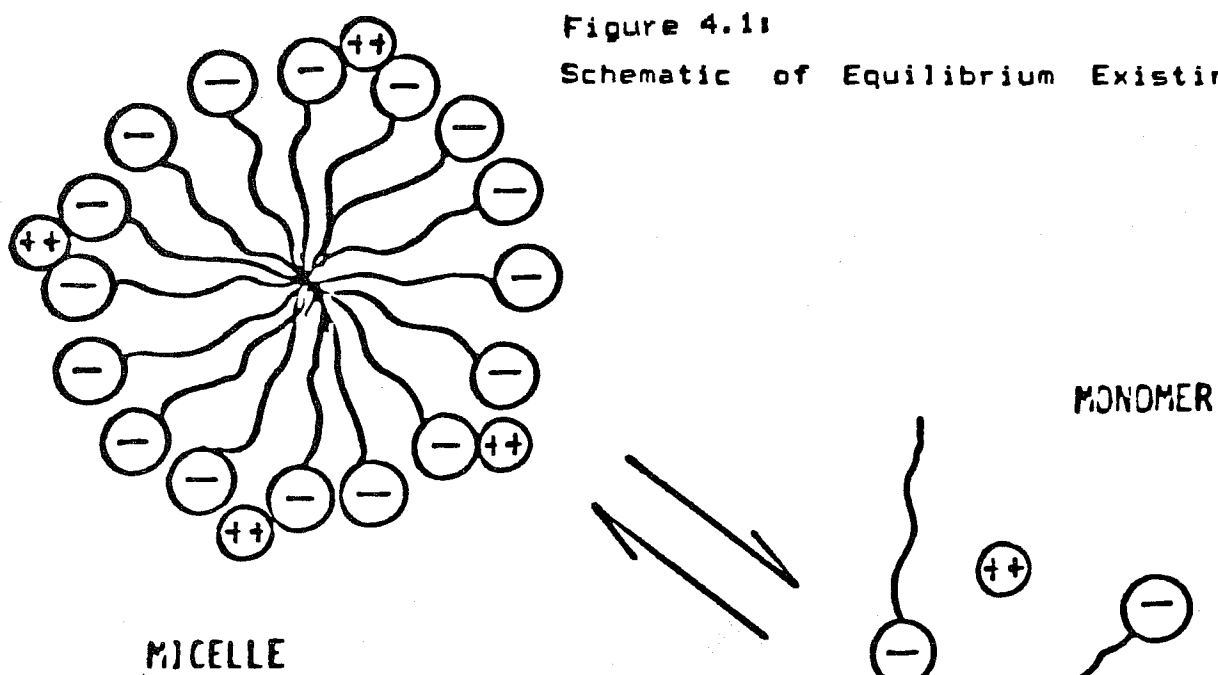
a [Mg<sup>+2</sup>]<sub>un</sub> = [MgCl<sub>2</sub>]

b [Na<sup>+</sup>]<sub>un</sub> = [NaCl] + [SDS]

c Calculated from eqs 16, 22, 27, and 28.

d This point is for CaCl<sub>2</sub>, not MgCl<sub>2</sub>.

Figure 4.11  
Schematic of Equilibrium Existing in System



PRECIPITATE

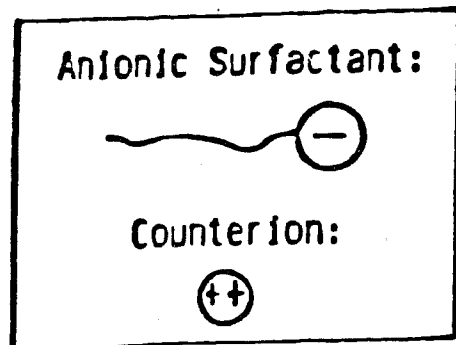
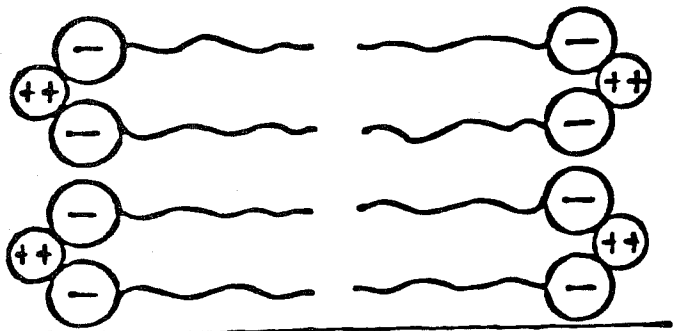


Figure 4.2: Effect of Unbound  $\text{Na}^+$  Concentration on CMC of Anionic Surfactant

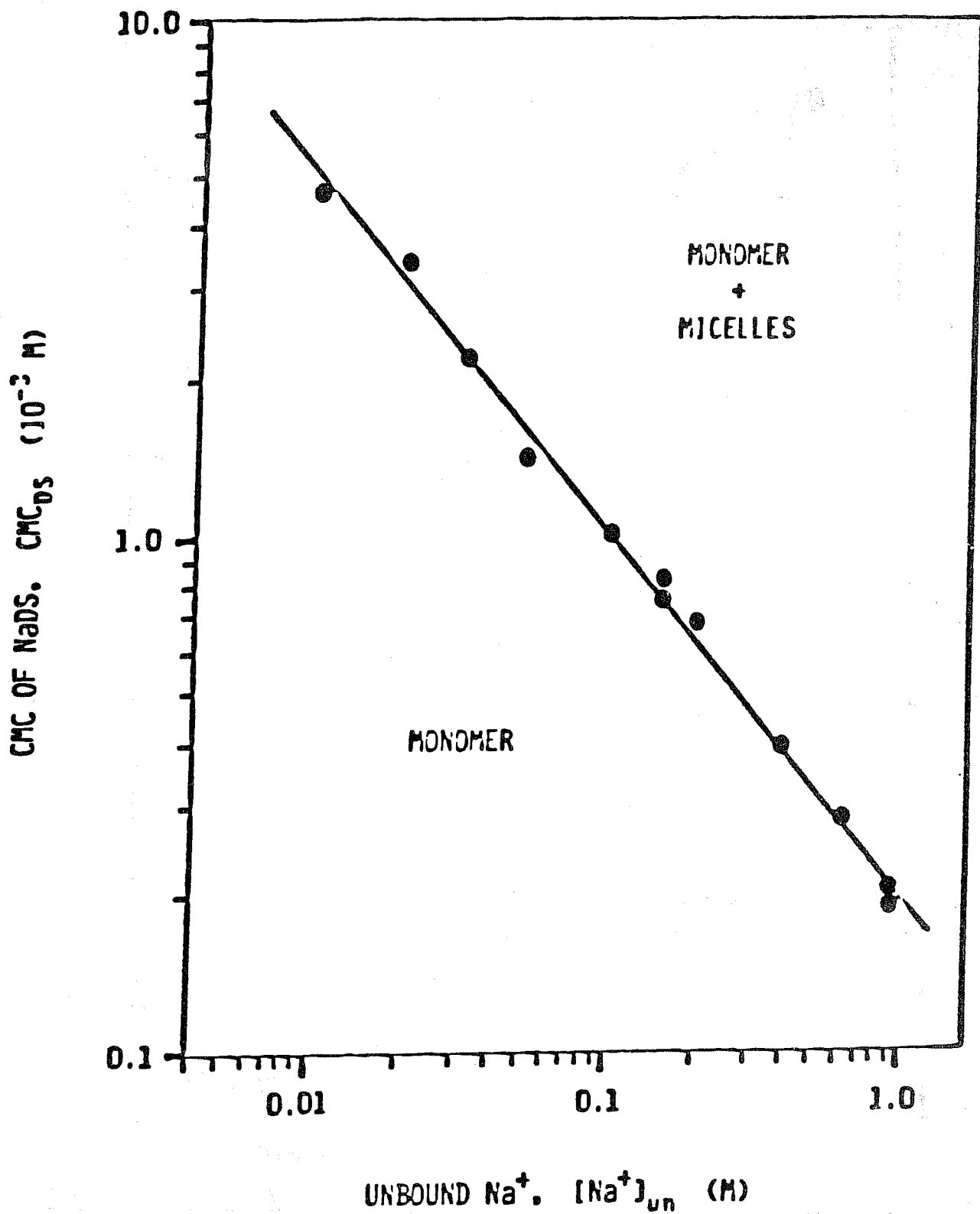


Figure 4.3: Precipitation Phase Boundary Without Added NaCl

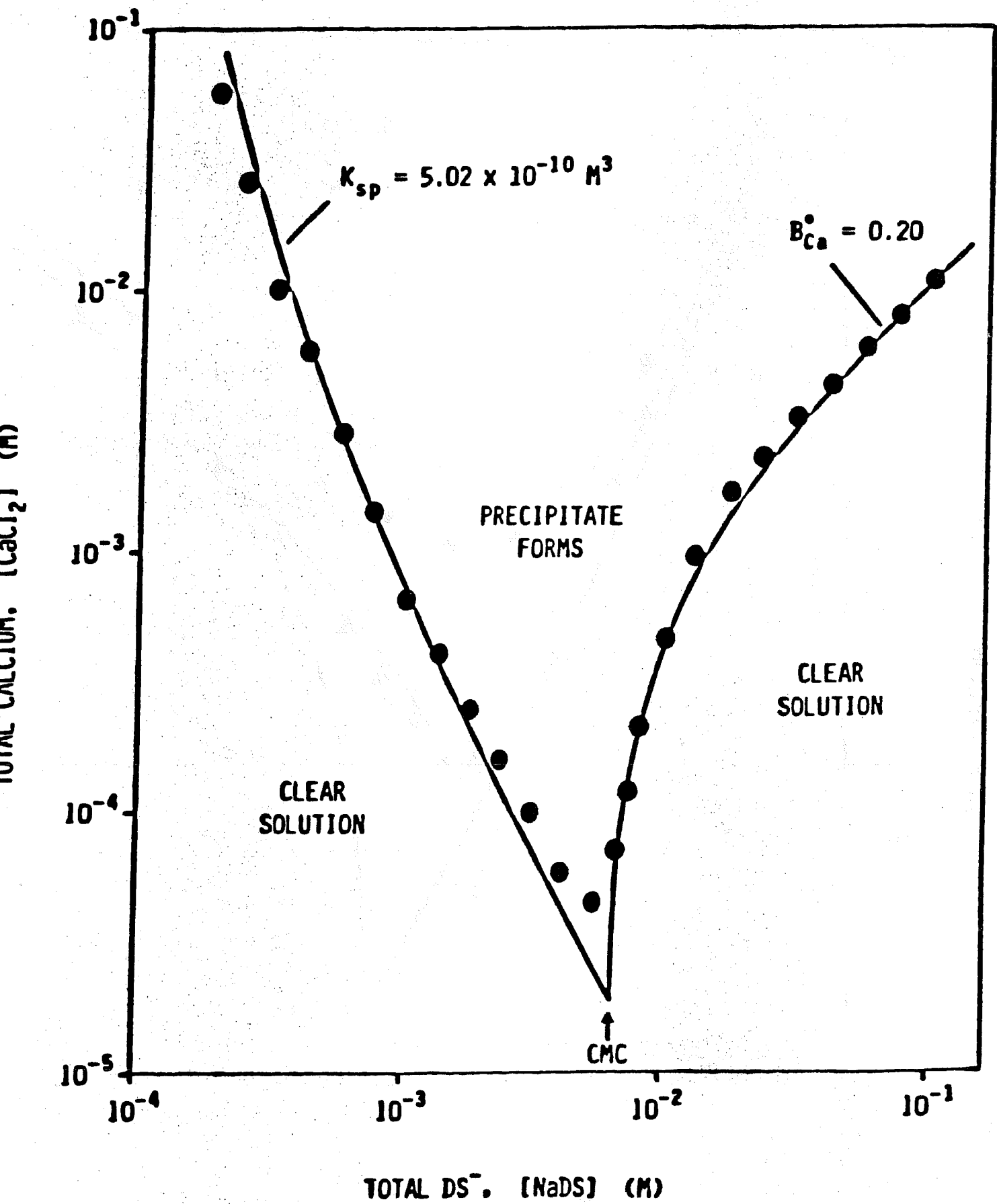
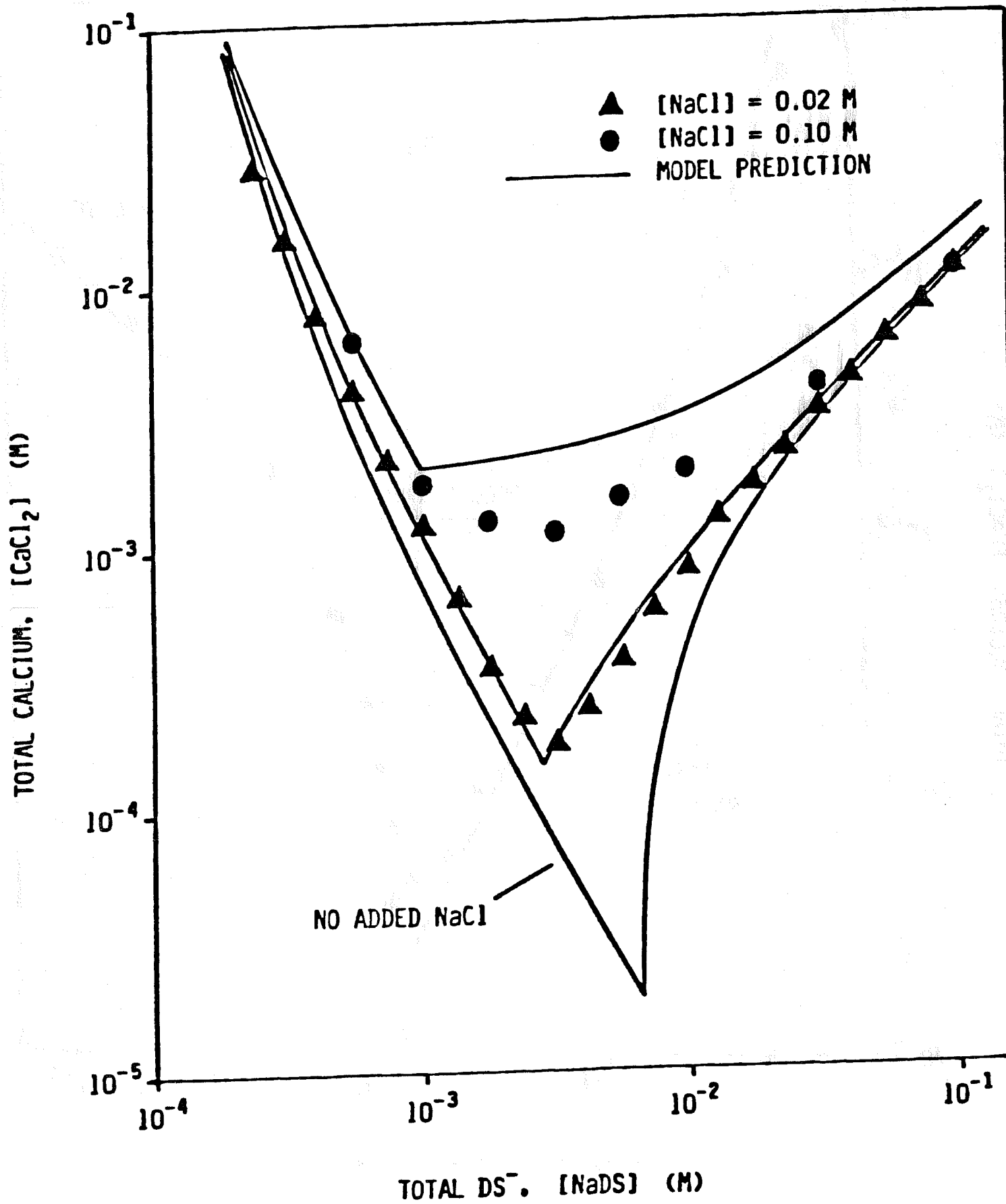


Figure 4.4: Precipitation Phase Boundary With Various Concentrations of Added NaCl



## CHAPTER 5

### HARDNESS TOLERANCE OF ANIONIC SURFACTANT SOLUTIONS: II. EFFECT OF ADDED NONIONIC SURFACTANT

#### ABSTRACT

Precipitation of anionic surfactant by calcium has been studied in the presence of added nonionic surfactant and added NaCl. A model is developed that can predict the precipitation boundary as a function of surfactant composition and concentration of added NaCl. The model uses a solubility product relationship between anionic surfactant monomer and unbound calcium, regular solution theory description of monomer-micelle equilibrium, and considers counterion binding of divalent and monovalent counterions onto the micelles. The model works well at moderate NaCl concentrations, but is less accurate at high NaCl concentrations. Calculations from the model confirm that mixed micelle formation is responsible for increased hardness tolerance in anionic surfactant solutions when nonionic surfactant is added.

#### INTRODUCTION

Hardness tolerance of an anionic surfactant is defined as the minimum concentration of multivalent cation necessary to cause precipitation of the surfactant. In Chapter 3, we discussed the precipitation of anionic surfactant with or without added monovalent electrolyte. A model was developed which could predict hardness tolerance as a function of surfactant concentration and monovalent electrolyte concentration. In an earlier paper<sup>2</sup>, we discussed salinity tolerance (minimum concentration of a monovalent electrolyte to cause precipitation) of an anionic surfactant in the presence of a nonionic surfactant. The nonionic surfactant was shown to enhance salinity tolerance substantially due to mixed micelle formation. In this chapter, we extend these previous two investigations to consider the effect of added nonionic surfactant on hardness tolerance of an anionic surfactant.

Hardness tolerance is a commonly encountered problem in the utilization of ionic surfactants. Builders (e.g., phosphates) are traditionally added to detergent formulations to prevent anionic surfactant precipitation<sup>3</sup>. In enhanced oil recovery by micellar flooding or surfactant assisted waterflooding, alcohols may be added to an injected slug to prevent precipitation<sup>4</sup>.

The addition of nonionic surfactants to anionic

surfactants to enhance hardness tolerance in practical applications is receiving increasing attention. Non-built heavy duty liquid laundry detergents may utilize mixtures of anionic and nonionic surfactants<sup>5,6</sup>. Mixed surfactant systems employing nonionic surfactant have been proposed for use in surfactant based enhanced oil recovery<sup>7</sup>. More generally, surfactant mixtures can have a number of synergistic advantages over the use of a single surfactant type<sup>8</sup>.

Conversely, the use of sequentially injected slugs of anionic and nonionic surfactant solutions is another potential candidate for surfactant enhanced volumetric sweep efficiency. The nonionic surfactant solution has a low adsorption to the reservoir minerals, and thus has a high chromatographic velocity relative to the anionic surfactant solution. Successful application of this approach requires the correct formulation of the respective surfactant solutions in monovalent electrolytes.

In this work, the precipitation phase boundary is measured for an anionic-nonionic surfactant mixture at different NaCl concentrations. Furthermore, a model is developed which can predict this phase boundary.

## EXPERIMENTAL

The experimental materials and methods are the same as used in chapter 4 with the following additions due to the inclusion of nonionic surfactant in these studies.

The nonionic surfactant (NPE) was a polydisperse nonylphenol polyethoxylate with an average of 10 ethylene oxide groups per molecule. The NPE has a trade name of Igepal CO-660 from GAF Corporation and was used as received.

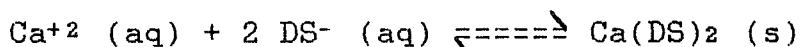
In order to determine if NPE incorporated itself into the precipitated crystals, the precipitate was filtered from the solution, washed with cold water, and dried at low heat. The crystals were then dissolved in water and the concentration of NPE in the solution determined using HPLC with UV detection. The precipitate formed from mixed surfactant solutions of various compositions was analyzed and found to contain no detectable nonionic surfactant contaminant (>99.98 % pure).

## THEORY

The model developed here is an extension of the hardness tolerance model developed in chapter 4, the main addition being that regular solution theory will be included to account for the equilibrium between surfactant monomer and micelles. Figure 5.1 is a schematic diagram which represents precipitation in these mixtures when micelles are present.

The anionic surfactant is present in 3 environments: 1) as monomer (unassociated molecules), 2) incorporated in mixed micelles, and 3) as precipitate. Nonionic surfactant is present 1) as monomer, and 2) in mixed micelles. Monovalent counterions (not shown in Figure 5.1 for clarity) and divalent counterions, both exist 1) as unbound (unassociated) species and 2) bound onto the micelle surface. In addition, the divalent counterion is present in any precipitate that forms. The anionic surfactant used is sodium dodecylsulfate (NaDS).

Nonionic surfactant does not participate in the precipitation reaction which is represented by:



This can be described by a solubility product relationship between unassociated species:

$$K_{sp} = [\text{Ca}^{2+}]_{un} ([\text{DS}^{-}]_{mon})^2 f_{ca} (f_{DS})^2 \quad (5.1)$$

where  $K_{sp}$  is the activity-based solubility product,  $[\text{Ca}^{2+}]_{un}$  is the concentration of unbound calcium,  $[\text{DS}^{-}]_{mon}$  is the monomer concentration of anionic surfactant, and  $f_{ca}$  and  $f_{DS}$  represent the activity coefficients of unbound  $\text{Ca}^{2+}$  and monomeric  $\text{DS}^{-}$  in solution, respectively.

An extended Debye-Huckel equation is used to describe the activity coefficient of the unassociated ions<sup>1</sup>.

$$\log(f_{ca}) = -0.5139(2)^2(I)^{0.5}/(1 + 1.9782(I)^{0.5}) \quad (5.2)$$

$$\log(f_{DS}) = -0.5139(1)^2(I)^{0.5}/(1 + 2.3079(I)^{0.5}) \quad (5.3)$$

$$I = \sum 0.5 c_i (z_i)^2 = [\text{NaCl}] + [\text{SDS}] + 3[\text{CaCl}_2] \quad (5.4)$$

where  $I$  is the ionic strength,  $c_i$  is the total concentration of ion  $i$  in solution,  $z_i$  is the valence of species  $i$ , and  $[\text{NaCl}]$ ,  $[\text{SDS}]$ , and  $[\text{CaCl}_2]$  are the total concentrations of each species represented.

On the precipitation phase boundaries, the amount of anionic surfactant and calcium present as precipitate is infinitesimal. Therefore, a material balance for each surfactant (anionic and nonionic) and counterion (calcium and sodium) present in solution on this boundary yields:

$$[\text{SDS}] = [\text{DS}^{-}]_{mon} + [\text{DS}^{-}]_{mic} \quad (5.5)$$

$$[\text{NPE}] = [\text{NPE}]_{mon} + [\text{NPE}]_{mic} \quad (5.6)$$

$$[\text{CaCl}_2] = [\text{Ca}^{2+}]_{un} + [\text{Ca}^{2+}]_b \quad (5.7)$$

$$[\text{Na}^+]_{tot} = [\text{NaCl}] + [\text{NaDS}] = [\text{Na}^+]_{un} + [\text{Na}^+]_b \quad (5.8)$$

where  $[\text{DS}^{-}]_{mic}$  represents the concentration of  $\text{DS}^{-}$  present in micelles,  $[\text{NPE}]$  is the total NPE concentration in solution,  $[\text{NPE}]_{mon}$  and  $[\text{NPE}]_{mic}$  represent the concentration of NPE present as monomer or in micelles, respectively,  $[\text{Ca}^{2+}]_b$  is

the concentration of calcium bound onto micelles, and  $[Na^+]_{tot}$ ,  $[Na^+]_{un}$ , and  $[Na^+]_b$  represent the total sodium concentration, the unbound sodium concentration, and the concentration of sodium bound onto micelles, respectively. The concentration of each counterion bound onto the micelle is related to its value of fractional counterion binding by:

$$\beta_{Ca} = 2[Ca^{+2}]_b/[DS^-]_{mic} \quad (5.9)$$

$$\beta_{Na} = [Na^+]_b/[DS^-]_{mic} \quad (5.10)$$

where  $\beta_{Ca}$  and  $\beta_{Na}$  are the fraction of micellar charge neutralized by the respective counterion.

Application of regular solution theory to describe monomer-micelle equilibrium<sup>8,9</sup> yields:

$$[DS^-]_{mon} = X_{DS} \gamma_{DS} CMC_{DS} \quad (5.11)$$

$$[NPE]_{mon} = X_{NPE} \gamma_{NPE} CMC_{NPE} \quad (5.12)$$

$$\ln(\gamma_{DS}) = (X_{NPE})^2 W/RT \quad (5.13)$$

$$\ln(\gamma_{NPE}) = (X_{DS})^2 W/RT \quad (5.14)$$

where  $X_{DS}$  and  $X_{NPE}$  are the micellar mole fraction of the respective surfactants,  $\gamma_{DS}$  and  $\gamma_{NPE}$  represent the activity coefficients of the respective surfactants in the micelle,  $CMC_{DS}$  and  $CMC_{NPE}$  are the CMC values of the respective pure component surfactants at the same unbound counterion concentrations as present in the system of interest (generally different than the CMC of the pure surfactant without additives),  $W$  is the regular solution theory interaction parameter,  $R$  is the gas constant, and  $T$  is absolute temperature.

Mole fractions used here are on a surfactant-only basis:

$$X_{DS} = [DS^-]_{mic} / \{ [DS^-]_{mic} + [NPE]_{mic} \} \quad (5.15)$$

$$X_{DS} + X_{NPE} = 1 \quad (5.16)$$

From eq 11, it is necessary to know  $CMC_{DS}$ , as a function of unbound electrolyte concentration. The calculation of this can be summarized by the following equations<sup>1</sup>:

$$K_2 S^2 = [Na^+]_{un} P + [Ca^{+2}]_{un} P^2 \quad (5.17)$$

$$\ln(CMC_{DS}) = K_3 + K_g \ln(P) \quad (5.18)$$

$$S = [Na^+]_{un} P (S_{Na}) / \{ CMC_{DS} P_{SDS} \} + [Ca^{+2}]_{un} P^2 (S_{Ca}) / \{ 0.5 CMC_{CaDS} (P_{CaDS})^2 \} \quad (5.19)$$

$$K_g = [Na^+]_{un} P (K_{g, Na}) / \{ CMC_{DS} P_{SDS} \} + [Ca^{+2}]_{un} P^2 (K_{g, Ca}) / \{ 0.5 CMC_{CaDS} (P_{CaDS})^2 \} \quad (5.20)$$

where  $K_2$ ,  $K_3$ , and  $K_g$  are constants,  $K_{g, Na}$  is the value of  $K_g$  when only  $Na^+$  is present,  $K_{g, Ca}$  is the value of  $K_g$  when only  $Ca^+$  is present,  $CMC_{SDS}$  and  $CMC_{CaDS}$  are the CMCs of pure sodium dodecylsulfate and pure calcium dodecylsulfate, without added

electrolyte,  $P$  is a term related to the electrical potential at the micelle surface,  $P_{SDS}$  and  $P_{CDS}$  are the values of  $P$  at  $CMC_{SDS}$  and  $CMC_{CDS}$ , respectively,  $S$  is the surface charge density of the micelle,  $S_{Na}$  is the surface charge density of the micelle when  $Na^+$  is the only counterion present in solution, and  $S_{Ca}$  is the surface charge density of the micelle when  $Ca^{+2}$  is the only counterion present in solution,

The purpose of the equations presented here is to predict the minimum calcium concentration required to cause precipitation at any surfactant concentration. The independent variables include total concentration of each surfactant, and concentration of added sodium chloride. Therefore when  $[SDS]$ ,  $[NPE]$ , and  $[NaCl]$  are set, the dependent variable of interest is  $[CaCl_2]$ . If  $K_{sp}$ ,  $\beta_{Ca}$ ,  $\beta_{Na}$ ,  $K_2$ ,  $K_3$ ,  $K_{g,Na}$ ,  $S_{Na}$ ,  $CMC_{SDS}$ ,  $P_{SDS}$ ,  $K_{g,Ca}$ ,  $S_{Ca}$ ,  $CMC_{CDS}$ ,  $P_{CDS}$ ,  $W/RT$ ,  $CMC_{NPE}$  are known, equations 1 - 20 can be solved simultaneously to obtain  $[CaCl_2]$ ,  $[Ca^{+2}]_{un}$ ,  $[Ca^{+2}]_b$ ,  $[DS^-]_{mon}$ ,  $[DS^-]_{mic}$ ,  $[NPE]_{mon}$ ,  $[NPE]_{mic}$ ,  $[Na^+]_{un}$ ,  $[Na^+]_b$ ,  $I$ ,  $f_{Ca}$ ,  $f_{DS}$ ,  $X_{DS}$ ,  $X_{NPE}$ ,  $\gamma_{DS}$ ,  $\gamma_{NPE}$ ,  $P$ ,  $CMC_{CDS}$ ,  $S$ , and  $K_g$ . Therefore, from the theory presented here, it is possible to predict hardness tolerance ( $[CaCl_2]$ ) for any surfactant concentration, with any anionic-nonionic surfactant composition, and for any amount of added salt.

## RESULTS AND DISCUSSION

### DETERMINATION OF PARAMETERS IN MODEL.

The value of  $K_{sp}$ ,  $K_2$ ,  $K_3$ ,  $K_{g,Na}$ ,  $S_{Na}$ ,  $CMC_{SDS}$ ,  $P_{SDS}$ ,  $K_{g,Ca}$ ,  $S_{Ca}$ ,  $CMC_{CDS}$ , and  $P_{CDS}$ , have been obtained for this system in Part I of this series<sup>1</sup>. It is now necessary to obtain values for  $CMC_{NPE}$ ,  $W/RT$ ,  $\beta_{Ca}$ , and  $\beta_{Na}$ .

$CMC_{NPE}$  was found to be approximately constant over the entire range of electrolyte concentrations of interest in this study at a value of  $4.2 \times 10^{-5}$  M.

Counterion binding on mixed anionic-nonionic micelles has been shown<sup>10,11</sup> to be a function of the micelle mole fraction of anionic surfactant,  $X_{DS}$ . Similarly, binding in mixed (monovalent and divalent) counterion systems is a function of the monovalent/divalent concentration ratio<sup>1</sup>. Currently, there is no known work that has measured counterion binding in systems containing both mixed surfactant and mixed counterions. Fortunately, the overall mole fraction of NPE (i.e.,  $[NPE]/([SDS]+[NPE])$ ) in the mixtures studied here does not exceed 0.1, so micellar mole fractions of  $DS^-$  are high. At high  $X_{DS}$ , values for counterion binding ( $\beta_{Na}$  and  $\beta_{Ca}$ ) are approximately equal<sup>10,11</sup> to the values of counterion binding on a pure anionic micelle<sup>1</sup> ( $\beta_{Na}^0 = 0.20$  and  $\beta_{Ca}^0 = 0.45$ ).

The following equations define the relationship between

the mixture CMC ( $CMC_{mix}$ ) and the monomer mole fraction of anionic surfactant ( $Y_{ds}$ ) at the CMC of the mixture:

$$Y_{ds} CMC_{mix} = [DS^-]_{mon} \quad (5.21)$$

$$(1 - Y_{ds}) CMC_{mix} = [NPE]_{mon} \quad (5.22)$$

The final parameter needed in the model is  $W/RT$ . Using equations 5.11-5.14, 5.16, 5.21, and 5.22,  $CMC_{mix}$  data as a function of  $Y_{ds}$  can be used to obtain a best-fit value of  $W/RT$  at a specific added electrolyte concentration and temperature. The curves shown in Figures 5.2, 5.3, and 5.4 are the results of such analysis at different unbound  $Na^+$  concentrations and regular solution theory can be seen to fit  $CMC_{mix}$  data very well. Only at the CMC is the unbound  $Na^+$  concentration equal to the total  $Na^+$  concentration. As shown in Figure 5, the resultant values of  $W/RT$  decrease as  $[Na^+]_{un}$  increases. This is due to the fact that as electrolyte concentration increases, the electrical potential at the micelle surface decreases, which implies a reduction in electrostatic repulsion between ionic groups in the micelle. This means that the synergistic effect of adding nonionic surfactant (which also reduces surface electrical potential<sup>10,11</sup>) is decreased as electrolyte concentration increases. The data in Figure 5.5 can be described by the relationship:

$$\ln(-W/RT) = -0.2105 \ln([Na^+]_{un}) + 0.1975 \quad (5.23)$$

Obviously, unbound  $Ca^{+2}$  will also affect the value of  $W/RT$ . To account for this, it is assumed that the mixture of  $Ca^{+2}$  and  $Na^+$  can be translated into an "equivalent"  $Na^+$  concentration. For any value of  $[Ca^{+2}]_{un}$  and  $[Na^+]_{un}$ ,  $CMC_{ds}$  can be calculated from equations 5.17-5.20. There is a corresponding unbound  $Na^+$  concentration,  $[Na^+]_{eq}$ , that gives the same value of  $CMC_{ds}$  in a  $NaDS + NaCl$  solution (without added divalent counterion). Assuming the same electrostatic effects for  $W/RT$  in the  $Na^+-Ca^{+2}$  mixture and the  $Na^+$ -only system (at the same value of  $CMC_{ds}$ ),  $W/RT$  for the  $Na^+-Ca^{+2}$  mixture can be calculated from equation 5.23 using  $[Na^+]_{eq}$  in the place of  $[Na^+]_{un}$ . When  $CMC_{ds}$  is known for given values of  $[Na^+]_{un}$  and  $[Ca^{+2}]_{un}$ , the equivalent  $Na^+$  concentration can be calculated by:

$$\ln(CMC_{ds}) = -0.69832 \ln([Na^+]_{eq}) - 8.5134 \quad (5.24)$$

Divalent magnesium is similar to divalent calcium in its effect on the CMC of anionic surfactants, yet has a much higher  $K_{sp}$ , so micellization can be studied over a much wider range<sup>1</sup>. Therefore, we will present effects of  $Mg^{+2}$  on CMC with the understanding that this is equivalent to the effect of  $Ca^{+2}$  on the CMC. For example, Figure 5.6 gives  $CMC_{mix}$  data for  $[Na^+]_{un} = 0.01175$  M and  $[Mg^{+2}]_{un} = 0.001$  M. For anionic surfactant only ( $Y_{ds} = 1$ ), the value of  $CMC_{ds}$  is equal to

1.750 x 10<sup>-3</sup> M. From equation 24, the unbound Na<sup>+</sup> concentration (without added divalent cation) required to give the same CMC<sub>Ds</sub>, is [Na<sup>+</sup>]<sub>eq</sub> = 0.0450 M. When this value is used in eq 24 for [Na<sup>+</sup>]<sub>un</sub>, it results in a calculated value of W/RT = -2.34. The actual value of W/RT determined experimentally in Figure 5.6 is W/RT = -2.15. It will be shown that the predictions of precipitation boundaries are not highly sensitive to the value of W/RT. Calculation of W/RT can be simplified by combining equations 5.23 and 5.24 to give:

$$\ln(-W/RT) = 0.3014 \ln(\text{CMC}_{Ds}) + 2.765 \quad (5.25)$$

### PRECIPITATION BOUNDARY PREDICTIONS FROM MODEL

At this point, all the parameters that are required to predict precipitation boundaries have been obtained as shown in Table 5.1. Using these values, equations 5.1-5.20 with eq 5.25, must be solved simultaneously to predict the hardness tolerance of an anionic-nonionic surfactant mixture with both monovalent and divalent counterions present.

Figure 5.7 shows the experimental and predicted precipitation boundary for the anionic-nonionic surfactant mixture, containing 10% nonionic surfactant (i.e., [NPE]/([SDS]+[NPE]) = 0.10), with no added NaCl. The precipitation phase boundary<sup>1</sup> for NaDS-only has also been included in Figure 5.7 to show the benefit of adding nonionic surfactant. It can be seen that by adding 10% NPE, the minimum hardness tolerance for the SDS + CaCl<sub>2</sub> system increases approximately 850%. This serves to demonstrate the tremendous potential of using anionic-nonionic mixtures in applications where the sensitivity of anionic surfactants to hard ions must be reduced. It is possible to understand why hardness tolerance increases with added nonionic surfactant by considering Figures 5.2-5.4 and 5.6. When a small amount of nonionic surfactant is added to anionic surfactant, CMC<sub>mix</sub> decreases rapidly due to a reduction of electrostatic repulsion in the micelles. From equation 21, as CMC<sub>mix</sub> decreases, the monomer concentration of anionic surfactant, [DS<sup>-</sup>]<sub>mon</sub>, also decreases. Therefore, a higher concentration of unbound Ca<sup>2+</sup> is required to cause precipitation to occur (equation 1). The curve in Figure 5.7 is a true prediction, without adjustable parameters.

One advantage of the model presented here is that, without additional data, it can predict the precipitation boundary of the NaDS + CaCl<sub>2</sub> system for any amount of added nonionic surfactant and any concentration of added NaCl. Figure 5.8 gives predictions for 10% added NPE with 0.02 M added NaCl. The predictions for this system show excellent agreement with the experimentally determined precipitation boundary except at very high CaCl<sub>2</sub> concentrations. Figure 5.9 gives results for 10% added NPE with 0.10 M added NaCl. The

curve labeled  $K_{g,ca} = 0.895$  and  $CMC_{cds} = 1.9 \times 10^{-3} \text{ M}$  is the a priori predictive model and it can be seen that the predictions for this system are not as accurate at these high salinities. The experimentally determined increase in minimum hardness tolerance is 1400% for the 0.02 M NaCl system and 5000% for the 0.10 M NaCl system, both compared to the NaDS-only system without added NaCl.

From Figure 5.9, it seems that the model has difficulty in giving good predictions at high  $\text{CaCl}_2$  concentrations. This corresponds to high NaCl concentrations, under which conditions hardness tolerance is increased ( $\text{CaCl}_2$  concentrations on the phase boundary are increased). The main reason for this is that the model is sensitive to the value of  $CMC_{cds}$  calculated from equations 5.17-5.20. An accurate value for  $CMC_{cds}$  is important because it greatly affects the monomer concentration of  $\text{DS}^-$  that is obtained from equation 5.11. If  $[\text{DS}^-]_{\text{mon}}$  has significant error, then the calculated value of  $[\text{Ca}^{+2}]_{\text{un}}$  will be greatly in error (equation 5.1). The parameters used in equations 5.17-5.20 must be obtained from data taken at low divalent counterion concentrations. The probable cause of the deviation between predictions and experimental data at high  $\text{CaCl}_2$  concentrations is the required extrapolation of these values. The values of  $CMC_{cds}$  and  $K_{g,ca}$  were obtained from experimental  $CMC_{cds}$  data<sup>1</sup>. If these values are changed, such that  $CMC_{cds} = 2.00 \times 10^{-3} \text{ M}$  and  $K_{g,ca} = 0.84$ , the calculations from the model improve substantially at high  $\text{CaCl}_2$  concentrations, as shown in Figure 5.9 for the 10% NPE + 0.10 M NaCl system. Table 5.2 gives a comparison between calculated and experimental values of  $CMC_{cds}$  using  $CMC_{cds} = 2.00 \times 10^{-3} \text{ M}$  and  $K_{g,ca} = 0.84$ . The only other parameters in Table 5.1 which are changed by changing the values of  $CMC_{cds}$  and  $K_{g,ca}$  are  $S_{ca}$  and  $P_{cds}$ . The use of these values still gives excellent prediction of CMC values (Table 5.2), while substantially improving the prediction of the precipitation phase boundaries. Results of this work serve to emphasize the need to fully investigate the effect of monovalent-divalent counterion mixtures on the CMC of anionic surfactants.

For the SDS-only solutions presented in reference 1, the CMC corresponded to the calculated minimum  $\text{CaCl}_2$  concentration for each precipitation boundary. In Figure 5.10, however, it is not possible to identify a CMC along any of the precipitation boundaries because micelles are present at all NaDS concentrations shown. At the CMC for an anionic-nonionic mixture, all surfactant is present as monomer so that the monomer mole fraction,  $Y_{ds}$ , is equal to the overall mole fraction. For a mixture containing 10% NPE, therefore,  $Y_{ds} = 0.9$ . This corresponds to a low  $CMC_{\text{mix}}$  in Figures 5.2-5.4 and 5.6, which implies a low  $\text{DS}^-$  monomer concentration. As the total surfactant concentration increases to a point which is far above the CMC, virtually all surfactant is present as micelles so the micellar mole fraction,  $X_{ds}$ , is equal to the

overall mole fraction (0.90 in this case). At this point, essentially all nonionic surfactant is present in the mixed micelles and the value of  $Y_{ds}$  is much higher than 0.9. This means (from Figures 5.2-5.4 and 5.6) that as the total surfactant concentration increases and the corresponding value of  $[DS^-]_{mon}$  increases. As  $[DS^-]_{mon}$  increases,  $[Ca^{+2}]_{un}$  must decrease as dictated by the solubility product (eq 5.1). Therefore, the curves in Figure 5.10 are at high  $[CaCl_2]$  values at low total surfactant concentration, but drop as total surfactant concentration increases.

The higher the concentration of micelles in solution, the higher the concentration of bound  $Ca^{+2}$ . Hence, a higher total  $Ca^{+2}$  concentration is necessary for the unbound calcium concentration to permit the solubility product to be exceeded. The minima in Figure 5.10 occur at the points where the amount of  $Ca^{+2}$  bound on micelles begins to account for a significant percentage of the total  $Ca^{+2}$  present in solution. At still higher surfactant concentrations, binding dominates so that virtually all of the  $Ca^{+2}$  in the mixture is bound onto the micelles and the hardness tolerance becomes proportional to the total surfactant concentration.

The precipitation boundary for 10% NPE without added NaCl (Figure 5.8) describes the data well at low NaDS concentrations. In this region, there are so few micelles in solution that binding is insignificant. Therefore, hardness tolerance depends entirely on the value of  $[DS^-]_{mon}$  calculated by regular solution theory. The agreement between predictions and experiments in this region implies that regular solution theory does an adequate job of calculating monomer-micelle equilibrium, a conclusion reached in other work<sup>8, 12</sup>.

Discrepancies between calculated and experimental values occur around the minimum point in the precipitation boundary; i.e., where the amount of  $Ca^{+2}$  bound on micelles becomes an important quantity. For the model to fit the data, a higher value of  $Ca^{+2}$  counterion binding ( $\beta_{ca}$ ) would be necessary in this region. However, as NaDS concentration continues to increase, the actual binding approaches the value of  $\beta_{ca}$  (0.20) which was used in the model. Figure 11 shows the values of  $\beta_{ca}$  that are required to fit the experimental precipitation data. Binding in mixed electrolyte systems is a complicated process and presently there are no theories available to describe these results. It has been shown, however, that binding depends on the  $Ca^{+2}/Na^+$  ratio in solution<sup>13, 14</sup>. It is not surprising, then, that a higher value for  $\beta_{ca}$  is observed around the minimum of the boundary without added NaCl, since there is a relatively high  $Ca^{+2}/Na^+$  ratio at this point. At the same time, a value of  $\beta_{ca} = 0.20$  predicts the precipitation boundary with 0.02 M added NaCl very well. This is probably due to a lower  $Ca^{+2}/Na^+$  ratio (because of added NaCl) in the region where binding becomes

important.

In order to test the sensitivity of the model to the value of  $W/RT$ , Figure 5.12 compares calculations from the model using  $W/RT = -5.00$ ,  $W/RT = 0.0$  (ideal solution), and  $W/RT$  obtained from equation 23. This figure shows that it is not possible to assume the micelles behave ideally under these conditions because significant errors result. Interestingly, even with an unreasonably low value of  $W/RT = -5.0$ , the calculated boundary does not agree with experimental results around the minimum. This seems to confirm the fact that the error in this region is the result of using too low a value for calcium binding,  $\beta_{Ca}$ , not to deficiencies in regular solution theory to model mixed micelle formation.

The precipitation boundaries obtained from the model were not sensitive to the value of  $CMC_{NPE}$  used. There was essentially no change in calculated quantities in the range of  $CMC_{NPE} = 30 \times 10^{-6} \text{ M}$  to  $55 \times 10^{-6} \text{ M}$ . Therefore, for the precipitation boundary without added NaCl, an inadequate description of counterion binding is responsible for the error in the predictions obtained from the model.

#### RELATIONSHIP TO PREVIOUS WORK

Fan et. al.<sup>15</sup> used a similar approach to that taken here to describe the effect of nonionic surfactant on precipitation of SDS by calcium and magnesium. In that work, several concentrations of added nonionic surfactant were used, whereas we only studied one nonionic surfactant concentration. However, no added monovalent electrolyte was added to those systems and the monomeric anionic surfactant concentration above the CMC was assumed to be affected only by the added divalent cation (not the monovalent cation).

Nishikido et. al.<sup>16</sup> found that the Krafft temperatures of divalent metal dodecylsulfates was lowered when nonionic surfactant was added, which corresponds to an increase in hardness tolerance.

Gerbacia<sup>17</sup> measured hardness tolerance in the same four component system presented here (with a different nonionic surfactant) and demonstrated that hardness tolerance increased as ionic strength was increased; which is the same result given in this study. In that work, the counterion binding of  $Ca^{+2}$  was shown to decrease as the  $Na^{+}/Ca^{+2}$  ratio increased, consistent with this work.

Noik et. al.<sup>18</sup> has presented the entire precipitation boundary for a four component mixture but they include butanol rather than nonionic surfactant. In that work, the increase in hardness tolerance, with added butanol, is attributed to a decrease in anionic surfactant monomer

concentration.

Shah et. al.<sup>19</sup> reported the influence of ethoxylated sulfonates on the hardness tolerance of an anionic surfactant, and demonstrated that hardness tolerance increases as the percent of ethoxylated sulfonate increases. Interestingly, they mention that precipitation boundaries merge to follow the same curve at high anionic surfactant concentrations (the same result seen in this study).

The general phenomena of reduction of surfactant monomer concentrations upon mixed micelle formation has been discussed in literature review articles<sup>8,20</sup>. Several authors<sup>15,21,22</sup> have identified that mixed micelle formation is the mechanism by which hardness tolerance is increased when nonionic surfactant is added.

## NOMENCLATURE

$c_i$	concentration of ion $i$ in solution, $\text{kmol/m}^3$
$[\text{CaCl}_2]$	total concentration of $\text{CaCl}_2$ in solution, $\text{kmol/m}^3$
$[\text{Ca}^{+2}]_b$	concentration of $\text{Ca}^{+2}$ bound on micelles, $\text{kmol/m}^3$
$[\text{Ca}^{+2}]_{un}$	concentration of unbound $\text{Ca}^{+2}$ in solution, $\text{kmol/m}^3$
CMC	critical micelle concentration, $\text{kmol/m}^3$
CMC <sub>CDs</sub>	CMC of pure $\text{Ca}(\text{DS})_2$ , $\text{kmol/m}^3$
CMC <sub>DS</sub>	CMC of SDS under various conditions, $\text{kmol/m}^3$
CMC <sub>mix</sub>	measured mixtures CMC values, $\text{kmol/m}^3$
CMC <sub>NPE</sub>	CMC of pure NPE, $\text{kmol/m}^3$
CMC <sub>SDS</sub>	CMC of pure NaDS, $\text{kmol/m}^3$
$[\text{DS}^-]_{mic}$	concentration of $\text{DS}^-$ present in micelles, $\text{kmol/m}^3$
$[\text{DS}^-]_{mon}$	concentration of $\text{DS}^-$ present as monomer, $\text{kmol/m}^3$
$f_{ca}$	activity coefficient of unbound $\text{Ca}^{+2}$ in solution
$f_{ds}$	activity coefficient of monomeric $\text{DS}^-$ in solution
$I$	ionic strength, $\text{kmol/m}^3$
$K_3, K_g$	constants
$K_2$	constant, $\text{Mm}^4\text{C}^{-2}$
$K_{g, Ca}$	value of $K_g$ when $\text{Ca}^{+2}$ is the only counterion present in solution
$K_{g, Na}$	value of $K_g$ when $\text{Na}^+$ is the only counterion present in solution
$K_{sp}$	solubility product, $\text{M}^3$
$[\text{Na}^+]_b$	concentration of $\text{Na}^+$ bound on micelles, $\text{kmol/m}^3$
$[\text{Na}^+]_{eq}$	concentration of $\text{Na}^+$ in solution which would have the same effect on the CMC of the anionic surfactant as the actual mixture of counterions in solution, $\text{kmol/m}^3$

$[\text{Na}^+]_{\text{tot}}$	total concentration of $\text{Na}^+$ ions in solution, $\text{kmol/m}^3$
$[\text{Na}^+]_{\text{un}}$	concentration of unbound $\text{Na}^+$ in solution, $\text{kmol/m}^3$
$[\text{NaCl}]$	total concentration of $\text{NaCl}$ in solution, $\text{kmol/m}^3$
$[\text{NPE}]$	total concentration of $\text{NPE}$ in solution, $\text{kmol/m}^3$
$[\text{NPE}]_{\text{mic}}$	concentration of $\text{NPE}$ present in micelles, $\text{kmol/m}^3$
$[\text{NPE}]_{\text{mon}}$	concentration of $\text{NPE}$ present as monomer, $\text{kmol/m}^3$
$P$	term related to $\Phi_0$
$P_{\text{CDs}}$	value of $P$ at the CMC of pure $\text{Ca}(\text{DS})_2$
$P_{\text{SDS}}$	value of $P$ at the CMC of pure $\text{NaDS}$
$R$	gas constant, $1.987 \text{ kcal}/(\text{kmol K})$
$S$	surface charge density of micelle, $\text{Cm}^{-2}$
$S_{\text{Ca}}$	surface charge density of micelle when $\text{Ca}^{+2}$ is the only counterion present in solution, $\text{Cm}^{-2}$
$[\text{SDS}]$	total concentration of $\text{NaDS}$ in solution, $\text{kmol/m}^3$
$S_{\text{Na}}$	surface charge density of micelle when $\text{Na}^+$ is the only counterion present in solution, $\text{Cm}^{-2}$
$T$	absolute temperature, $\text{K}$
$W$	regular solution theory interaction parameter, $\text{kcal/kmol}$
$X_{\text{DS}}$	mole fraction of $\text{DS}^-$ in the micelle
$X_{\text{NPE}}$	mole fraction of $\text{NPE}$ in the micelle
$Y_{\text{DS}}$	mole fraction of $\text{DS}^-$ in the monomer
$z_i$	valence of species $i$ in solution
$\beta_{\text{Ca}}$	fractional counterion binding of $\text{Ca}^{+2}$ on micelle
$\beta_{\text{Na}}$	fractional counterion binding of $\text{Na}^+$ on micelle
$\beta_{\text{Ca}}^0$	fractional counterion binding of $\text{Ca}^{+2}$ on micelle in absence of nonionic surfactant
$\beta_{\text{Na}}^0$	fractional counterion binding of $\text{Na}^+$ on micelle

in absence of nonionic surfactant

$\gamma_{DS}$  activity coefficient of  $DS^-$  in the micelle

$\gamma_{NPE}$  activity coefficient of NPE in the micelle

## REFERENCES

1. Stellner, K.L.; Scamehorn, J.F. Langmuir, In Press.
2. Stellner, K.L.; Scamehorn, J.F. J. Am. Oil Chem. Soc. **1986**, 63, 566.
3. Nagarajan, M.K., Paine, H.L. J. Am. Oil Chem. Soc., **1984**, 61, 1475.
4. LaLanne-Cassou, C.; Carmona, I.; Fortney, L.; Samii, A.; Schechter, R.S.; Wade, W.H.; Weerasooriya, U.; Weerasooriya, V.; Yiv, S., SPE Paper No. 12035, Presented at the 58th Annual Technical Conference and Exhibition of the Society of Petroleum Engineers, San Francisco, October, 1983.
5. Cox, M.F.; Borys, N.F.; Matson, T.P. J. Am. Oil Chem. Soc. **1985**, 62, 1139.
6. Kravetz, L.; Scharer, D.H.; Stupel, H. Tr. Mezhdunar. Kongr. Poverkhn. Akt. Veshchestvam 7th 1978, 3, 192.
7. Novosad, J.; Maini, B.; Batycky, J. J. Am. Oil Chem. Soc. **1982**, 59, 833.
8. Scamehorn, J.F. In "Phenomena in Mixed Surfactant Systems"; Scamehorn, J.F., Ed.; American Chemical Society: Washington, 1986, p. 1.
9. Scamehorn, J.F.; Schechter, R.S.; Wade, W.H. J. Dispersion Sci. Technol. **1982**, 3, 261.
10. Rathman, J.F.; Scamehorn, J.F. J. Phys. Chem. **1984**, 88, 5807.
11. Rathman, J.F.; Scamehorn, J.F. Langmuir **1987**, 3, 372.
12. Nguyen, C.M.; Rathman, J.F.; Scamehorn, J.F. J. Colloid Interface Sci. **1986**, 112, 438.
13. Koshinuma, M. Bull. Chem. Soc. Japan. **1983**, 56, 2341.
14. Corkill, J.M.; Goodman, J.F. Trans. Faraday Soc. **1962**, 58, 206.
15. Fan, X.-J., Stenius, P., Kallay, N., Matijevic, E., J. Colloid Interface Sci. **1988**, 121, 571.
16. Nishikido, N.; Akisada, H.; Matuura, R. Mem. Fac. Sci., Kyushu Univ., Ser. C **1977**, 10, 91.

17. Gerbacia, W.E.F. J. Colloid Interface Sci. 1983, 93, 556.
18. Noik, C.; Baviere, M.; Defives, D. J. Colloid Interface Sci. 1987, 115, 36.
19. Shah, D.O.; Walker, R.D., Annual Report for DOE Contract DE-AC1979BC10075, p. III-25 - III-27.
20. Rosen, M.J., In "Phenomena in Mixed Surfactant Systems"; Scamehorn, J.F., Ed.; American Chemical Society: Washington, 1986, p. 144.
21. Cox, M.F.; Matheson, K.L. J. Am. Oil Chem. Soc. 1985, 62, 1396.
22. Chiu, Y. In "Solution Behavior of Surfactants", Volume 2, Mittal, K.L., Ed.; Plenum Press: New York, 1980, p. 1415.

Table 5.1  
Summary of Parameters Used in Model.

Parameter	Value	Source
$K_{sp}$	$5.02 \times 10^{-10} \text{ M}^3$	Reference 1
$\beta_{Ca}$	0.20	This Paper
$\beta_{Na}$	0.45	This Paper
$K_2$	$2.8724 \times 10^5 \text{ Mm}^4 \text{C}^{-2}$	Reference 1
$K_3$	-10.5396	Reference 1
$K_{g, Na}$	0.69832	Reference 1
$S_{Na}$	$7.960 \times 10^{-3} \text{ Cm}^{-2}$	Reference 1
$CMC_{NPE}$	$4.2 \times 10^{-5} \text{ M}$	This Paper
$CMC_{SDS}$	$6.652 \times 10^{-3} \text{ M}$	Reference 1
$P_{SDS}$	2736.32	Reference 1
$K_{g, Ca}$	0.895	Reference 1
$S_{Ca}$	$6.816 \times 10^{-2} \text{ Cm}^{-2}$	Reference 1
$CMC_{CDS}$	$1.900 \times 10^{-3} \text{ M}$	Reference 1
$P_{CDS}$	118.52	Reference 1
W/RT	From eq 23 or 25	This Paper

Table 5.2  
 Comparison Between Calculated and Experimental  
 Values of CMC<sub>ds</sub> with Added NaCl and MgCl<sub>2</sub> (all  
 Concentrations in mM).  $K_{g,ca} = 0.84$ ,  
 $CMC_{cds} = 2.0 \times 10^{-3} \text{ M}$ .

[NaCl]	[Mg <sup>2+</sup> ] <sub>un</sub> <sup>a</sup>	[Na <sup>+</sup> ] <sub>un</sub> <sup>b</sup>	Calc. <sup>c</sup> CMC <sub>ds</sub>	Exper. CMC <sub>ds</sub>	error
0.0	0.100	4.5762	4.5762	4.450	+2.8%
0.0	0.300	3.1445	3.1445	2.800	+12.3%
0.0	1.000	1.9659	1.9659	1.930	+1.9%
10.0	1.000	11.807	1.8071	1.750	+3.3%
20.0	0.500	22.046	2.0464	1.900	+7.7%
20.0	3.000	21.143	1.1425	1.150	-0.7%
100.0	0.600 <sup>d</sup>	101.01	1.0070	0.965	+4.4%

a [Mg<sup>2+</sup>]<sub>un</sub> = [MgCl<sub>2</sub>]

b [Na<sup>+</sup>]<sub>un</sub> = [NaCl] + [SDS]

c Calculated from eqs 17 - 20

d This point is for CaCl<sub>2</sub>, not MgCl<sub>2</sub>

Figure 5.1: Schematic of Equilibrium Existing in System

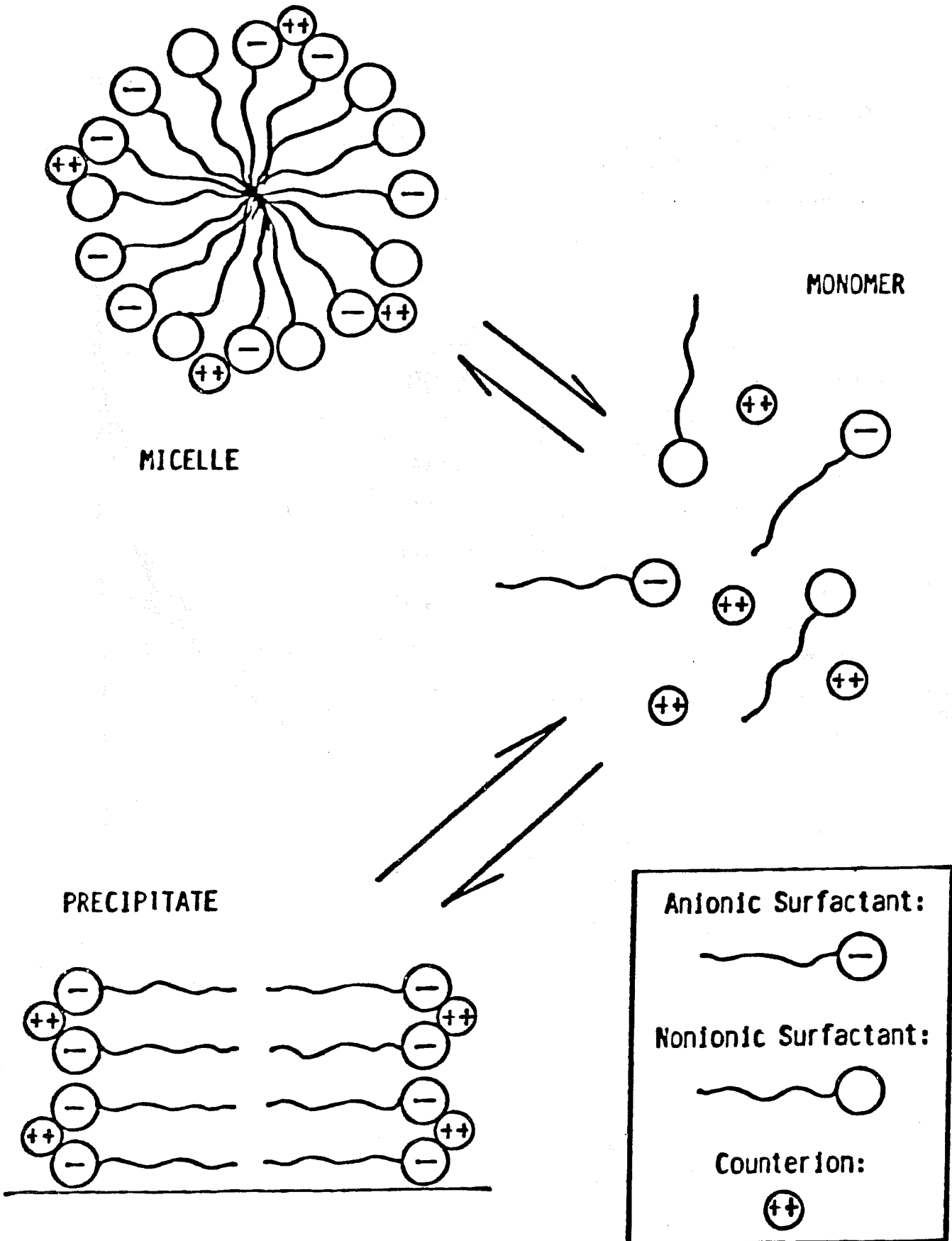


Figure 5.2: CMC of Mixed Surfactant System at  $[Na^+]_{un} = 0.01$  M

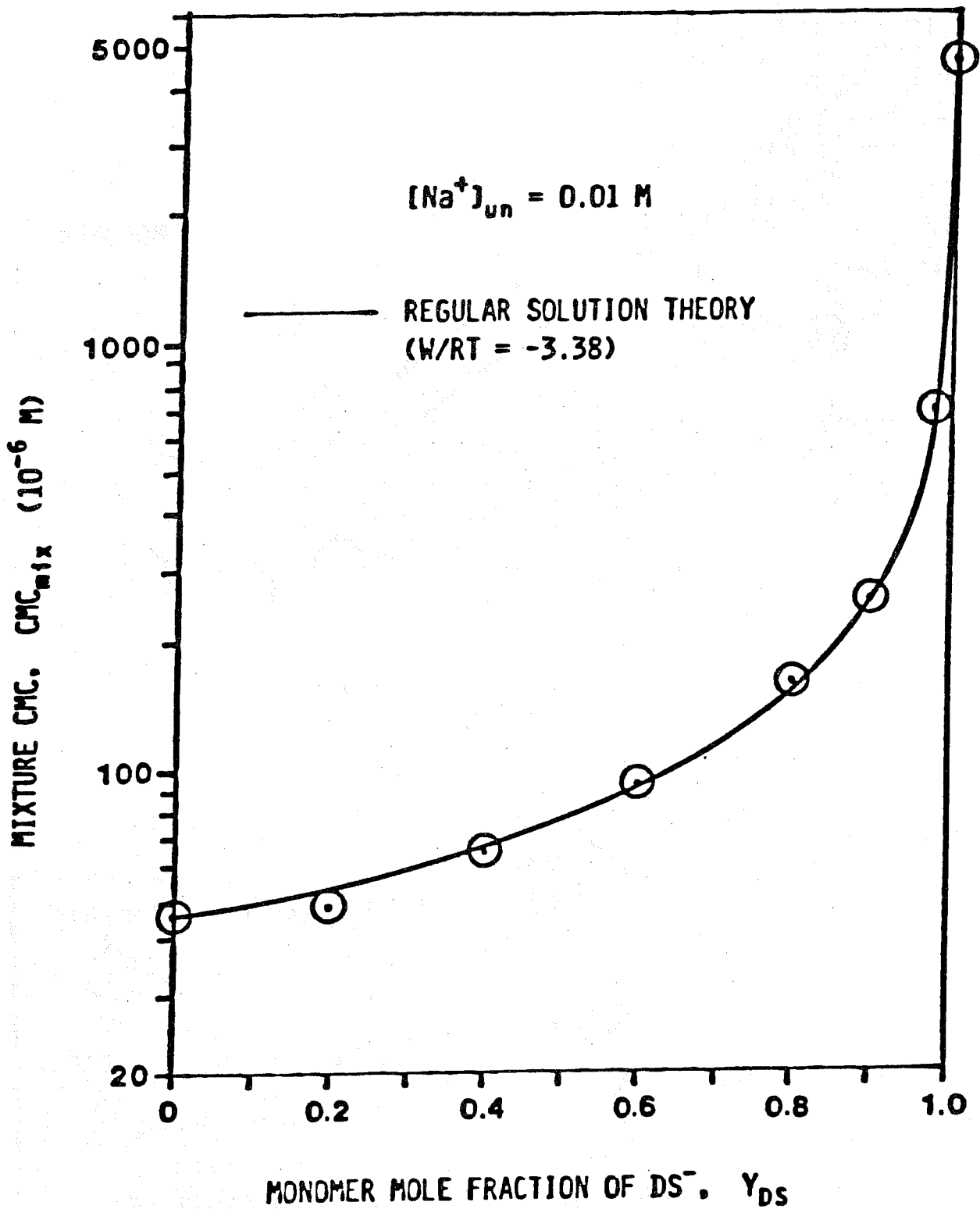


Figure 5.3: CMC of Mixed Surfactant System at  $[Na^+]_{un} = 0.02 M$

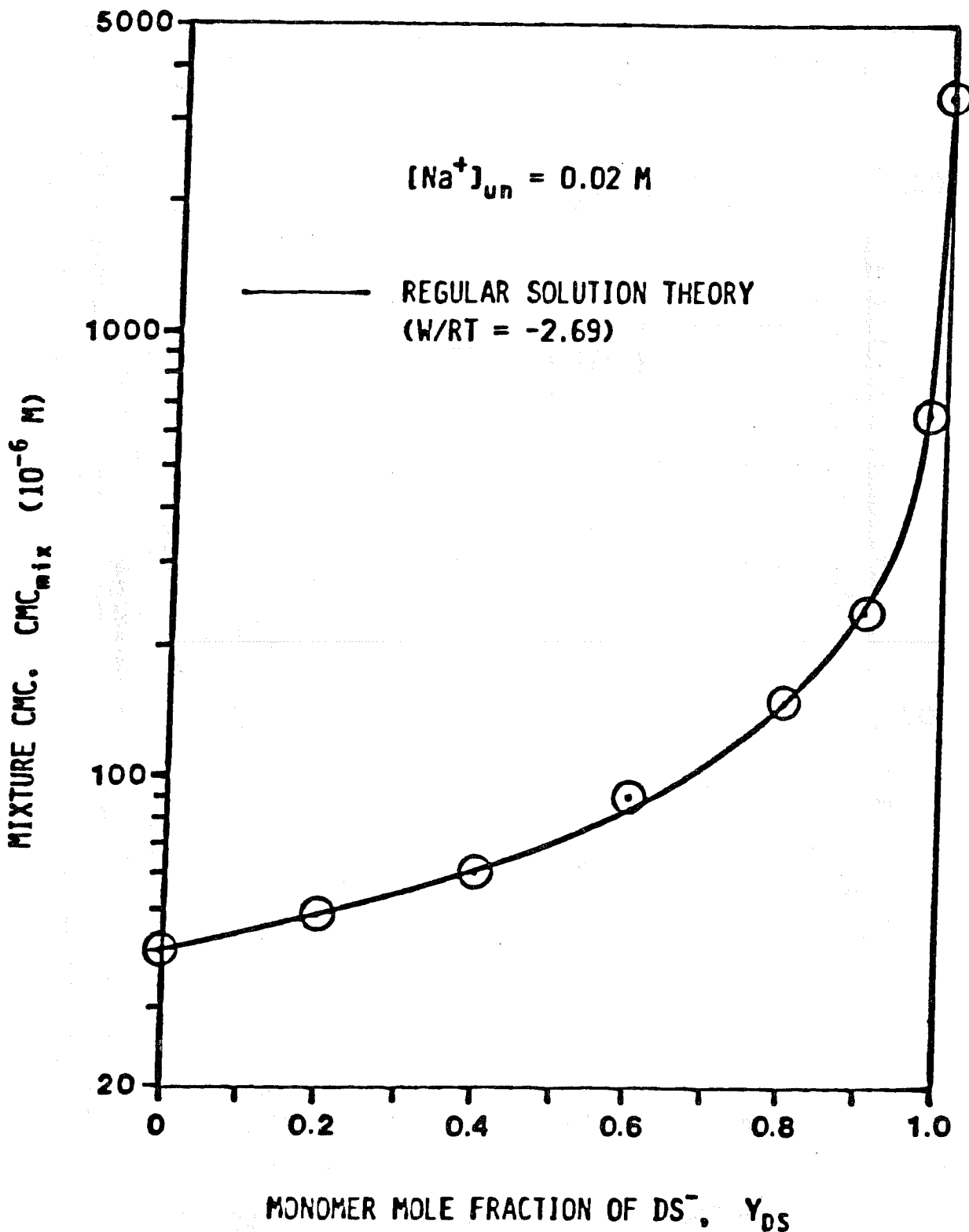


Figure 5.4: CMC of Mixed Surfactant System at  $[Na^+]_{un} = 0.10 \text{ M}$

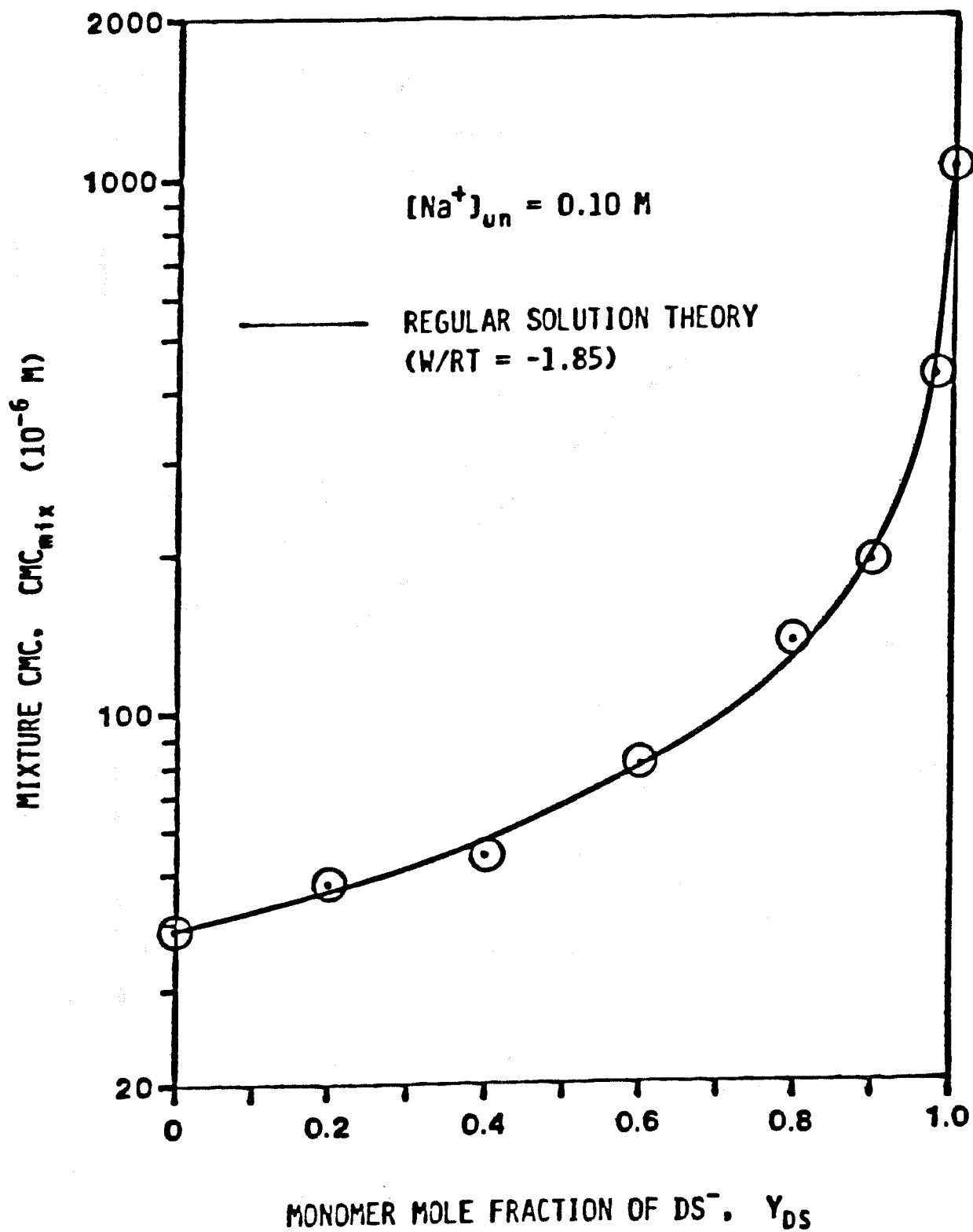


Figure 5.5: Effect of Unbound Na<sup>+</sup> Concentration on W/RT

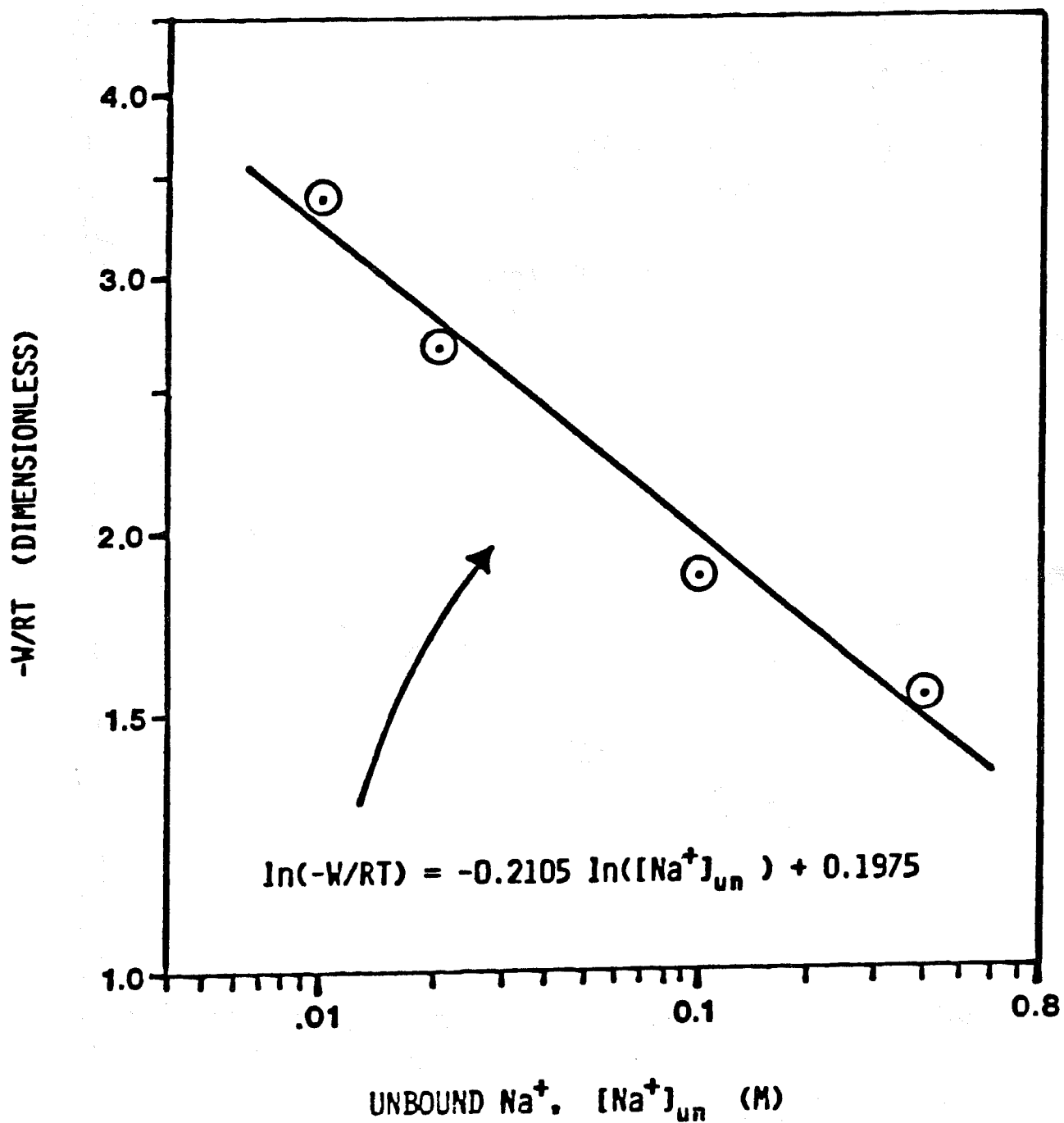


Figure 5.6: CMC of Mixed Surfactant System With Mixed Electrolytes Present

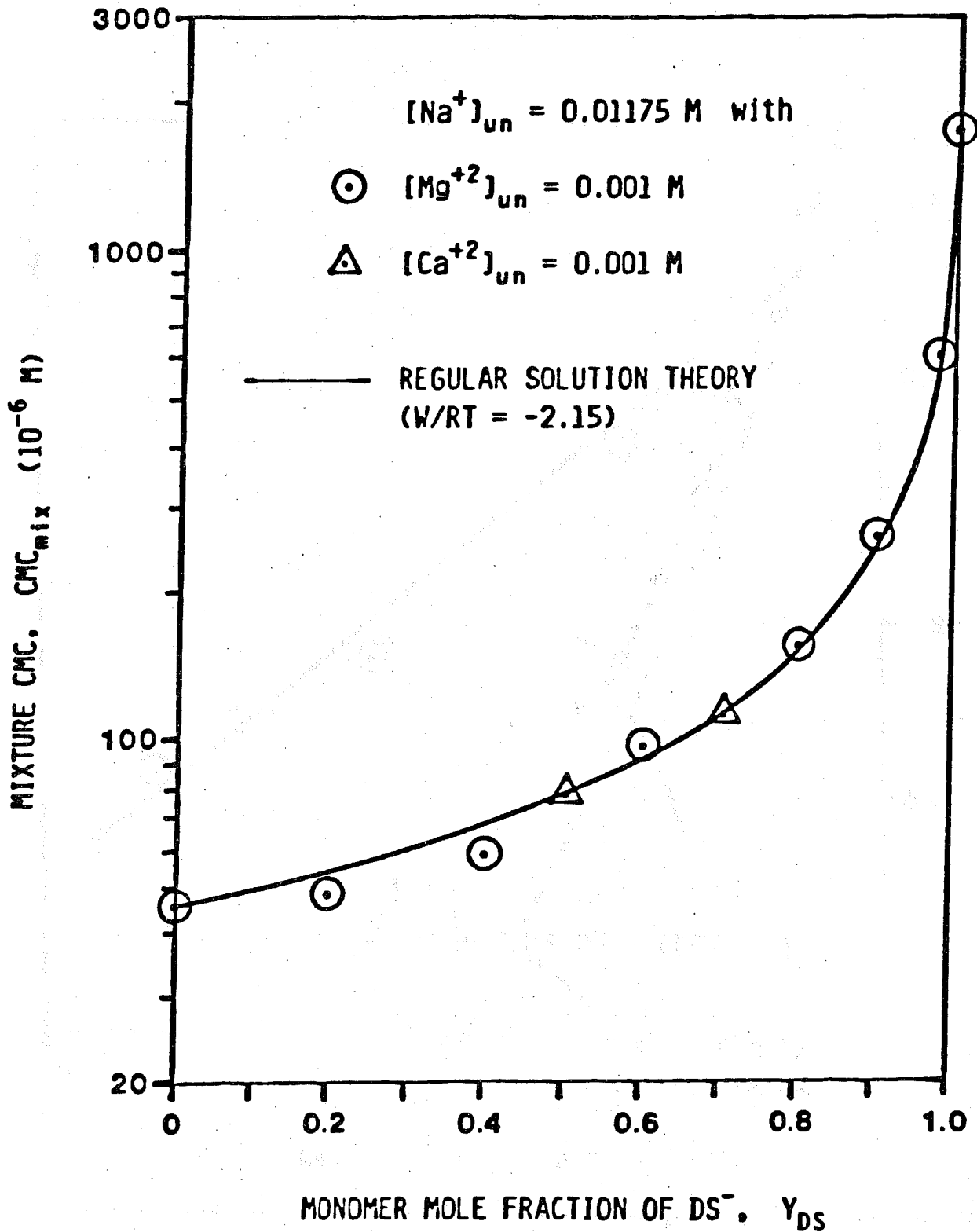


Figure 5.7: Precipitation Phase Boundary Without Added NaCl and With and Without Added Nonionic Surfactant

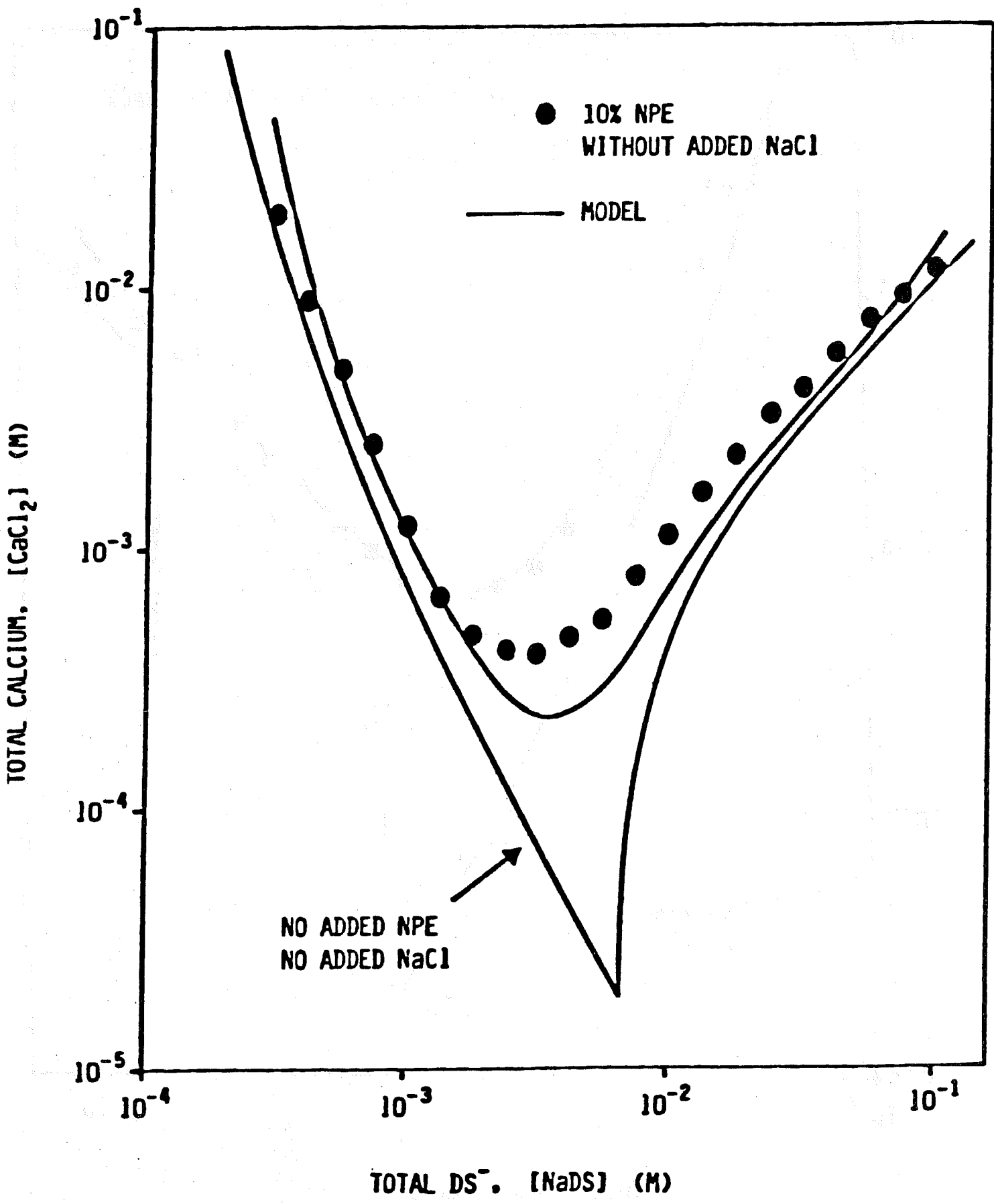


Figure 5.8: Precipitation Phase Boundary With Nonionic surfactant and 0.02 M Added NaCl and Without Added Nonionic Surfactant or Added NaCl

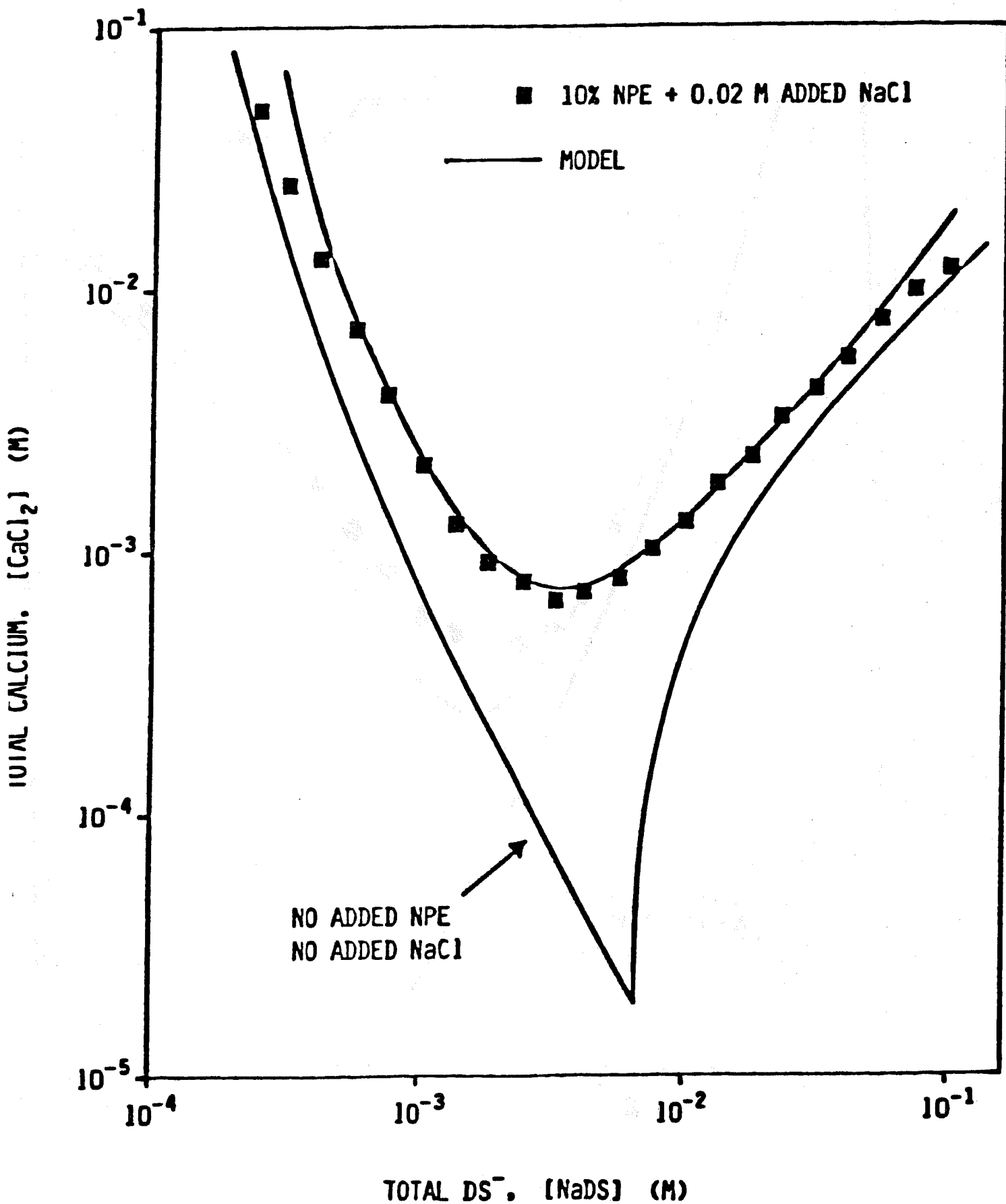


Figure 5.9: Precipitation Phase Boundary With Nonionic surfactant and 0.10 M Added NaCl and Without Added Nonionic Surfactant or Added NaCl

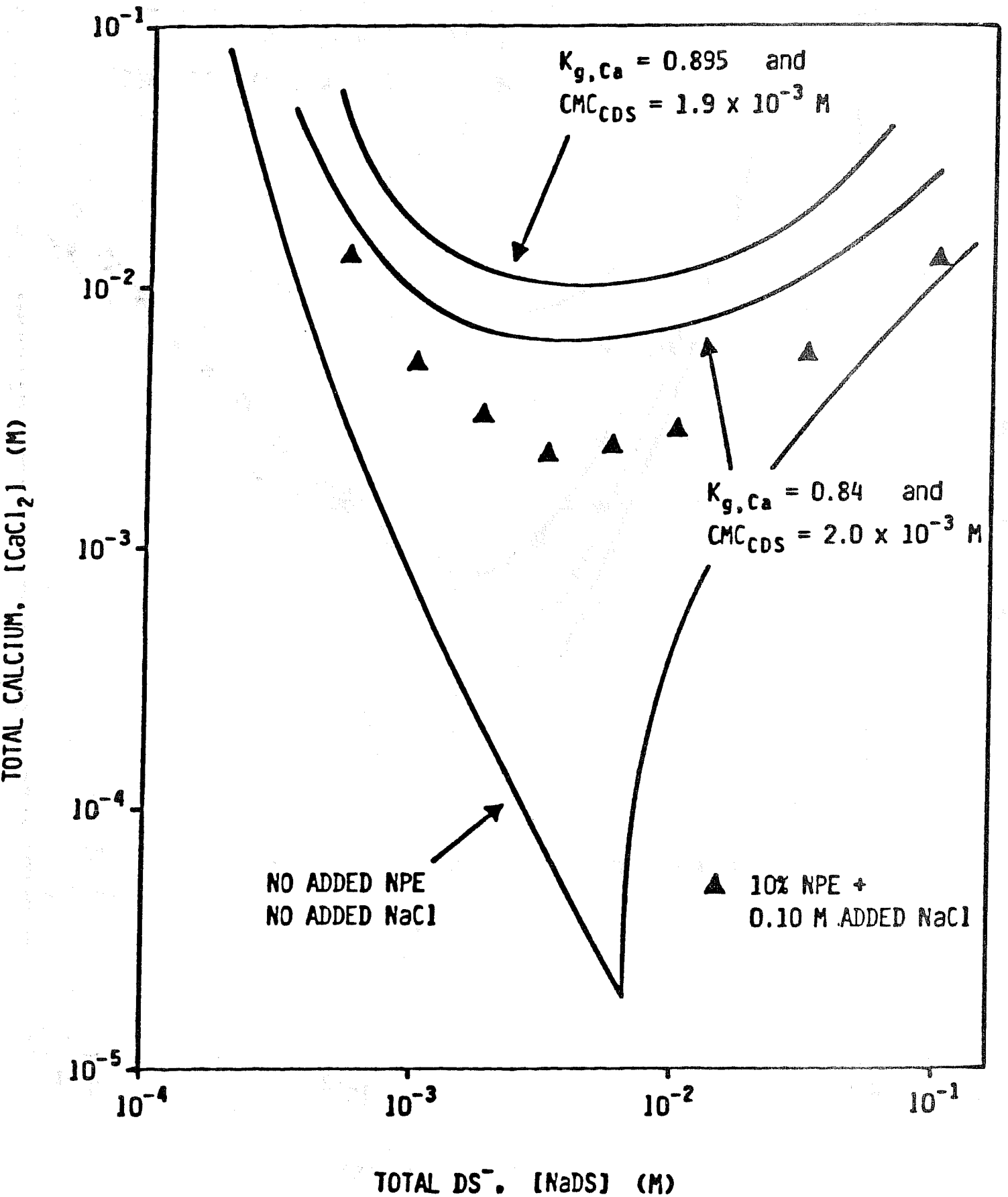


Figure 5.10: Comparison of Precipitation Phase Boundaries With Predictions Using Modified Model Parameters

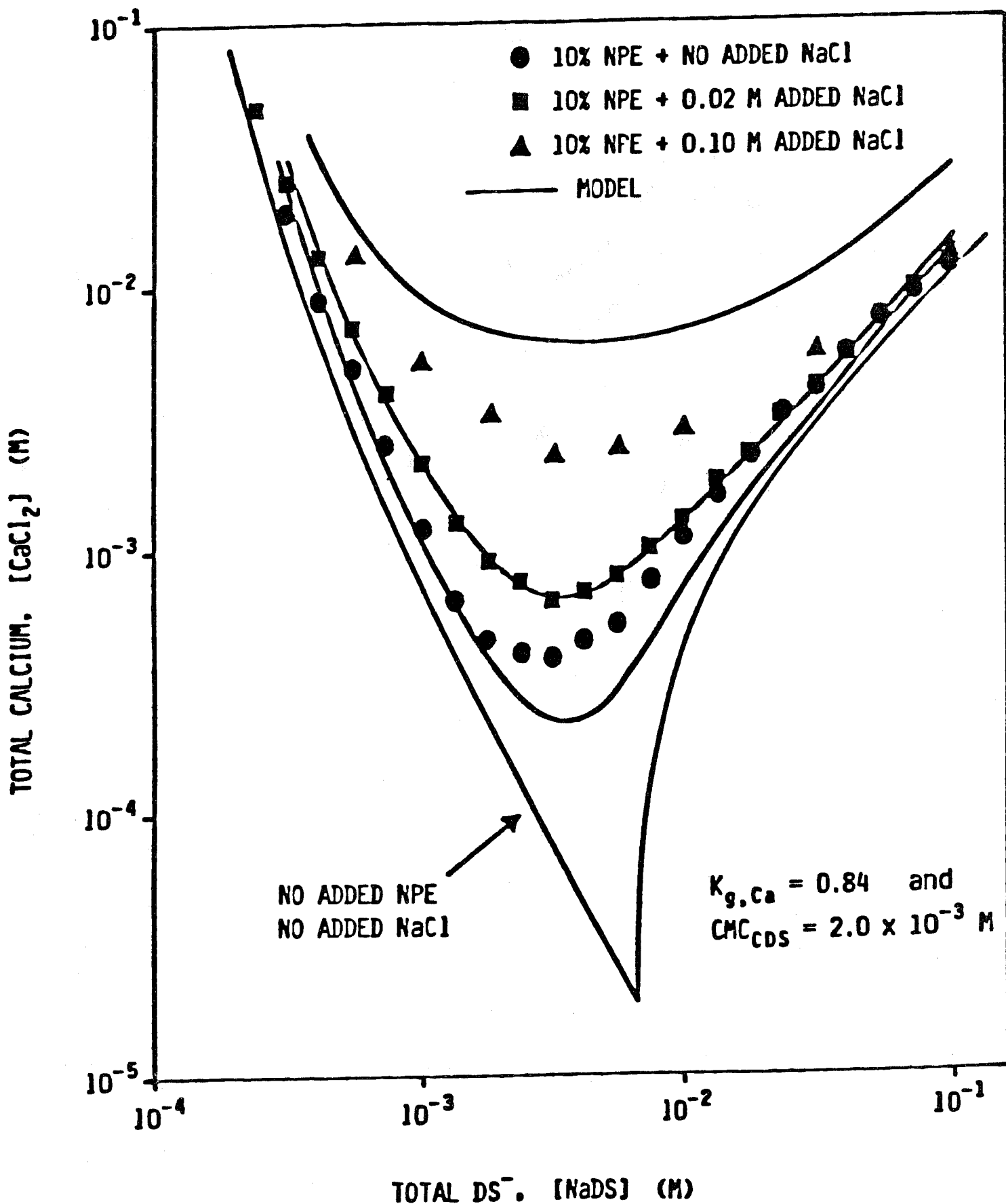


Figure 5.11: Values of Fractional Counterion Binding of Calcium Required to Describe System With Nonionic Surfactant and No Added NaCl

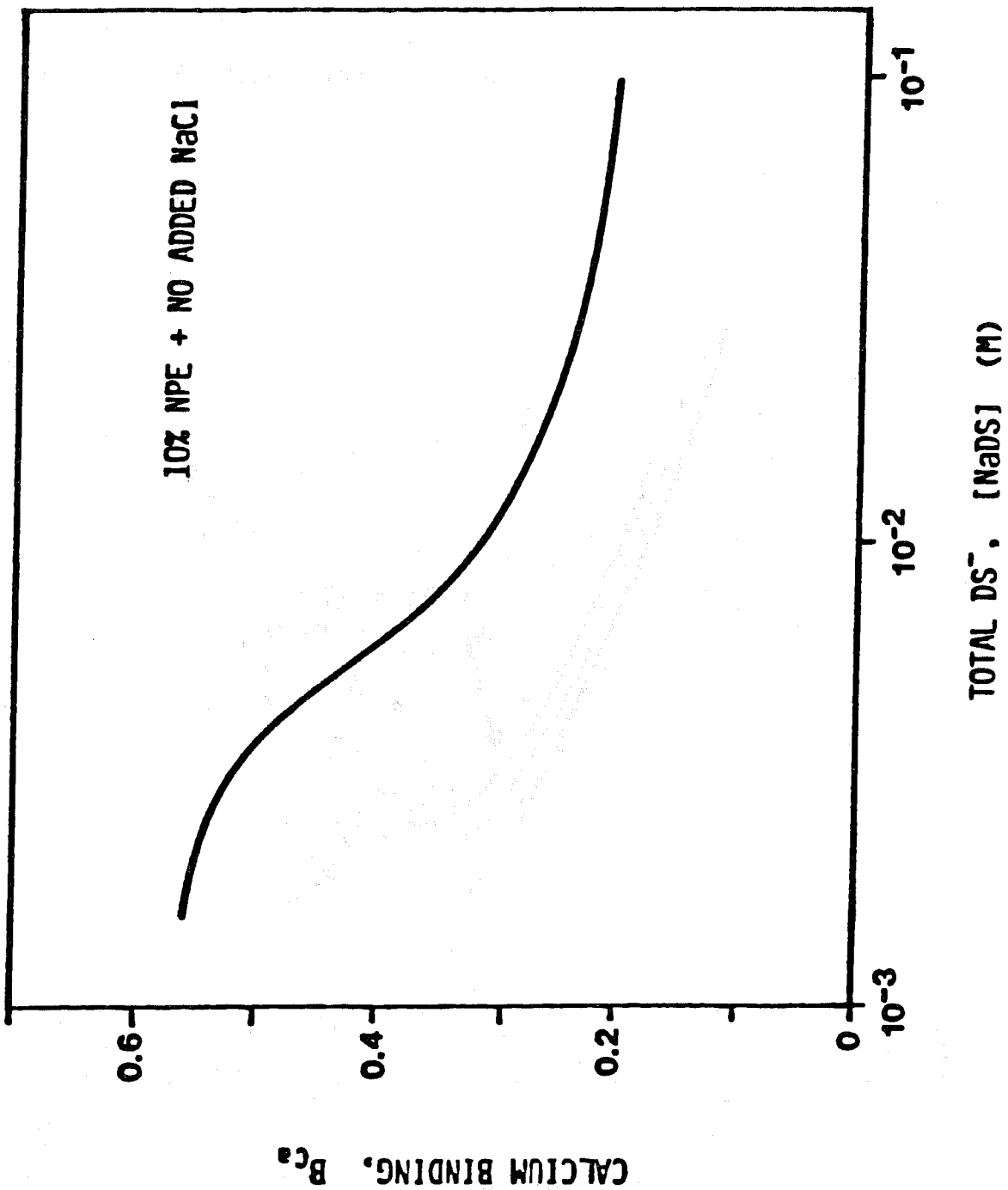


Figure 5.12: Effect of W/RT on Predicted Precipitation Phase Boundaries

